AD-A068 015 OFFICE OF THE PROJECT MANAGER HIGH ENERGY LASER REDS--ETC F/6 20/6
OPTICAL QUALITY OF TILTED SPHERICAL MIRROR UNSTABLE RESONATORS.(U)
JAN 79 R W JONES, J C NIXON, C CASON

UNCLASSIFIED DRCPM-HEL-79-2 NL

1 OF 2
AD
A068015

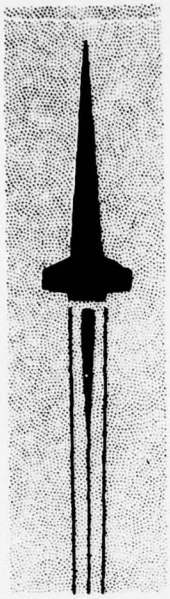

LEVEL II

12

TECHNICAL REPORT DRCPM-HEL-79-2

OPTICAL QUALITY OF TILTED SPHERICAL MIRROR UNSTABLE RESONATORS

R. William Jones, James C. Nixon, and Charles Cason
High Energy Laser Laboratory

and

James F. Perkins
University of Alabama

January 1979

U.S. ARMY MISSILE RESEARCH AND DEVELOPMENT COMMAND

Redstone Arsenal, Alabama 35809

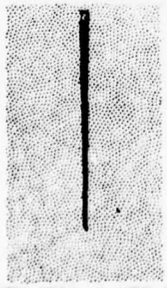

Approved for public release; distribution unlimited.

DMI FORM 1000, 1 APR 77

DISPOSITION INSTRUCTIONS

DESTROY THIS REPORT WHEN IT IS NO LONGER NEEDED. DO NOT RETURN IT TO THE ORIGINATOR.

DISCLAIMER

THE FINDINGS IN THIS REPORT ARE NOT TO BE CONSTRUED AS AN OFFICIAL DEPARTMENT OF THE ARMY POSITION UNLESS SO DESIGNATED BY OTHER AUTHORIZED DOCUMENTS.

TRADE NAMES

USE OF TRADE NAMES OR MANUFACTURERS IN THIS REPORT DOES NOT CONSTITUTE AN OFFICIAL INDORSEMENT OR APPROVAL OF THE USE OF SUCH COMMERCIAL HARDWARE OR SOFTWARE.

UNCLASSIFIED

SECURITY CLASSIFICATION OF THIS PAGE (When Data Entered)

REPORT DOCUMENTATION PAGE

READ INSTRUCTIONS BEFORE COMPLETING FORM

1. REPORT NUMBER: DRCPM-HEL-79-2	2. GOVT ACCESSION NO.
3. RECIPIENT'S CATALOG NUMBER	
4. TITLE (and Subtitle): OPTICAL QUALITY OF TILTED SPHERICAL MIRROR UNSTABLE RESONATORS.	5. TYPE OF REPORT & PERIOD COVERED: Technical Report
6. PERFORMING ORG. REPORT NUMBER	
7. AUTHOR(s): R. William Jones, James C. Nixon, Charles Cason, James F. Perkins - University of Alabama	8. CONTRACT OR GRANT NUMBER(s)
9. PERFORMING ORGANIZATION NAME AND ADDRESS: Commander, US Army Missile Research and Development Command, Attn: DRCPM-HEL-79-2, Redstone Arsenal, Alabama 35809	10. PROGRAM ELEMENT, PROJECT, TASK AREA & WORK UNIT NUMBERS: 1X263314D093, AMCMS 623314.0930012
11. CONTROLLING OFFICE NAME AND ADDRESS: Commander, US Army Missile Research and Development Command, Attn: DRDMI-TI, Redstone Arsenal, Alabama 35809	12. REPORT DATE: January 1979
	13. NUMBER OF PAGES: 115
14. MONITORING AGENCY NAME & ADDRESS (if different from Controlling Office)	15. SECURITY CLASS. (of this report): UNCLASSIFIED
	15a. DECLASSIFICATION/DOWNGRADING SCHEDULE

16. DISTRIBUTION STATEMENT (of this Report)

Source = Office of the Project Manager High Energy Laser

17. DISTRIBUTION STATEMENT (of the abstract entered in Block 20, if different from Report)

Approved for public release; distribution unlimited.

18. SUPPLEMENTARY NOTES

19. KEY WORDS (Continue on reverse side if necessary and identify by block number)

Collimated output
Spherical mirrors
Experimental interferometry
Optical path differences
U and Z configurations

20. ABSTRACT (Continue on reverse side if necessary and identify by block number)

A new class of resonators has recently been proposed which has the property of having different magnifications M_x and M_y in orthogonal directions perpendicular to the propagation direction; the most interesting cases are those with collimated output analagous to conventional confocal unstable resonators. The designs utilize spherical mirrors which are tilted substantially

(ABSTRACT continued)

DD FORM 1 JAN 73 1473 EDITION OF 1 NOV 65 IS OBSOLETE

410 990

UNCLASSIFIED

SECURITY CLASSIFICATION OF THIS PAGE (When Data Entered)

(ABSTRACT concluded)

from the mirror normal. The conventional orientation requires the mirror normal to be along (or very nearly parallel to) the propagation direction. Use of spherical mirrors by this new class of resonators eliminates the difficulties of fabricating mirrors with more complex figures, which would otherwise be required to achieve the desired asymmetric magnification. The critical problem of keeping beam-quality degradation (aberrations) due to mirror tilt within acceptable limits has been examined experimentally and analytically. The results confirm the possibility of achieving acceptable small aberrations for large tilt angles (convex mirror tilt as large as 70°, corresponding to 140° beam deflection) to operation at infrared wavelengths.

A confirmation of the tilted spherical mirror resonator concept was validated theoretically and experimentally by choosing a convex/concave mirror set with small radii of curvature (small f number). The deliberately exaggerated aberrations were compared by experimental interferometry and computational plots of optical path differences. The results of experiment and theory agreed quantitatively.

The following conclusions were drawn from this work:

1) The sense of relative tilt of the spherical mirrors affects the aberrations.

2) The dominant terms contributing to aberrations are of the form y^3 and x^2y with y^3 predominating for high aspect ratio resonators.

3) The concept has many advantages over toroidal resonators used with linear chemical lasers. Chemical laser development programs experiment with varying values of x_c, thereby requiring several sets of toroidal mirrors for beam extraction. The present concept has the ability to vary M_x continuously to account for planned variations in x_c of interest in chemical laser development experiments, thereby requiring no more than one resonator.

CONTENTS

		Page
I.	INTRODUCTION	3
II.	THEORETICAL CALCULATIONS	3
III.	EXPERIMENTAL RESULTS	20
IV.	SUMMARY AND CONCLUSIONS	23
Appendix A.	EQUATIONS FOR THREE-DIMENSIONAL RAY TRACING	101
Appendix B.	EFFECTS OF INCREMENTS TO MIRROR SPACING L AND TO CONCAVE-MIRROR TILT ANGLE θ_2	109

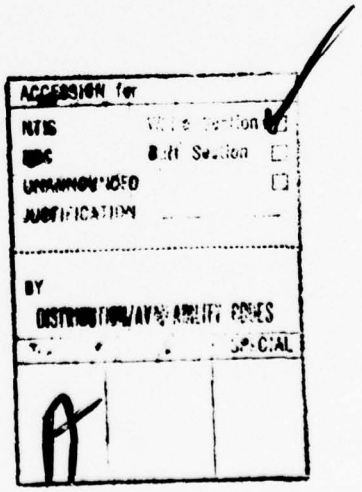

I. INTRODUCTION

This new class of resonators, which possesses certain unique and desirable features, was proposed and discussed earlier.[1,2] The basic design equations were derived and experimentally confirmed, and a report was given of a preliminary interferometric study of optical quality expected from such resonators. This class of resonators is useful provided only that the output optical quality can be maintained at an acceptably high level. A more detailed, combined theoretical-computational study of expected optical properties has subsequently been performed. It forms the subject of this report.

This study considers the effect of one complete passage from convex to concave mirror on an initially collimated beam. This is essentially the conventionally aligned travelling-wave (or ring) resonator configuration. Standing-wave resonators, with or without beam inverters, are also of considerable interest, but they are not considered here. Both cases of relative sign of spherical-mirror tilt angles are considered; these are referred to as U and Z configurations. The Z configuration is preferred over the U configuration in optical quality.

A two-dimensional treatment (i.e., one which neglects one of the two transverse dimensions) is useful as a conceptual vehicle and as a means of obtaining useful, though only approximate, estimates of output beam quality. This is discussed first. A three-dimensional ray-tracing approach is then discussed and its predictions are compared with experiments. The most important part of this study is the experimental study, which is an extension and refinement of the preliminary interferometric study reported earlier.

II. THEORETICAL CALCULATIONS

A. Two-Dimensional Approximation

The two-dimensional approximation has the advantages of greater ease of detailed calculations, easier visualization, and feasibility of obtaining approximate closed-form predictions of optical

---

[1] Cason, Charles, Jones, R. W., and Perkins, J. F., Optical Resonators with Tilted Spherical Mirrors, US Army Missile Research and Development Command, Redstone Arsenal, Alabama, September 1977, Report No. H-77-9.

[2] Cason, Charles, Jones, R. F., and Perkins, J. F., "Unstable Optical Resonators with Tilted Spherical Mirrors, "Optics Letters, Vol. 6, No. 2, June 1978, pp. 145-147.

quality. On the other hand, it is certainly not highly accurate quantitatively, and it sheds no light on the appearance of interferograms and their behavior with respect to variation of experimental parameters.

An approach based on local wave-front curvature was pursued first; this led to a closed-form approximate prediction of the magnitude of the principal contribution (the y^3 term) to the aberration resulting from tilting the spherical mirrors. The assumptions and approximations underlying this approach are perhaps obscure, so calculations were also carried out for one particular set of parameters using a ray-slope and an optical-path-difference (OPD) approach. The latter two calculations agreed with results of the former (local wave-front-curvature) approach, thereby lending it credibility.

The two basic types of configurations, U-type and Z-type, are illustrated in Figures 1(a) and 1(b). The basic design equations derived earlier make no distinction between these two types of design. The various treatments of aberrations as given here, however, clearly distinguish between the two types.

1. Wave-Front Curvature Approach. Figures 1(a) and 1(b) present the two basic types of configurations. The combination of mirror curvatures, separation, and tilt angles for the central ray will be chosen such that the curvatures in the y-z and x-z plane introduced at the convex mirror, after modification by passage to the concave mirror, (will be compensated by the concave mirror), and the emergent central portion of the beam will again be collimated. This condition will not be exactly satisfied for noncentral portions of the beam, as schematically related to off-center rays sketched in Figures 1(a) and 1(b). Behavior at noncentral portions of the beam between curved mirrors differs from that at the central position in two respects:

a) The local tilt angles of the mirrors are slightly different from the central values.

b) The distance between points of reflection by the two mirrors is slightly different for the off-center case.

The increments in tilt angles at the convex and concave mirrors, respectively, in going to an off-center case are labelled $\delta\theta_1$ and $\delta\theta_2$ initially. These two values are (approximately, but to a high order) equal. This can be shown as follows:

$$\frac{\delta\theta_1}{\delta\theta_2} = \pm \frac{\frac{a \sec \theta_1}{R_1}}{\frac{b \sec \theta_2}{R_2}} = \mp \frac{1}{M_y}\left(\frac{-R_2}{R_1}\right)\frac{\sec \theta_1}{\sec \theta_2} ,$$

$$= \mp \frac{M}{M_y}\frac{\sec \theta_1}{\sec \theta_2} \quad .$$

From Equation (32)[3], it is noted

$$\frac{M}{M_y} = \sqrt{\frac{M_x M_y}{M_y}} = \sqrt{\frac{M_x}{M_y}} \quad .$$

By Equation (28)[4], it follows that

$$\frac{M}{M_y} = \frac{\sec \theta_2}{\sec \theta_1} \quad .$$

Combining these two equations gives

$$\frac{\delta\theta_1}{\delta\theta_2} = \mp 1 \quad .$$

The positive sign applies to the U configuration (from its shape); the negative sign applies to the Z configuration. For simplicity, δ is used to denote the common magnitude of $\delta\theta_1$ and $\delta\theta_2$.

a. Increment in Separation Required to Maintain Confocality: The basic confocality condition required to obtain collimation of the output beam in a localized region is

$$L_{req} \ (\delta = 0) = \frac{1}{2}\left[- |R_1| \cos \theta_1 + R_2 \cos \theta_2\right] \quad .$$

The incremental value [i.e., change in L required to maintain confocality as the ray of interest moves from the center toward the upper

---

[3] Op. cit., Cason et al., Optical Resonators . . .

[4] Ibid.

portion of Figures 1 (a) and 1 (b)] can be obtained by expanding about the central angle. For the incremental ray, $\delta\theta_1$ is considered the negative of δ (i.e., δ is a positive quantity). This gives

$$\Delta L_{req} = \frac{1}{2}\,\delta\left[-\,|R_1|\,\sin\,\theta_1 \pm R_2\,\sin\,\theta_2\right] \quad .$$

b. Actual Increment in Separation of Reflection Points: First, only the difference in Z-coordinates of the points of reflection of a ray from each of the mirrors is considered. By geometrical construction, it can be seen that

$$\Delta Z \approx -\,\delta\left[-\,|R_1|\,\sin\,\theta_1 \pm R_2\,\sin\,\theta_2\right] \quad .$$

From separate numerical examination, it is found that the increment in path length due to the change in y coordinates is small compared to the preceding change in z coordinate. The incremental focal length then is the difference between these quantities, and it follows that

$$\Delta F = \Delta L_{req} - \Delta Z = \frac{3}{2}\,\delta\left[-\,|R_1|\,\sin\,\theta_1 \pm R_2\,\sin\,\theta_2\right] \quad .$$

c. Radius of Curvature of Emerging Wavelet: Next the local radius of curvature of the wave reflected from the concave mirror at the displaced position is determined for a mirror spacing adjusted such that the center portion of the emergent wave is collimated. From the lens equation, it follows that

$$\frac{1}{R_0} = \frac{1}{F_{2y}} - \frac{1}{(F_{2y}+\Delta F)} \approx \frac{\Delta F}{(F_{2y})^2}$$

where F_{2y} is the y-coordinate effective focal length of Mirror 2 (concave mirror); namely, $1/2\ R_2\ \cos\ \theta_2$.

If it is assumed that the equation for the curve of constant phase (obtained by setting x = 0 in the equation for the surface of constant optical phase) is

$$z - A\,y^3 = 0 \quad ,$$

the following is readily obtained:

$$\frac{d^2z}{dy^2} = 6\,A\,y \quad .$$

By definition, the left-hand side of this equation is the reciprocal of the local radius of curvature. That is

$$\frac{1}{R_0} = 6\,A\,y \quad .$$

Substitution in the preceding equation gives

$$z = \frac{1}{6\,R_0}\,y^2$$

for the curve of constant phase. Introducing the earlier expression for R_0 gives

$$z = \frac{2}{3}\,\frac{\Delta F}{R_2^2\cos^2\theta_2}\,y^2 \quad ,$$

where ΔF is given by the preceding expression. Here y is used to denote the displacement at the output position; hence, $y = R_2\,\delta\cos\theta_2$. Combining all of these gives

$$z = \frac{1}{R_2^3\cos^3\theta_2}\left[-|R_1|\,\sin\theta_1 \pm R_2\,\sin\theta_2\right]y^3 \quad .$$

By inspection, the value of z for a given value of y is always smaller in magnitude for the Z configuration than for the U configuration. (Only the magnitude, but not the sign, of z as predicted by this equation is of significance, because the value of z has opposite signs for rays incident on opposite sides of the convex mirror).

As a numerical example, a case with $R_1 = -290$ cm, $R_2 = 675$ cm, $\theta_1 = 55°$, $y = 9.176$ cm (corresponds to δ 0.01) is considered. The associated value of θ_2 is 38.76°. Using the preceding formula for the Z configuration, the following is obtained:

$$z = \frac{1}{(675 \times 0.77977)^3} \times 185.035 \times (9.176)^3 = 0.000\ 980 \text{ cm} \quad .$$

For the U configuration, the following is obtained

$$z = \frac{1}{(675 \times 0.77977)} \times (-660.144) \times (9.176)^3 = -0.003\ 497 \text{ cm} \quad .$$

The expression for z as a function of y can alternatively be written as an explicit function of the magnifications M_x and M_y, rather than the angles θ_1 and θ_2, although this has not been done here. There are equations from which θ_2 can be determined, when θ_1, R_1, and R_2 are specified.[5]

This detailed discussion has been given for the wave-front curvature approach in the y-z plane because it gives an explicit expression in terms of resonator parameters. Alternative approaches which have been used will be more briefly discussed. The function of the latter has been essentially limited to numerical and analytical confirmation of the preceding approach for one set of resonator parameters.

2. Ray Slope Approach. A two-dimensional ray-trace calculation was carried through numerically for the reference case with $R_1 = -290$ cm, $R_2 = 675$ cm, $\theta_1 = 55°$; here the small parameter, again labelled δ (the distance between points of intersection of two incident rays with convex mirror and measured in units of radius of curvature of convex mirror) was treated. Numerical results agreed with the wave-curvature results. Treatment was done semi-analytically with various quantities expressed as expansions in powers of δ. From the latter, the y^3 dependence of z (y^2 dependence of slope) was confirmed as found from the wave-curvature approach.

3. OPD Approach. Direct numerical and semi-analytical expansion-type calculations were made to determine the OPD for the previously mentioned reference case. Results again confirmed the wave-curvature results.

4. Beam-Quality Predictions. Deterioration of the optical quality of the output beam is essentially determined by the root-mean-square (rms) value of variations in optical path length, z, measured in units of wavelength, relative to a suitable reference plane for a collimated output beam. The rms variations are considerably smaller than peak-to-peak or center-to-peak variations, and the choice of reference plane is important.

In the two-dimensional approximation, the center-to-peak variation, z_{cp}, (approximately half the peak-to-peak variation) can be expressed as

$$z_{cp} \approx C_{03}\, y_{max}^{\,3} = C_{03}\, y^3$$

---

[5] Ibid.

where y_{max} is the half-width of the output beam, and C_{03} is a certain expansion coefficient (use of the double subscript is for consistency with the later three-dimensional calculations). From the preceding equation, the approximate prediction for C_{03} is

$$C_{03} \approx \frac{1}{R_2^3 \cos^3 \theta_2} \left[- |R_1| \sin \theta_1 \pm R_2 \sin \theta_2 \right] \quad .$$

The rms value for an untilted reference plane is obtained by simple integration

$$z_{rms,nt}^2 = \frac{\int_{-y}^{y} \left[z(y) \right]^2 dy}{2y} = \frac{C_{03}^2}{2y} \int_{-y}^{y} y^6 \, dy \quad ,$$

$$z_{rms,nt}^2 = \frac{1}{7} C_{03}^2 y^6 \quad .$$

The factor of 7 reduction is naturally of considerable practical significance. It follows that

$$z_{rms,nt} = 0.378 \, z_{cp} \quad .$$

The preceding equations assume a reference plane which is perpendicular to the central ray of the output beam. There is no a priori reason why the reference plane must be so chosen. A reference plane which optimizes the beam quality can be chosen (i.e., to allow for a tilted reference plane (this is closely related to allowance for a tilted reference beam in interferometry, as discussed later), as given by the equation

$$z_{ref} = C_t \, y \quad .$$

The integral involved is

$$z_{rms,t} = \frac{1}{2y} \int_{-y}^{y} \left[C_{03} y^3 - C_t y \right]^2 dy$$

$$= \frac{1}{2y} C_{03}^2 \int_{-y}^{y} \left[y^3 - By \right]^2 dy$$

where

$$B = \frac{C_t}{C_{03}} \quad .$$

The following is readily obtained:

$$z_{rms,t}^2 = \frac{1}{7} C_{03}^2 y^6 f(B) \quad ,$$

where

$$f(B) = 1 - \frac{14 B}{5 y^2} + \frac{7 B^2}{3 y^4} \quad .$$

To minimize f(B), its derivative is taken with respect to B and set equal to zero. The following is obtained:

$$B_{opt} = \frac{3}{5} y^2 \quad .$$

The minimum value of f(B) is then

$$f_{opt}(B) = \frac{4}{25} = 0.160 \quad .$$

This represents a further substantial reduction in the OPD which is effective in deterioration of beam quality. For optimal reference-plane tilt, the following is obtained:

$$z_{rms,opt}^2 = \frac{4}{175} C_{03}^2 y^6 \quad .$$

The minimized rms value itself can then be written as

$$z_{rms,opt} = 0.151 C_{03} y^3 \quad .$$

This is less by a factor of approximately 13 than the peak-to-peak OPD. It is the square of this factor which is important in determining beam-quality deterioration.

Some numerical examples are given in Tables 1 through 3, which are representative of the mirror pair studied interferometrically: an example chemical-laser resonator design, and a CO_2 pulsed electron-beam

laser, respectively. From these estimates, the optical quality should be quite acceptable at infrared wavelengths, when rms and reference-plane-tilt effects are accounted for, except for the rather extreme case of the mirrors being used for the interferometric testing in the case of Table 1. This pair of mirrors is considered at full aperture primarily because they provide useful interferometric structure at visible wavelengths, thereby, facilitating quantitative experimental studies of aberrations.

TABLE 1. TWO-DIMENSIONAL APPROXIMATE OPD PREDICTIONS (IN MICRONS) FOR A Z CONFIGURATION TRAVELLING-WAVE RESONATOR WITH R_1 = -290 cm, R_2 = 675 cm, Y = y_{max} = 7.62 cm, FOR VARIOUS VALUES OF CONVEX-MIRROR TILT ANGLE θ_1*

θ_1 (deg)	z_{cp}	$z_{rms,nt}$	$z_{rms,opt}$
10	0.393	0.149	0.059
20	0.855	0.323	0.129
30	1.481	0.560	0.224
45	3.168	1.198	0.479
50	4.165	1.574	0.630
55	5.614	2.122	0.849
60	7.866	2.973	1.189
65	11.709	4.426	1.770
70	19.233	7.270	2.908

*This corresponds to the resonator mirrors used in the interferometric study. The second column gives the center-to-edge values; the third column gives the rms OPD for an ultilted reference plane; the fourth column gives the rms OPD relative to an optimally-tilted reference plane.

Such two-dimensional estimates would be considered quite uncertain if standing alone. In later sections of this report results of more detailed calculations will be presented. These rather simple sorts of estimates give useful semi-quantitative guidance to the expected degree of optical-quality degradation for an ideally aligned system. On the other hand, the two-dimensional considerations give no indication what-

TABLE 2. TWO-DIMENSIONAL APPROXIMATE OPD PREDICTIONS (IN MICRONS) FOR A Z CONFIGURATION TRAVELLING-WAVE RESONATOR WITH R_1 = -1481 cm, R_2 = 3703 cm, Y = y_{max} = 7.5 cm, FOR VARIOUS VALUES OF CONVEX-MIRROR TILT ANGLE θ_1*

θ_1 (deg)	z_{cp}	$z_{rms,nt}$	$z_{rms,opt}$
10	0.013	0.005	0.002
20	0.028	0.010	0.004
30	0.048	0.018	0.007
45	0.100	0.038	0.015
50	0.130	0.049	0.020
55	0.174	0.066	0.026
60	0.240	0.091	0.036
65	0.352	0.133	0.053
68.6	0.491	0.185	0.074

*This corresponds to a typical MADS chemical-laser resonator. The second column gives the center-to-edge values; the third column gives the rms OPD for an untilted reference plane; the fourth column gives the rms OPD relative to an optimally-tilted reference plane.

ever of the sensitivity of optical quality to various systems parameters, including increments to mirror separation L, and concave-mirror-tilt-angle θ_2 for a specified value of θ_1.

The two-dimensional results give no information about expected shapes of interferograms. Using information gathered from experiments and three-dimensional calculations, a brief discussion of the behavior of reference-plane tilt can be given. In Figure 2, the $C_{03}\ y^3$ dependence is plotted as a function of z in the solid curve. If the reference-plane is chosen to be that indicated by the dashed line, instead of the xy plane itself, the maximum OPD will clearly be reduced. If it is assumed that Z configurations have an x^2y term in the OPD series-expansion expression with the same sign as that of the y^3 term, a

TABLE 3. TWO-DIMENSIONAL APPROXIMATE PREDICTIONS OF (IN MICRONS) FOR A Z CONFIGURATION TRAVELLING-WAVE RESONATOR WITH R_1 = -1180 cm, R_2 = 2640 cm, Y = y_{max} = 10 cm, FOR VARIOUS VALUES OF CONVEX-MIRROR TILT ANGLE θ_1*

θ_1 (deg)	z_{cp}	$z_{rms,nt}$	$z_{rms,opt}$
10	0.057	0.022	0.009
20	0.124	0.047	0.019
30	0.216	0.082	0.033
45	0.468	0.177	0.071
50	0.619	0.234	0.094
55	0.839	0.317	0.127
60	1.184	0.448	0.179
65	1.778	0.672	0.269
70	2.952	1.116	0.446

*This corresponds to a typical CO_2 E-beam laser.

The second column gives the center-to-edge values; the third column gives the rms OPD for an untilted reference plane; the fourth column gives the rms OPD relative to an optimally-tilted reference plane.

qualitative property of an interferogram of an aligned system can be predicted with the reference beam tilted as shown by the dashed line. The x^2y term will cause the OPD to increase for positive y when x is varied in either direction from zero, i.e., the surface for positive y will curve upward with respect to variations in x. Hence, tilted planes parallel to that indicated by the dashed line, but corresponding to smaller values of z, will intersect the surface in closed curves. Similarly, for negative values of y, tilted planes parallel to that indicated by the dashed line, but corresponding to larger values of z, will intersect the surface in closed curves. This is the qualitative nature of the interferograms for a suitable aligned system with tilted reference beam for Z configurations.

B. Three-Dimensional Calculations

The major portion of the theoretical-computational part of this study has been concerned with developing and applying three-dimensional ray-tracing computational methods and with correlating the results (primarily in the form of quasi-interferograms) with the experimental interferograms. The development of computational methods progressed from step-by-step hand calculations to the use of a programmable pocket calculator, then to a Fortran program which initially treated each of the spherical mirrors by a separate set of equations, and finally to a Fortran program which treats mirror reflections, ray intersections, and coordinate rotations by subroutines in such a way that possible future generalizations to more than two spherical mirrors should be simplified.

Equations employed in ray tracing are derived in Appendix A. Their present application assumes a collimated beam incident on the convex mirror. Given x and y coordinates of an incident ray measured relative to the central ray, the computer program calculates the path of the ray through the system and determines (a) direction cosines after reflection from the concave mirror, measured in a coordinate system with the positive z-axis parallel to the central ray and (b) the OPD between the ray considered and the central ray. The OPDs are of primary interest, and are calculated for a position close to the concave mirror. Double-precision arithmetic was used to obtain reliable values of OPDs.

The input data include half-widths of the desired output beam and the number of mesh points along x and y (usually 9 × 9) in the x and y directions. Coordinates x and y of incident rays are obtained by dividing corresponding desired coordinates of output rays by magnifications M_x and M_y, which are computed by the program from input values of R_1, R_2, and θ_1. Unless otherwise specified, the program uses the values of mirror spacing L and concave-mirror tilt angle θ_2 which result in a collimated output beam. Values of these parameters are determined by an initial portion of the program. The first page of computer output is a table of calculated OPDs over the specified mesh; the OPDs are given in microns; mirror spacing and radii of curvature are given in centimeters.

As might be expected, there is a good deal of order in the calculated OPDs; their functional dependence on x and y can be well represented by a relatively small number of terms of a Taylor's expansion. The number of terms which are retained is somewhat arbitrary and has been increased from time to time. Terms $C_{03}\, y^3$ and $C_{21}\, x^2 y$ are of primary importance. Values of the coefficients C_{03} and C_{21} are not the

same (as they may be in some contexts in which the terminology of "coma" is employed). The quadratic terms $C_{20}\ x^2$ and $C_{02}\ y^2$ can be important if the system is not properly adjusted. These terms have been included in the function-fitting process to be able to investigate the effects of adjusting L and θ_2 to values slightly different from their ideal values. A cross-term $C_{22}\ x^2\ y^2$ and fourth-order terms of the form $C_{40}\ x^4$ and $C_{04}\ y^4$ are also considered.

The computer program evaluates the series coefficients from the table of calculated OPDs and prints these. It also calculates and prints a table of residuals showing the difference between the directly calculated OPDs and values obtained from the truncated series expansion; these typically seem to be of the order of less than one percent to few percent of the OPDs themselves. The coefficient C_{tilt} corresponding to a reference plane defined by $z = C_{tilt}\ y$, which minimizes the rms OPD is also determined and printed. A table is printed (as the last page of output for each case) of the rms values of OPD for various values of reference-beam tilt measured in units of the optimal value. Inspection of this table indicates substantial reductions in the rms OPD, as would be expected from the discussion in connection with two-dimensional calculations. The even more pronounced reduction as compared to peak values of OPD can be seen by comparison to those listed in the OPD table.

If L and/or θ_2 are set to values incremented slightly from their proper values, there will be curvature in either or both the x and y directions, i.e., C_{20} and/or C_{02} will differ appreciably from zero. Expected values of these coefficients can be derived analytically and compared with results of the function-fitting process applied to the ray-tracing OPD calculations. This is discussed in Appendix B. Agreement between analytically predicted and "function-fitting" calculated values is felt to be a confirmation of proper functioning of the computer program.

The primary experimental data regarding optical quality from the tilted spherical mirror resonator are in the form of interferograms. While providing very precise and detailed information about the optical systems, interferograms do not immediately (without an intervening measurement and data-reduction process) lead to quantities predicted by the calculations. Therefore, it seemed useful to convert the calculated results into the form of computer-simulated quasi-interferograms. For this purpose the computer generates a fairly large array (usually 49×49) of OPDs obtained by evaluation of the truncated series expansion at each of the array points. The array of numerical values is converted

to an array of alpnabetic characters or blanks and used to generate a one-page printer plot whose general apperance simulates that of an interferogram. Successive characters of the alphabet correspond to incremental OPDs of one wavelength (0.6328 μm). The interspersing of blanks with letters of the alphabet has the result that (at least in the central portion of the plot) light areas are interspersed with dark areas and properly simulate an interferogram. With only 26 characters available, the resolution is limited. As a result, it often happens that casual inspection of outer portions of such plots suggests spurious fringe pattern, because the eye tends to interpret contiguous light areas as all belonging to a light fringe. This difficulty can be avoided by concentrating on dark areas and keeping in mind that a particular dark fringe is always represented by the same letter of the alphabet. In one sense, the quasi-interferograms give more information than genuine interferograms because the sign and the magnitude of the OPD relative to the center are represented.

The computer program will optionally produce multiple quasi-interferograms corresponding to a specified set of reference-beam tilts from a single set of OPD calculations (Figures 3 through 14). The observed progression of shapes as tilt is systematically varied has proven interesting and useful because reference-beam tilt can also be varied experimentally. Inspection of quasi-interferograms leads to some interesting observations for a properly-aligned system (which was treated computationally prior to investigating effects of incremented values of L and θ_2):

1) There is symmetry in x, as would be expected since the entire optical system is assumed to have such symmetry.

2) For Z configurations and small-to-moderate values of θ_1, the pattern is symmetric in y to a fairly high degree of approximation (the OPDs are approximately antisymmetric).

3) For Z configurations there is a regular progression of shapes as reference-beam tilt is increased from zero to its optimal value and beyond. Specifically, the pattern changes from a single central oval to a pair of ovals (symmetrically spaced about y = 0) which move further apart and are separated by an increasing number of fringes.

These observed properties are useful in experimental adjustment of L and θ_2, because the symmetry in y is a rather good "signature". Calculations made with values of L and/or θ_2 which are incremented from their ideal values produce quasi-interferograms which are noticeably lacking in the y-symmetry property.

From one point of view, the tilted-spherical-mirror resonator concept can be described as a scheme in which a large degree of astigmatism is introduced by the tilt of the convex mirror, and is cancelled

by suitable choice of mirror spacing and the tilt of the concave mirror. Quasi-interferograms can be used to illustrate cancellation of curvature in either the x or y coordinates (simultaneous cancellation along both coordinates is achieved by the properly adjusted tilted-mirror resonator). For this purpose, a small value (10°) was chosen for θ_1 so that the effects to be illustrated would not be masked by other aberrations. The sequence of quasi-interferograms is presented in Figures 15 through 19. The basic case, i.e., the properly adjusted system, shows very little aberration of any sort; hence, it produces a rather structureless quasi-interferogram. When a small increment ΔL (labelled XINCL) in mirror spacing is introduced, curvature of the same sign is introduced along both x and y axes; the characteristic hill or valley shape is evident in Figure 16. Instead, if L is kept at its proper value but a small increment $\Delta\theta_2$ (labelled XINCT) to concave-mirror tilt is introduced, curvatures with opposite sign along the x and y axes are introduced. This leads to the characteristic "X" pattern representing a saddle-point type of surface, as seen in Figure 17. For a specified value of ΔL (or of $\Delta\theta_2$) an increment of the other parameter can be chosen, such as to cancel the curvature in either the x or y dimension. Such cases are presented in the Figure 18 and 19 plots, which show vertical and horizontal fringes. It should be emphasized that such cancellation could be obtained if there were additional sources of astigmatism present in the system. When one is free to adjust L and θ_2, curvature can be eliminated in the x and y dimensions; i.e., coefficients C_{20} and C_{02} are reduced to zero. This is the criterion which defines the tilted-spherical-mirror resonator concept. It should emphasize that this cancellation can also be obtained if other sources of astigmatism are present. This small value of θ_1 was deliberately chosen to illustrate avoiding complicating the plots with substantial amounts of aberrations other than those associated with x^2 and y^2 expansion terms. For more realistic cases with larger values of θ_1, the quasi-interferograms do not have such a simple appearance.

A number of calculations were made for $\theta_1 = 45°$ for various non-zero values of ΔL and $\Delta\theta_2$ (as well as reference-beam tilts); results are shown in Figures 20 through 43. The coefficient of either the x^2 or y^2 term can also be reduced to zero by suitable choice of one of the increments when the other is specified. Reduction to (approximately) zero of the C_{20} x^2 term shows up most clearly; the plot shows that there is very little OPD variation along x for y = 0. When the coefficient of y^2 is reduced to zero, the corresponding quasi

interferogram is somewhat more involved because there is still an appreciable amount of aberration present associated with other expansion terms. What is especially noticeable is that the y-symmetry is decidedly absent; this emphasizes usefulness of the y-symmetry property in making experimental adjustments. If the signs of ΔL and $\Delta\theta_2$ are reversed, the y^2 coefficient still vanishes, there is still a lack of y-symmetry, and the plot is essentially just the mirror image of the plot obtained without reversal of signs. This mirror-image property applies for any pair of magnitude of ΔL and $\Delta\theta_2$. In the special case of zero magnitude of these increments, the mirror image of the pattern is simply (to a rather good approximation) identical with the pattern itself; i.e., the y-symmetry property is characteristic of proper adjustment of L and θ_2.

The y-symmetry property is not exact, though it seems to hold well for Z configurations (which are of greatest interest because they have fewer aberrations than U configurations) up to large values of θ_1. Presumably, this property results from the fact that the principal terms in the series expansion of the OPD are of odd power in y (specifically, they are the y^3 and x^2y terms).

For cases where comparisons have been made, the three-dimensional ray-tracing calculations predict optical-quality parameters which are not greatly different from those obtained by the much simpler approach based on the two-dimensional approximation. Some specifics will be given in the following paragraphs.

For the representative MADS-type chemical-laser resonator with $\theta_1 = 68.6°$ and output-beam dimensions of 3 × 15 cm, the detailed calculations give a center-to-peak OPD along the y-dimension (for x = 0) of approximately 0.49 μm, in agreement with the two-dimensional prediction of Table 2. The rms value of the OPD for an untilted reference plane is calculated to be 0.188 μm as compared to a two-dimensional prediction of 0.185 μm. The minimized (with respect to reference-plane tilt) rms value of OPD is calculated to be 0.075 μm as compared to the two-dimensional prediction of 0.074 μm. The agreement is rather good. This is partly due to the fact that the flow dimension is small compared to the cross-flow dimension, so that the resonator is, in fact, something of a strip.

For the typical CO_2 resonator at $\theta_1 = 55°$, detailed calculations give a center-to-peak OPD along the y-dimension (for x = 0) of approximately 0.837 μm and a center-to-corner OPD of approximately 1.49 μm; by comparison the two-dimensional center-to-edge prediction of Table 3 is 0.839 μm. The rms value of OPD for an untilted reference plane is 0.448 μm compared to a two-dimensional prediction of 0.317 μm. The

minimized rms OPD is calculated to be 0.169 μm as compared to a two-dimensional prediction of 0.127 μm.

For the mirror parameters associated with the experimental studies, calculations have been carried out for a range of values of θ_1, for which the results are listed in Table 4.

TABLE 4. THREE-DIMENSIONAL RAY-TRACING PREDICTIONS (IN MICRONS) OF OPD FOR A Z CONFIGURATION TRAVELLING-WAVE RESONATOR WITH $R_1 = -290$ cm, $R_2 = 675$ cm, $x_{max} = y_{max} = 7.62$ cm, FOR VARIOUS VALUES OF CONVEX-MIRROR TILT ANGLE θ_1*

θ_1 (deg)	z_{cp}	$z_{rms,nt}$	$z_{rms,opt}$
10	0.393	0.230	0.091
20	0.855	0.496	0.194
30	1.481	0.848	0.330
45	3.171	1.764	0.678
50	4.171	2.287	0.876
55	5.626	3.031	1.157
60	7.892	4.159	1.582
70	19.450	9.529	3.667

*This corresponds to the resonator mirrors used in the interferometric study. The second column gives the center-to-edge values (taken along y for x = 0); center-to-corner values are somewhat larger but are not listed here. The third column gives the rms OPD for an untilted reference plane; the fourth column gives the rms OPD relative to an optimally-tilted reference plane.

These results may be directly compared with the two-dimensional predictions for the same case as given in Table 1. The three-dimensional predictions of the optimized rms OPD range from only 25% to 50% larger than the two-dimensional predictions, even for this case which is a resonator with larger aberrations.

The adjustment of L and θ_2, when R_1 and R_2 are fixed and θ_1 is set, is a central feature of this resonator concept. As alluded to earlier, a significant aspect of the recent studies has been development of criteria and procedures for making the appropriate adjustments. The question naturally arises as to the quantitative degree of sensitivity of rms OPD to variations in L and θ_2. Some numerical results are plotted in Figures 44 through 46. It was found that the numerically-determined values are in fairly good agreement with predictions that can be made on the basis of the intially somewhat questionable assumption that aberrations other than those of quadratic type are insensitive to adjustment of L and θ_2, and that these other aberrations are odd in y and hence "noninteracting" with the quadratic aberrations introduced by variations in L and/or θ_2. Following the approach of Appendix B, the ratio of the coefficients C_{20} and C_{02} to ΔL and/or $\Delta\theta_2$ can then be determined. With these assumptions, values of rms OPD can be predicted as a function of ΔL for $\Delta\theta_2 = 0$ and as a function of $\Delta\theta_2$ for $\Delta L = 0$. These predictions are plotted as the smooth curves in Figures 45 and 46. The numerically-determined values agree satisfactorily with the curves. The OPD contributions from increments to L and to θ_2 are not additive (though the magnitude of the combined effect of specified increments to both parameters can be predicted).

For the system being studied experimentally at moderate values of θ_1 (45° and 55°), it appears that L should be adjusted to within a few millimeters, and θ_2 to within a few milliradians in order that wave-curvature effects not increase the overall aberration substantially beyond the minimal value which is inherent in the tilted-spherical mirror design. These are not very stringent restrictions on experimental adjustments.

III. EXPERIMENTAL RESULTS

The results of this section agree quantitatively with the computational results obtained in the three-dimensional calculations of wavefront OPDs. A set of mirrors was chosen to give a moderate number of fringes across the output aperture and could be compared directly to calculated quasi-interferograms. This test represented an extreme case compared to the aberrations which would be present in the proposed high aspect ratio resonator mirrors[6] but provided a direct correlation between theory and experiment.

---

[6] Ibid.

Two types of resonator concepts were tested, the Z configuration and the U configuration. The schematics of these configurations are shown in Figures 1(a) and 1(b). Most of the interferograms were taken with the Z configuration experimental setup. Only two photographs were taken in the U configuration. All agreed well with the analytical predictions of OPD.

Schematics of the experimental setup for the Z and U configurations are shown in Figures 47(a) and 47(b). In both cases a plane wavefront is produced by passing a helium-neon laser beam through a spatial filter (microscope objective plus pinhole) and collimating the resultant spherically divergent wavefront with a high quality objective lens of 6-in. diameter. This plane wavefront is then split into two components with a glass beamsplitter. One component (reference beam) is reflected directly into a focusing lens to a camera. The other portion (test beam) passes through the beamsplitter to the convex resonator mirror, reflects to the concave resonator mirror, and is directed back through the beamsplitter into the camera by means of appropriately positioned mirror flats.

To obtain the best quality interferograms, an alignment procedure for adjustment of the resonator mirrors is necessary. First, the angles θ_1, θ_2 and the separation between the mirrors is setup in gross agreement with the theoretical predictions[7] (Figure 1). With the reference beam blocked, the beam passing through the resonator and focusing lens is observed. The concave resonator mirror is tilted (variation of θ_2) with simultaneous compensation of the turning flat mirror to keep the beam on the optical axis of the focusing lens. The optimal setting of θ_2 is obtained with the sharpest focal point.

For any given value of θ_1 there is only one value of θ_2 and L which minimize the aberrations introduced in the tilted spherical mirror configurations. The mirror separation L is not as critical as θ_2 to set up experimentally. No variation from the theoretically determined value was necessary.

The interferograms were obtained by superimposing the focal points of the two beams from the beamsplitter (by tilting the turning flat). There is a certain arbitrariness in this adjustment— the interferogram obtained depends strongly upon the angle between the reference beam and the test beam (wavefront tilt). This variability made it difficult to compare exactly the quasi-interferograms obtained analytically with the experimental interferograms.

---

[7] Ibid.

Figures 48 through 54 illustrate the effect of variation of wavefront tilt (reference beam tilt) upon the appearance of the interferograms. A direct side-by-side comparison of theory and experiment is given in many of these and the following cases shown. The agreement is seen to be very good. These cases are for nominal alignment with $\theta_1 = 45°$ in the Z configuration. A vignetting of the 6-in. square theoretical OPD plots is a result of the concave mirror being tilted with respect to the optic axis (Figure 1). The mirror is round and when viewed from the output end (2b), it produces a test beam having an elliptical cross section of 6-in. major axis by 6 cos θ_2 in. minor axis. This has been taken into account by not drawing an interferogram in the portions of the theoretical plots not seen.

Effects of misalignments ($\Delta L, \Delta\theta_2$) for $\theta_1 = 45°$ are shown in Figures 55 through 58. Figure 55 shows the result of a change in separation (ΔL) between the convex and concave mirrors (closer together by 1 cm). Figures 56 and 57 result from varying θ_2 approximately ±7 mrad ($\Delta\theta_2$) about the correct angular position. The mirror symmetry introduced about the vertical axis for $\Delta\theta_2$ of +7 mrad is evident in the interferograms. An increase in deviation of θ_2 of 14 mrad increases the aberrations as seen by the increased number of fringes in Figure 58.

The U configuration was tested for $\theta_1 = 45°$. Figures 59 and 60 are interferograms obtained for two settings of reference beam tilt. The aberrations increase with increasing θ_1 as shown in Figures 61-74 for $\theta_1 = 70°$. Figures 61-64 show a variation in reference beam tilt for the nominally aligned position of resonator mirrors. A comparison of this set of figures with the similar set at $\theta_1 = 45°$ (Figures 48 through 54 show that the essential features of the interferograms are the same, but that the aberrations are worse (more fringes) in the 70° case.

Variations in ΔL and $\Delta\theta_2$ for $\theta_1 = 70°$ show the same general features as for $\Delta\theta_1 = 45°$. Figures 65 and 66 are interferograms taken for $\Delta L = \pm 2$ cm variation about the nominal separation in spherical mirrors. Figures 67 and 68 show $\Delta\theta_2 = \pm 7$ mrad. Figures 69 and 70 give a variation of $\Delta\theta_2 = \pm 14$ mrad. The mirror symmetry of these interferograms in ΔL and $\Delta\theta_2$ is evident in the figures. These interferograms were taken in the Z configuration.

The interferograms for the U configuration show worse phase front errors than the Z configuration. Figures 71 and 72 are interferograms at $\theta_1 = 70°$ for two cases of reference beam tilt. These interferograms as well as the theoretical counterparts are not symmetric about the vertical axis. These are due to the higher order even terms contributing to the phase error in the series expansion of the OPD.

Figures 73 and 74 are a return to the $\theta_1 = 70°$, Z configuration and show a tilt of the concave mirror out of the plane of rotation of θ_1 and θ_2 (in the vertical direction of +7 mrad). The mirror symmetry of the interferograms about the horizontal axis for these misalignments is seen.

IV. SUMMARY AND CONCLUSIONS

Advantages of this relatively new type of resonator have been noted earlier; these include asymmetric magnification ($M_x \neq M_y$) combined with collimated output, a considerable measure of experimental and design flexibility, and the relative ease of fabrication and adjustment of spherical-figure mirrors (as used in the present designs) as constrasted to the case of toroidal mirrors (which are otherwise used to achieved asymmetric magnification). The disadvantages of tilted-spherical-mirror resonators is the additional deterioration of output optical quality resulting from the substantial mirror tilt angles which are involved; a quantitative investigation of this effect seemed clearly in order. Investigation of the optical quality is proceeding in stages. A preliminary interferometric investigation was already reported in connection with the initial examination of the resonator concept.[8,9]

This study has considered in a rather detailed manner the effect on optical quality resulting from one complete passage from convex to concave mirror (essentially a conventionally aligned travelling-wave configuration) of an input collimated beam. Comparison of computational and experimental results has been facilitated by presenting computed results in a format similar in appearance to interferograms. Computational and experimental results, including shapes of interferograms and their behavior as a function of reference-beam tilt angle, incremental mirror separation, and incremental concave mirror tilt angle, are in satisfactory agreement. The considerable reduction in root-mean-square OPD which results from using a slightly tilted reference plane has been confirmed; this simply implies that in a practical device, a major

---

[8] Ibid.

[9] Op. cit., Cason et al., Unstable Optical Resonators . . .

portion of the distinctive tilted-mirror effect consists of a slight angular displacement of far-field peak intensity relative to that of the nominal position. Small angular pointing errors are correctable by a tracker.

The experimental and computational studies have both clearly shown that the Z configuration is to be preferred over the U configuration as regards output optical quality. The principal tilted-spherical-mirror aberrations in a properly adjusted system arise from contributions to optical path differences which are proportional to y^3 and to x^2y. For a high-aspect-ratio resonator, only the y^3 contribution will be of substantial significance; the magnitude of this contribution was found to scale as y^3/R^2. Formulas are given for determining the magnitude of this contribution in a one-transverse-dimension approximation without extensive numerical computations, though three-dimensional ray-tracing calculations are required to evaluate the detailed effects. Tables are given of results of approximate and detailed calculations for selected systems.

Certain additional aspects of this general class of resonators could be investigated by extensions of methods used in the present study. First, the effect of repeated propagation of a beam through the resonator (satisfying the round-trip consistency condition) should be investigated; this will include effects of decentered alignment. Secondly, and more importantly, the studies should be extended to somewhat more involved configurations than those considered here. In particular, an investigation needs to be made of standing-wave tilted-spherical-mirror configurations, which involve a more complex optical path including a turning flat or inverter associated with each of the two spherical mirrors. In such an investigation an effort should naturally be made to find methods of optimizing optical quality as well as achieving other desirable features (e.g., reduced sensitivity to laser-medium inhomogeneities). Distances between turning flats or inverters and their associated spherical mirrors are additional experimental variables, suitable adjustment of which may possibly lead to improvement of optical quality as compared to the travelling-wave configuration, as well as providing variations in magnifications M_x and M_y. An especially desirable goal in this connection is finding combinations of parameters such that aberration effects are reduced to very small magnitudes. While there is no compelling reason for expecting this to be possible, it cannot be ruled out in advance, particularly because in typical chemical-laser configurations, only the y^3 aberration term should be of substantial significance.

The effects of beam inverters associated with either or both spherical mirrors in a standing-wave device should be investigated, not only as a possible means of reducing empty-resonator aberrations but also

because beam inversion could be quite helpful in reducing deleterious effects of spatial nonuniformity of gain and index of refraction in the laser gain medium. It is also desirable to investigate the latter effects separately, perhaps by wave-optics calculations and by experiments. The effects of beam inversion in travelling-wave resonators should also be considered; it should be noted that inversion in travelling-wave resonators can be accomplished with an odd number of flat turning mirrors without the necessity of special inverting optical components.

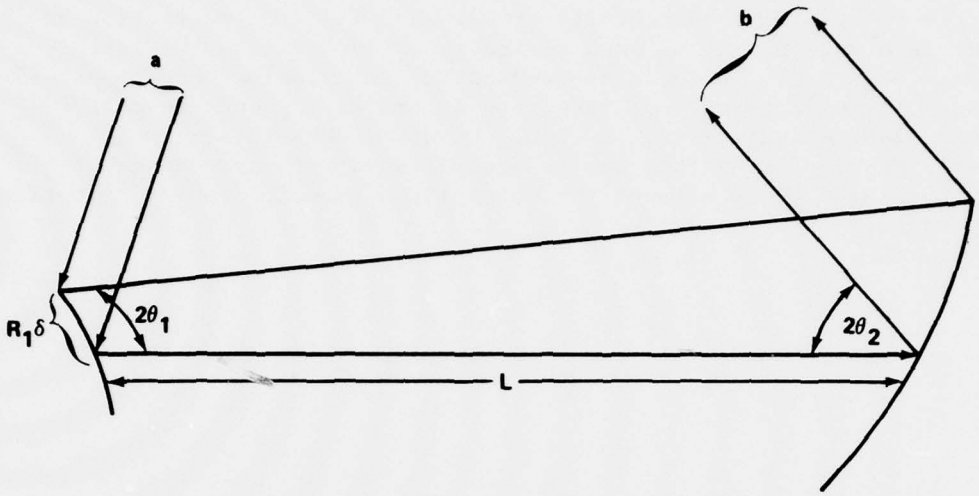

Figure 1(a). Schematic drawing of U configuration resonator.

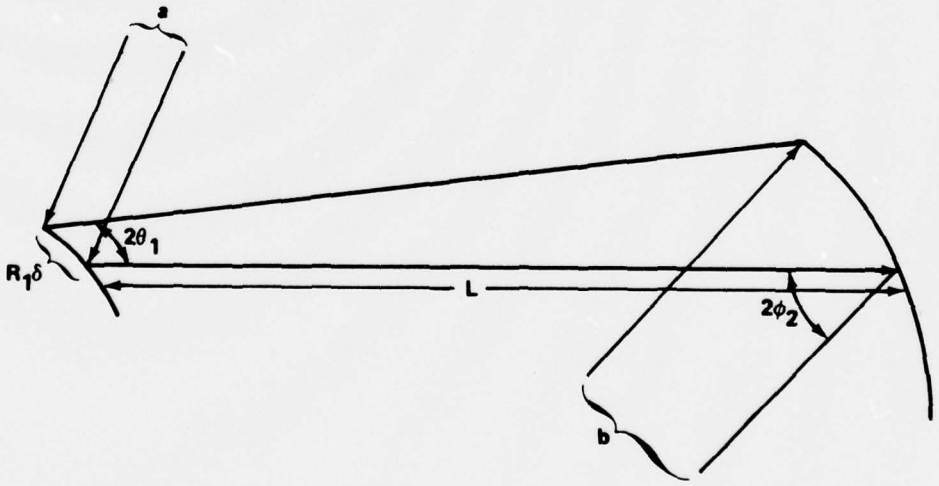

Figure 1(b). Schematic drawing of Z configuration resonator.

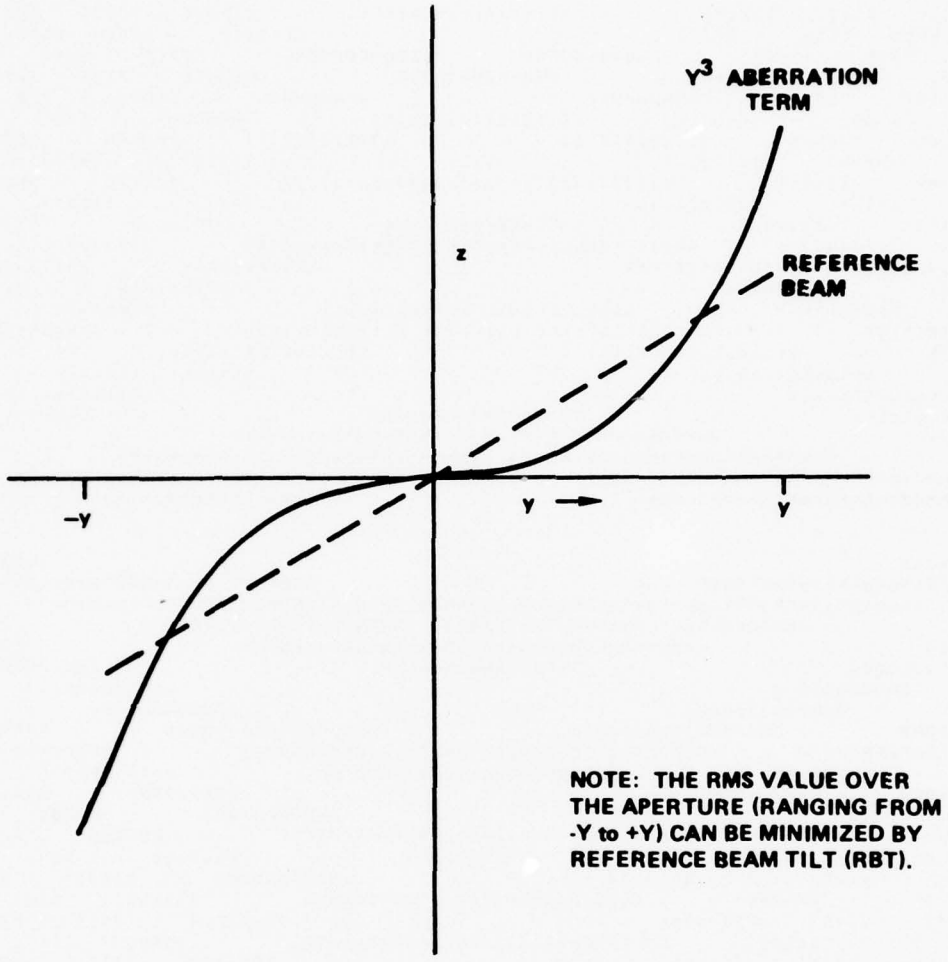

Figure 2. Dependence of the y^3 aberration term.

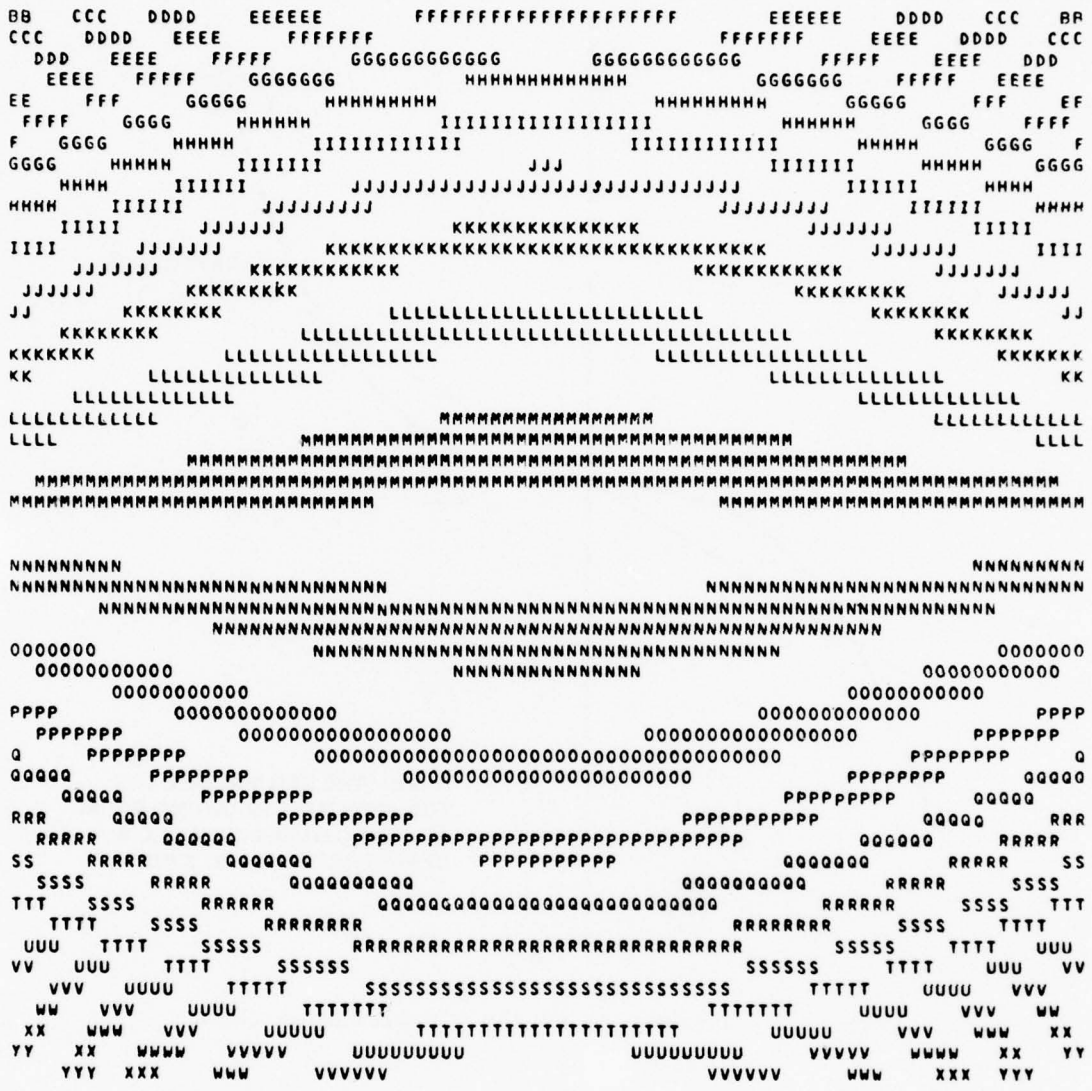

Figure 3. Computer-generated quasi-interferogram Z configuration, $\theta_1 = 45°$, nominal values of L and θ_2, reference-beam tilt (RBT) (optimal value of RBT) = 0.222 (-0.370), in units of 10^{-4} rad.

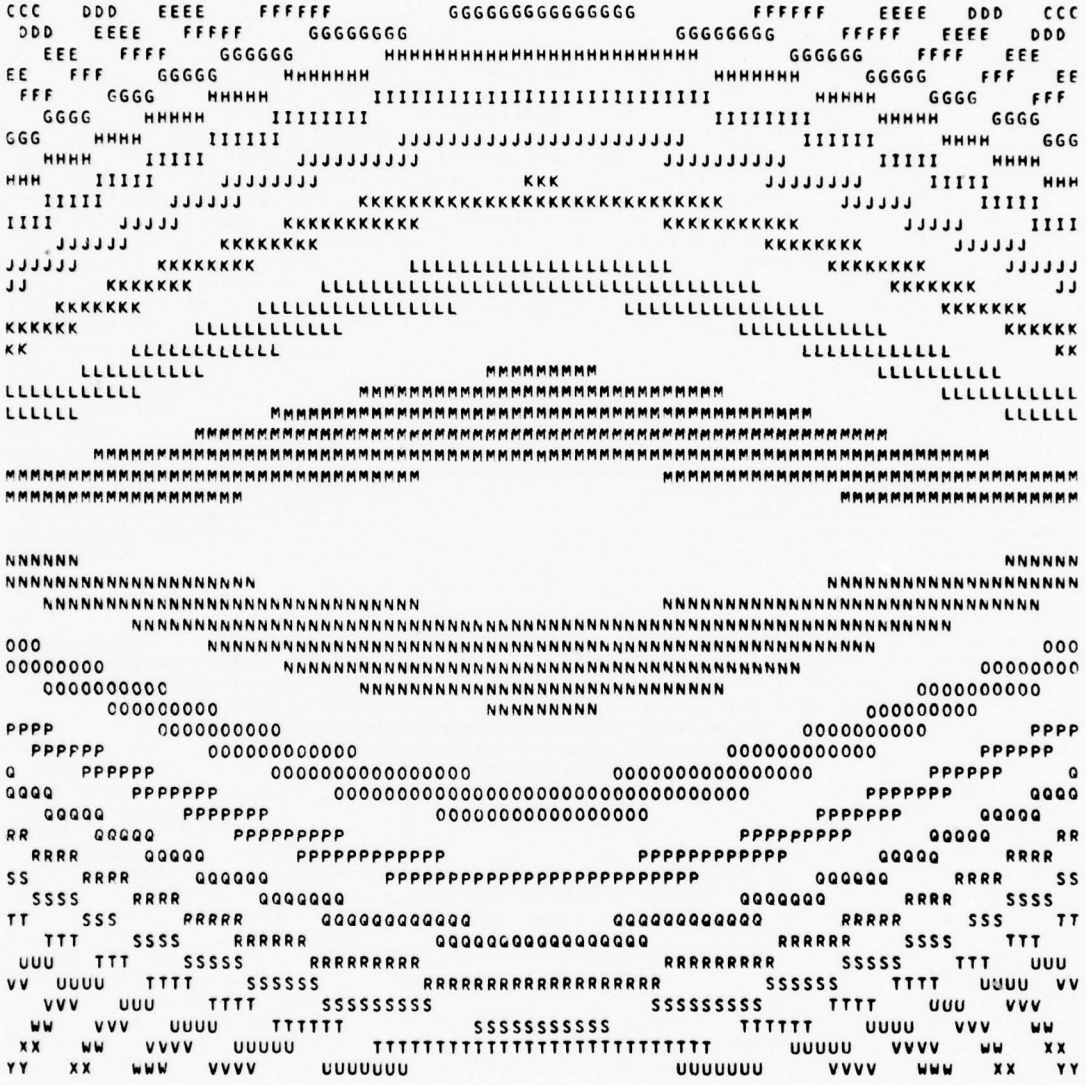

Figure 4. Z configuration, θ_1 = 45°, RBT = 0.148 (-0.370).

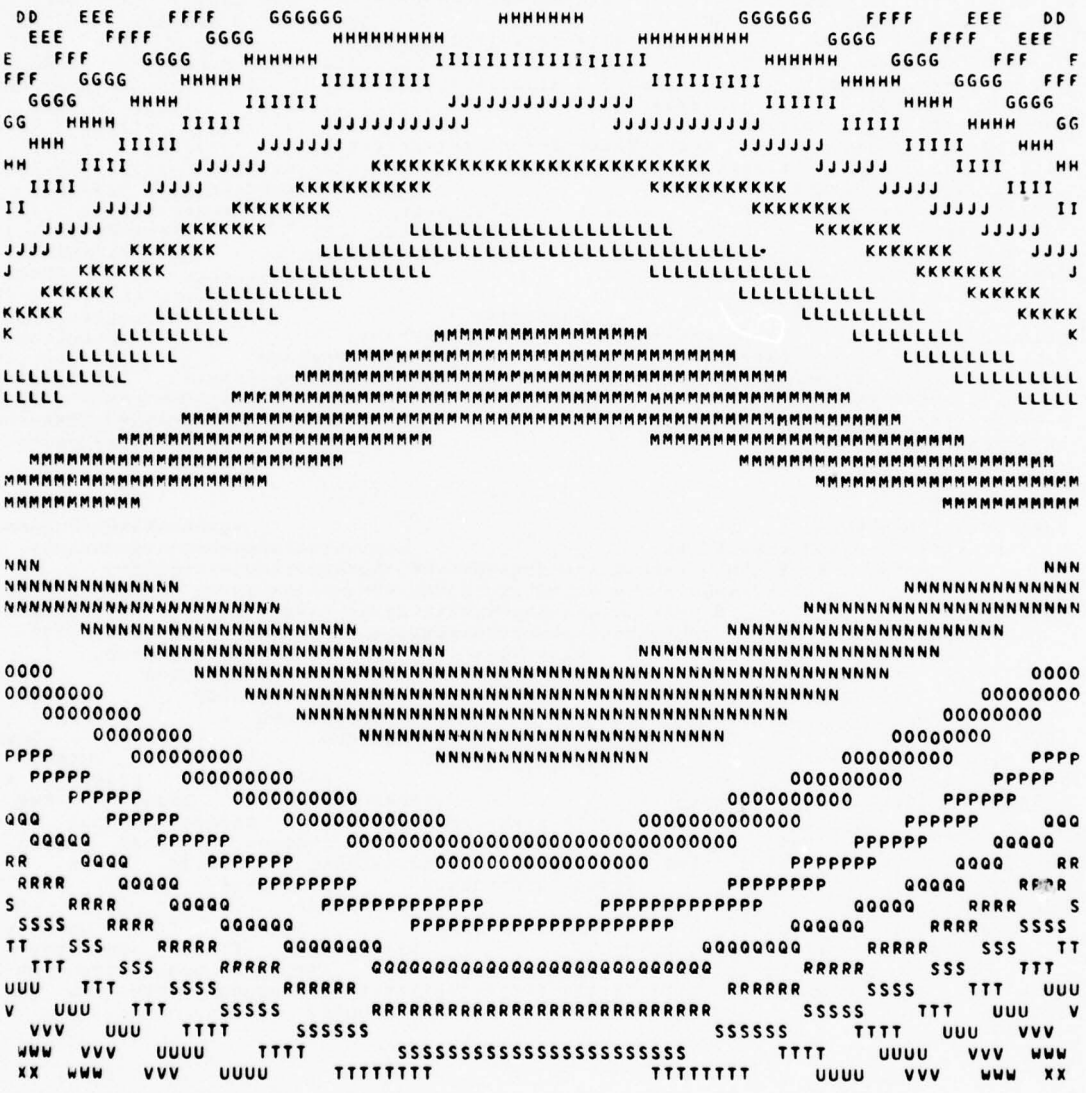

Figure 5. Z configuration, θ_1 = 45°, RBT = 0.074 (-0.370).

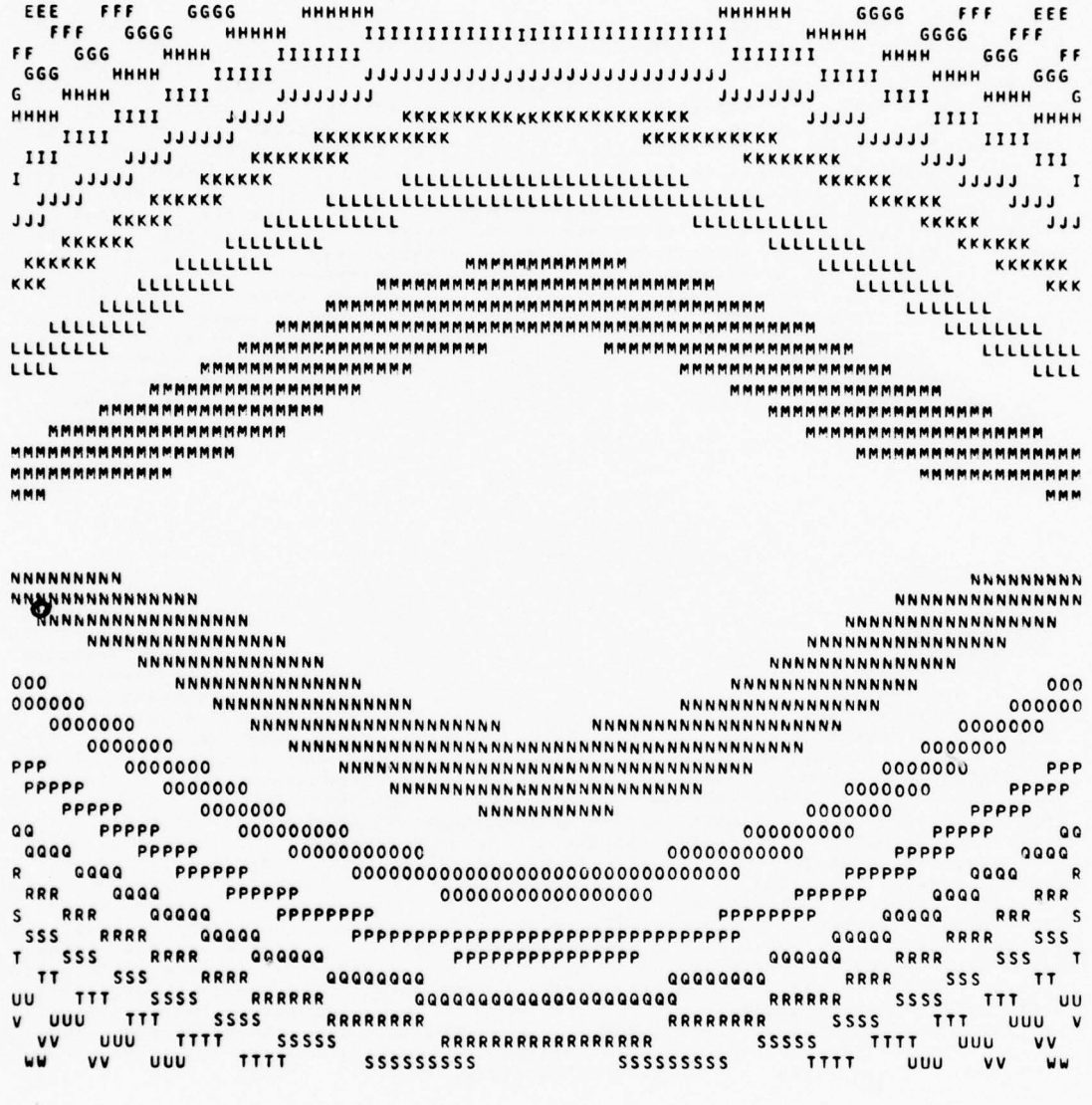

Figure 6. Z configuration, θ_1 = 45°, RBT = 0.000 (-0.370).

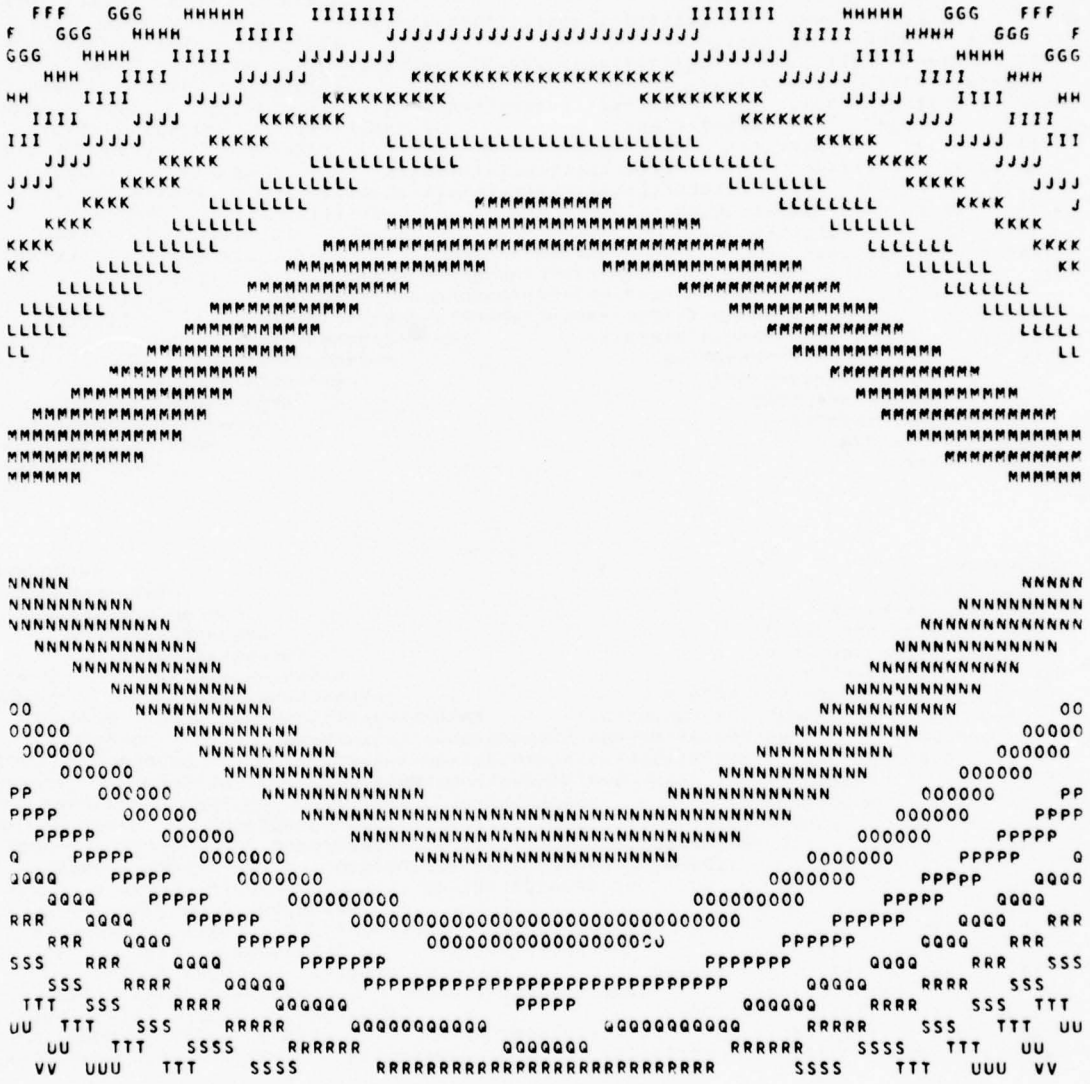

Figure 7. Z configuration, θ_1 = 45°, RBT = -0.074 (-0.370).

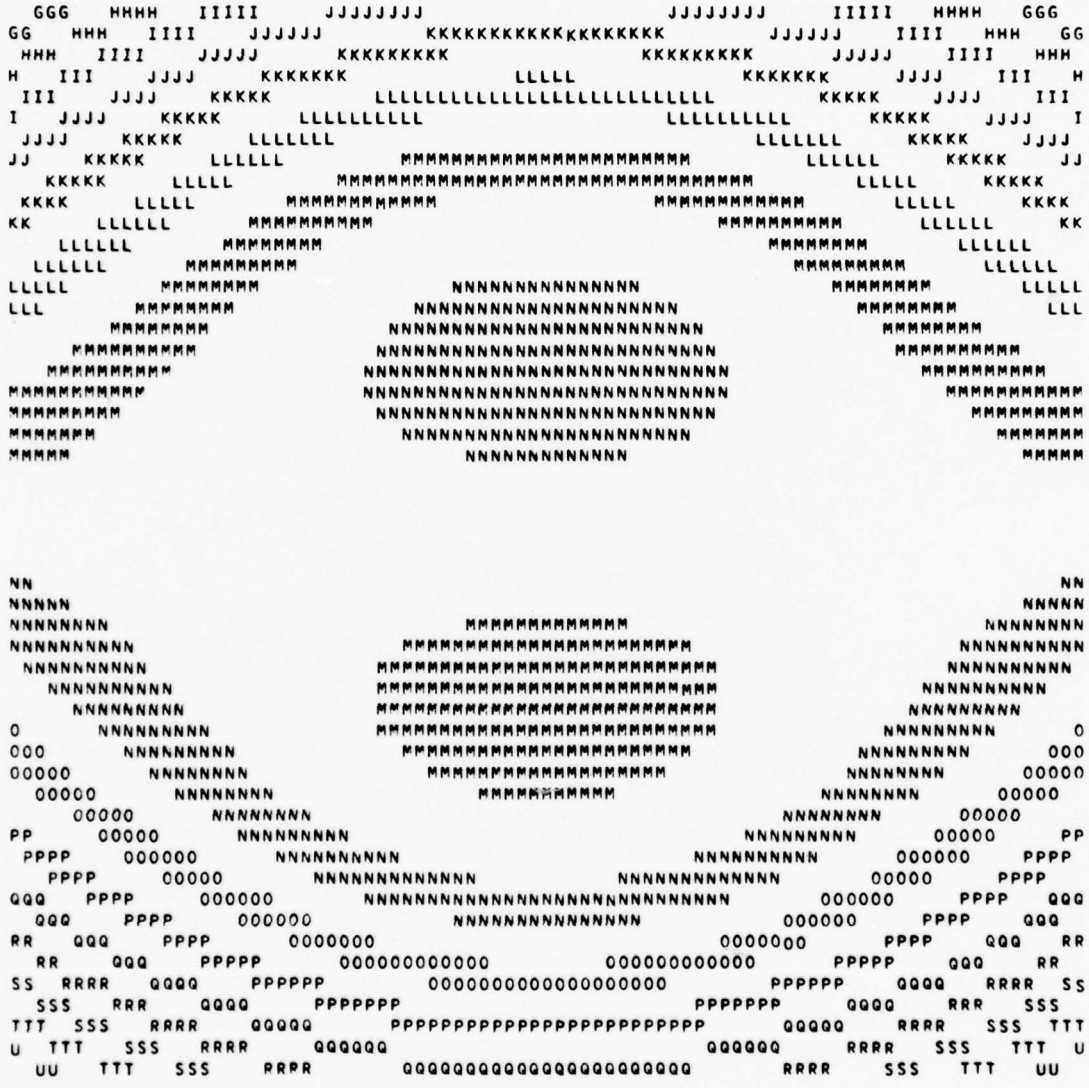

Figure 8. Z configuration, θ_1 = 45°, RBT = -0.148 (-0.370).

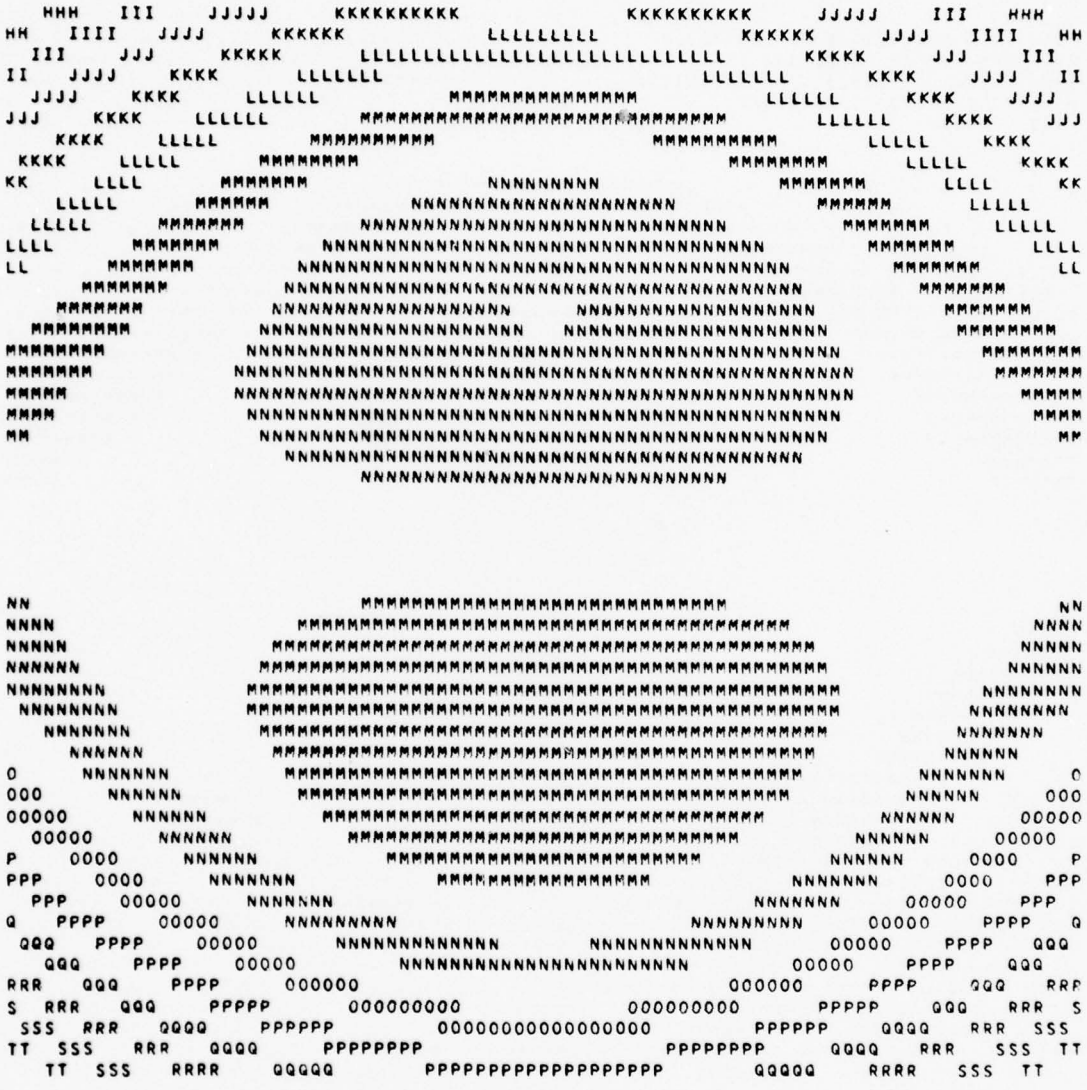

Figure 9. Z configuration, θ_1 = 45°, RBT = -0.222 (-0.370).

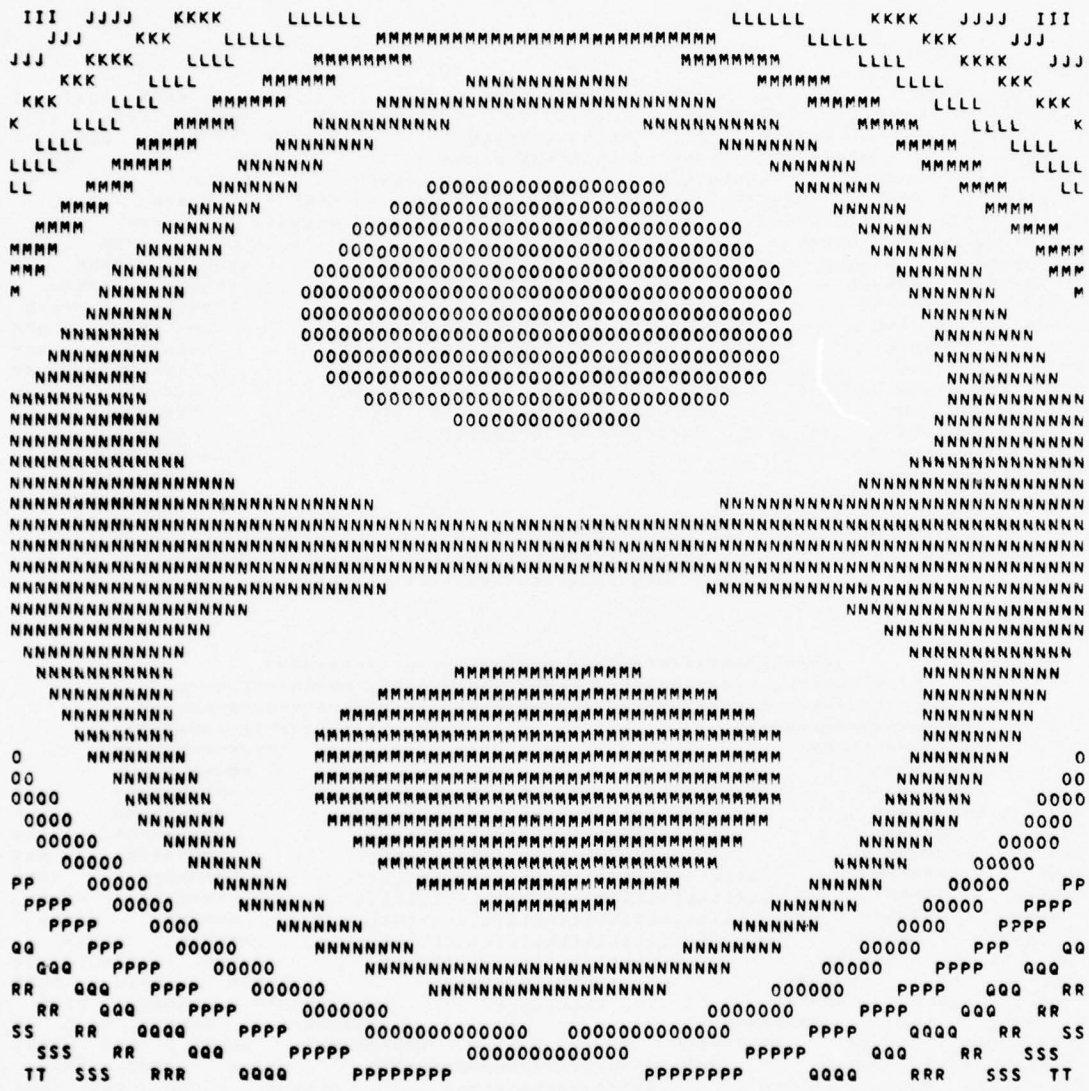

Figure 10. Z configuration, θ_1 = 45°, RBT = -0.296 (-0.370).

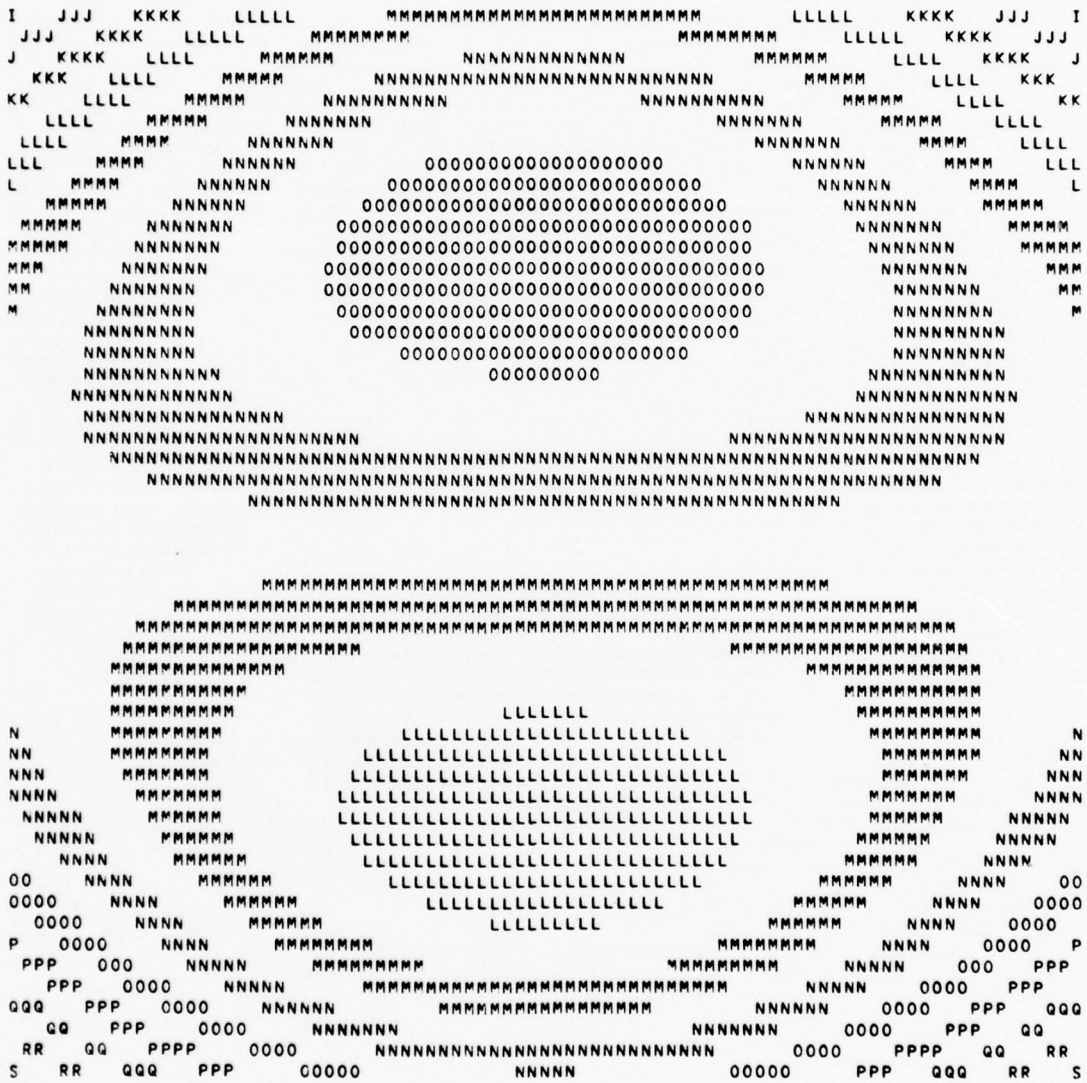

Figure 11. Z configuration, θ_1 = 45°, RBT = -0.370 (-0.370).

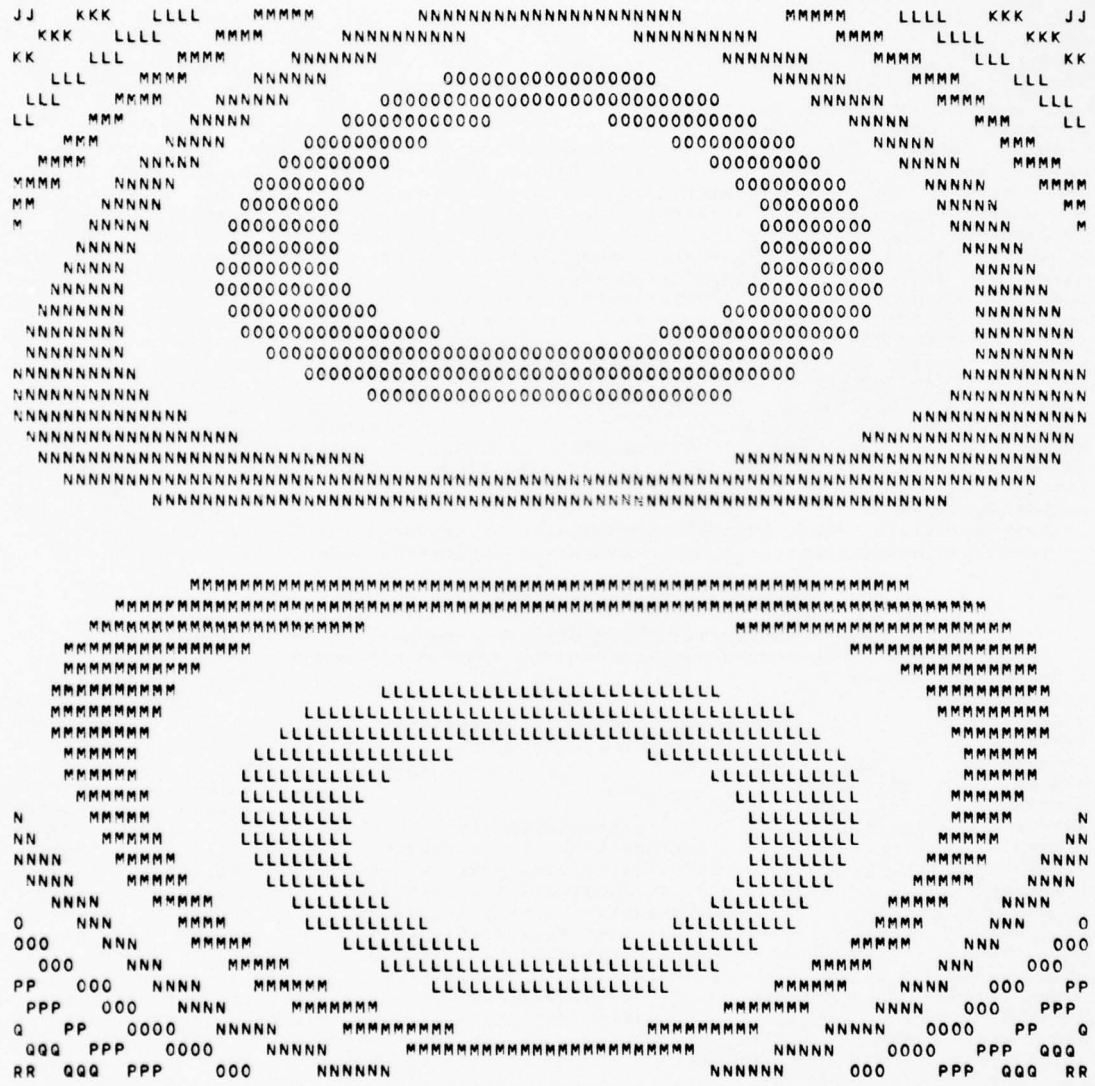

Figure 12. Z configuration, θ_1 = 45°, RBT = -0.444 (-0.370).

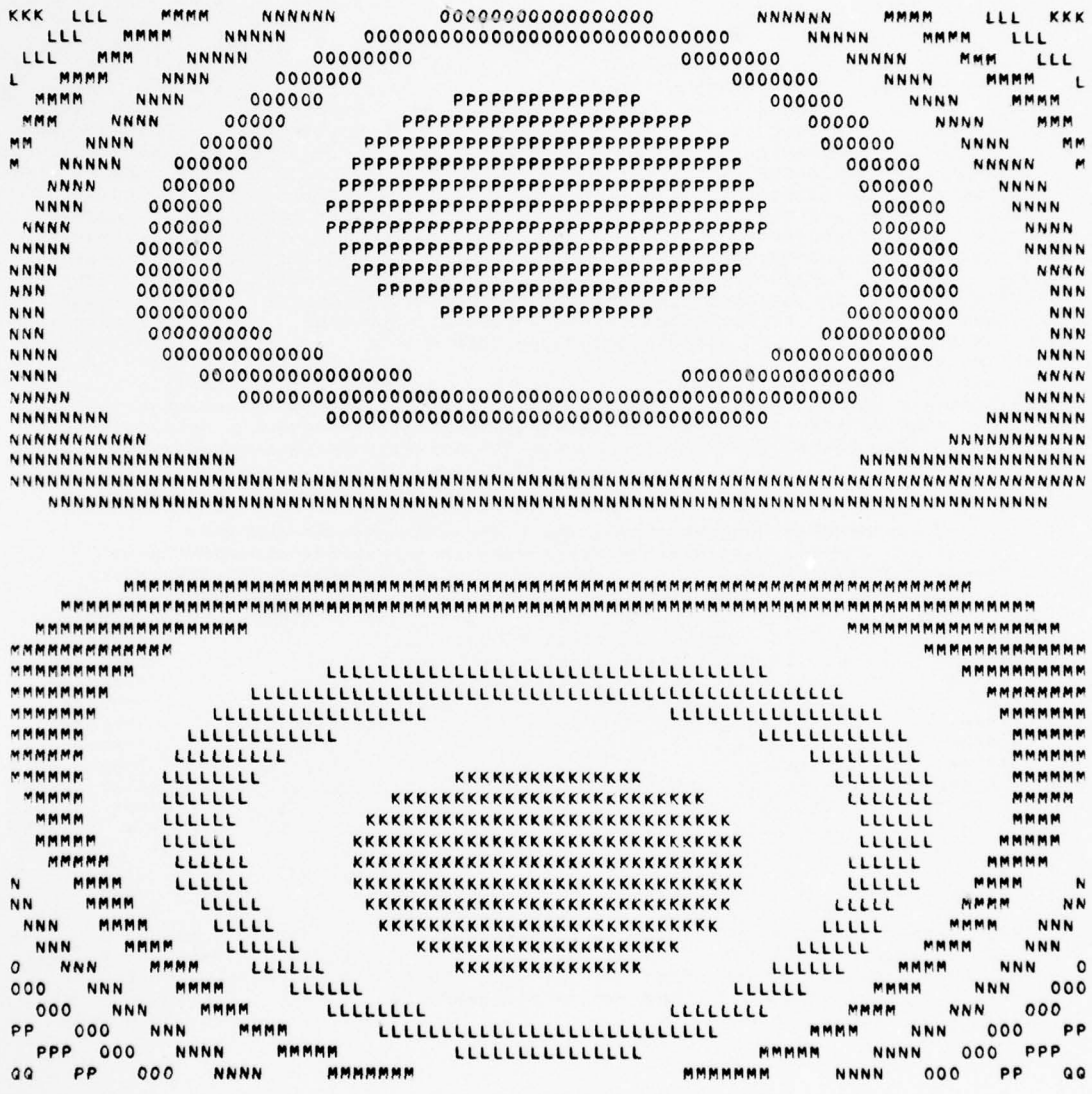

Figure 13. Z configuration, θ_1 = 45°, RBT = -0.518 (-0.370).

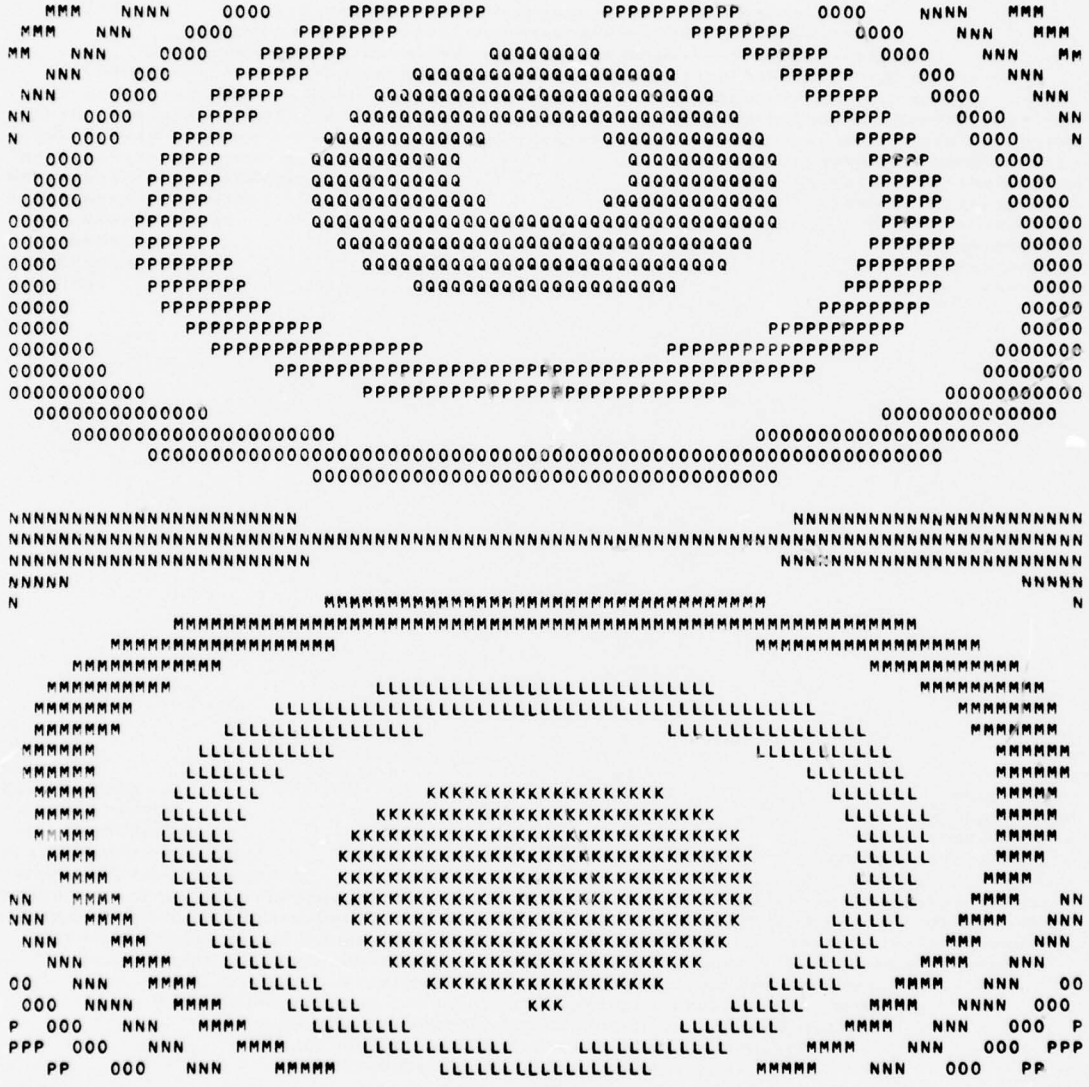

Figure 14. Z configuration, θ_1 = 45°, RBT = -0.592 (-0.370).

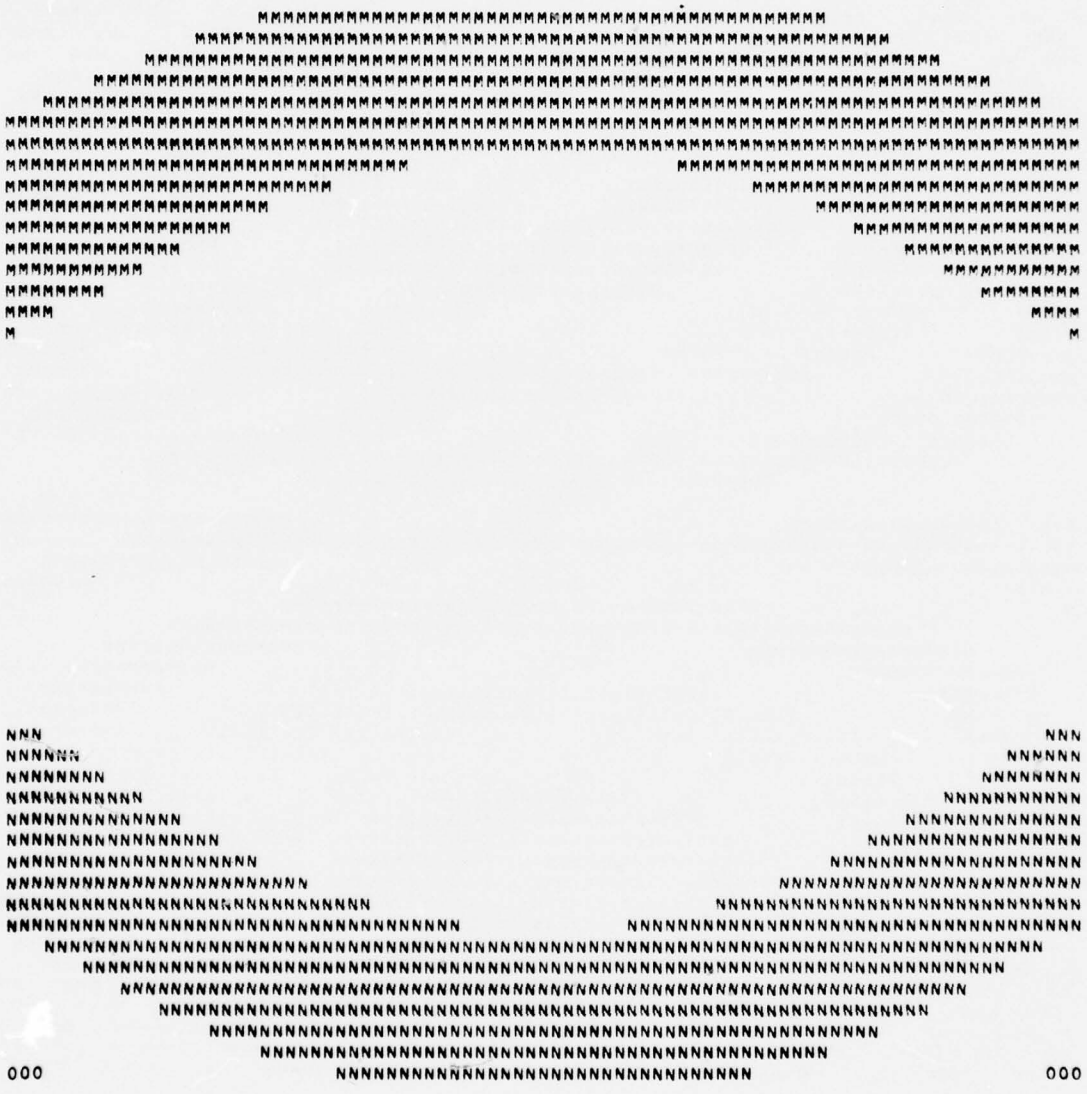

Figure 15. Z configuration, θ_1 = 10°, RBT = 0, nominal values of L and θ_2, i.e., $\Delta L = 0$, $\Delta\theta_2 = 0$.

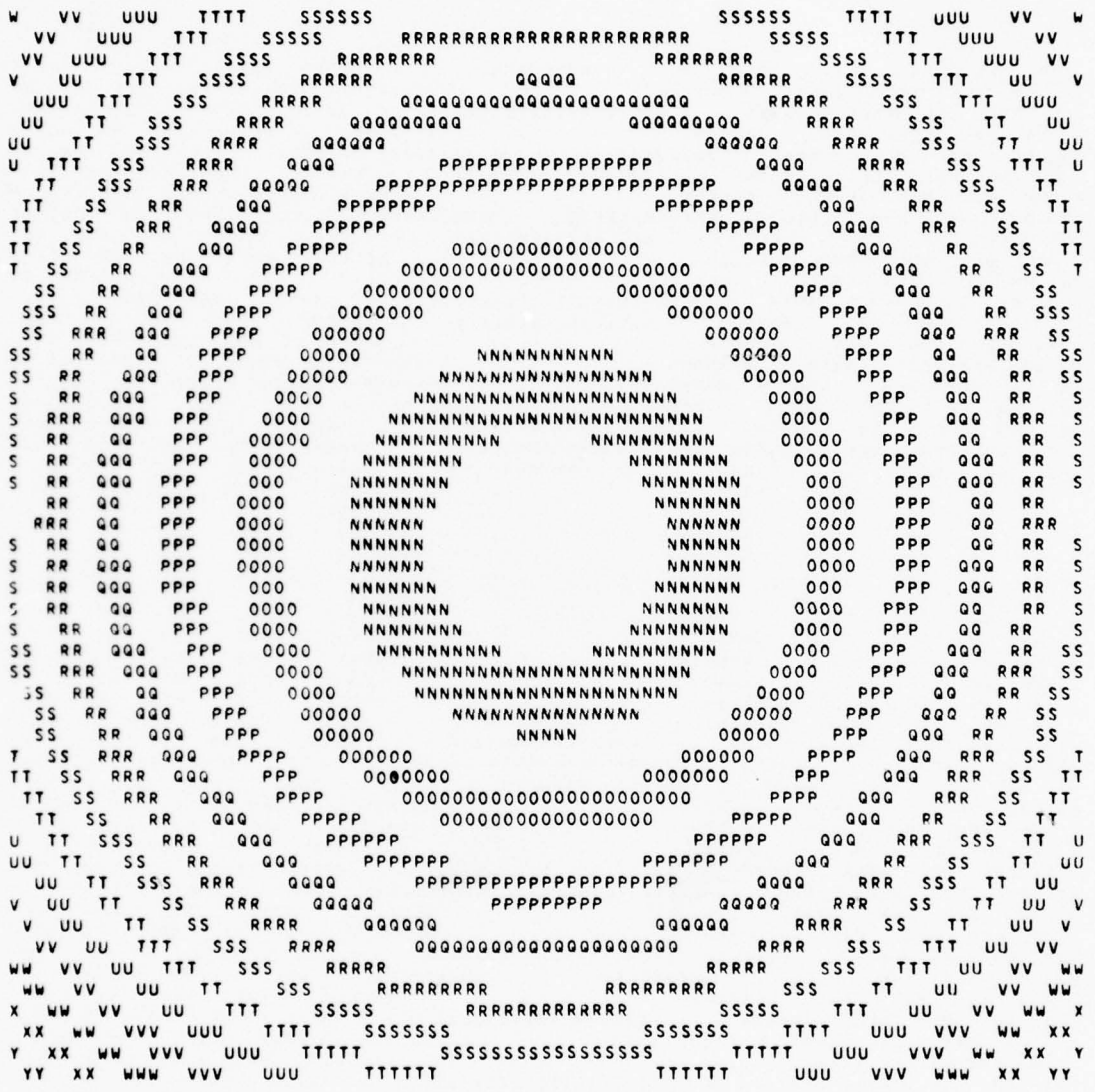

Figure 16. Z configurations, $\theta_1 = 10°$, RBT = 0, $\Delta L = 1.3097$ cm, $\Delta\theta_2 = 0$.

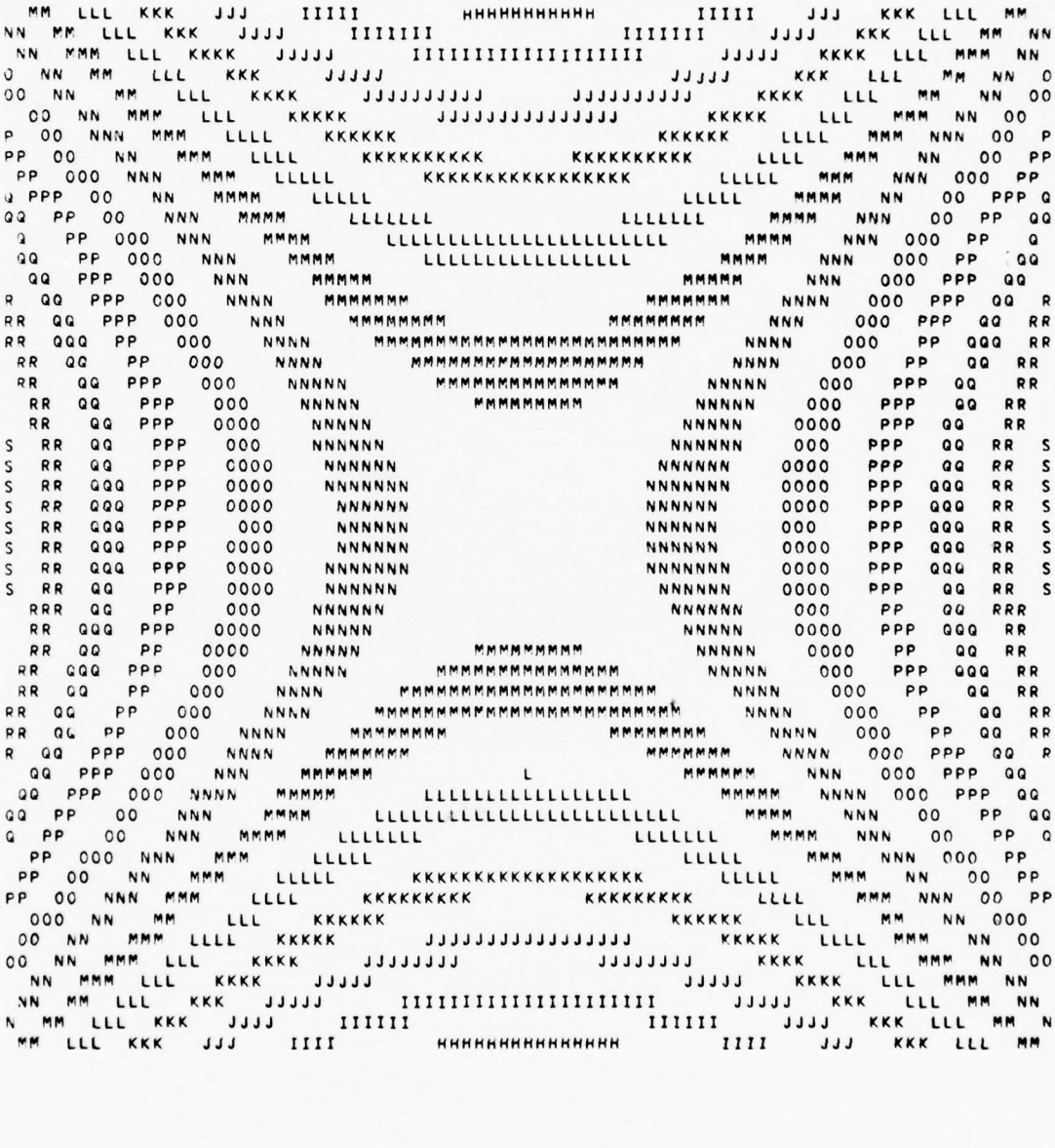

Figure 17. Z configuration, θ_1 = 10°, RBT = 0, ΔL = 0, $\Delta\theta_2$ = -0.04233 rad.

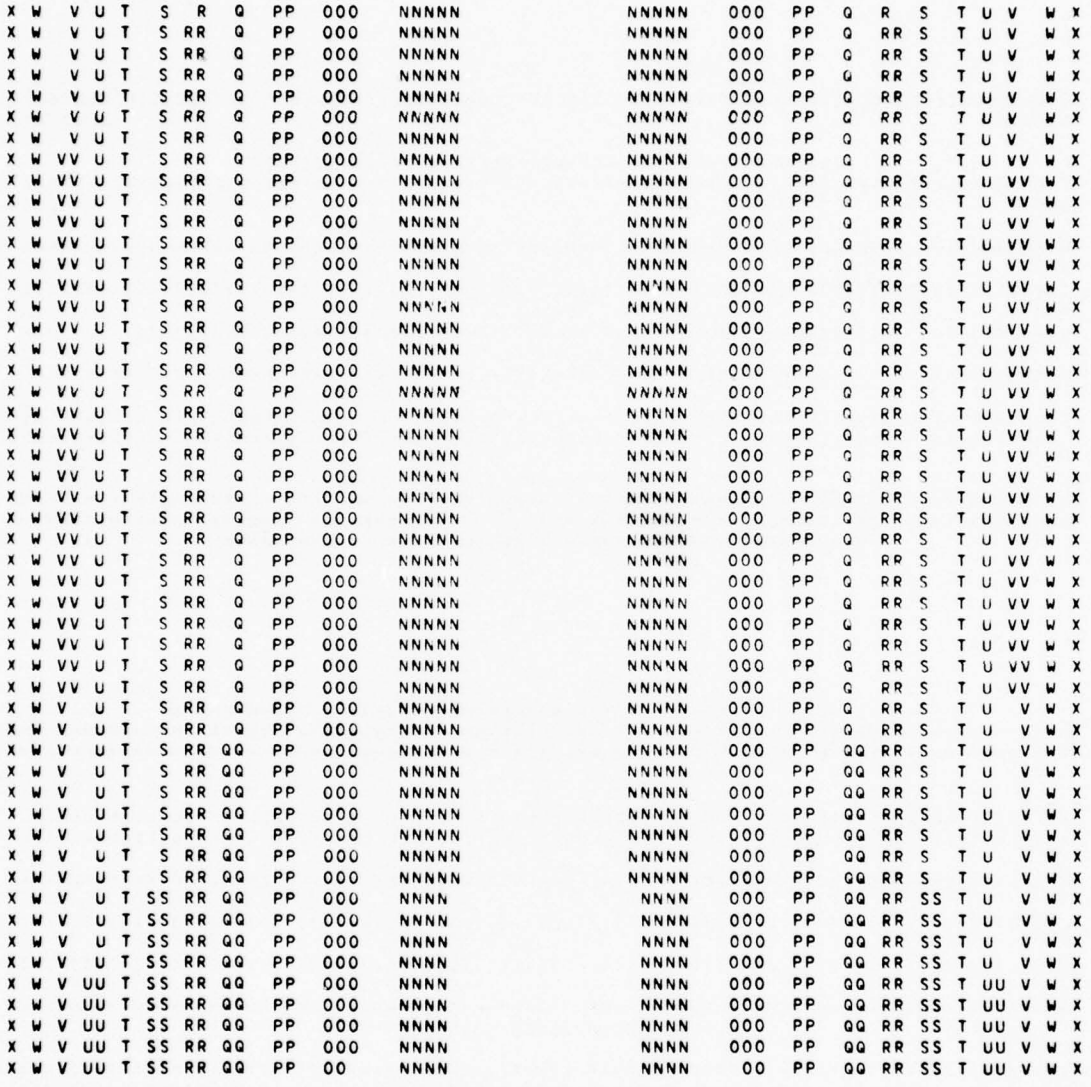

Figure 18. Z configuration, $\theta_1 = 10°$, RBT = 0, $\Delta L = 1.3097$ cm, $\Delta\theta_2 = -0.04233$ rad. The curvature along the y-coordinate has been reduced to approximately zero.

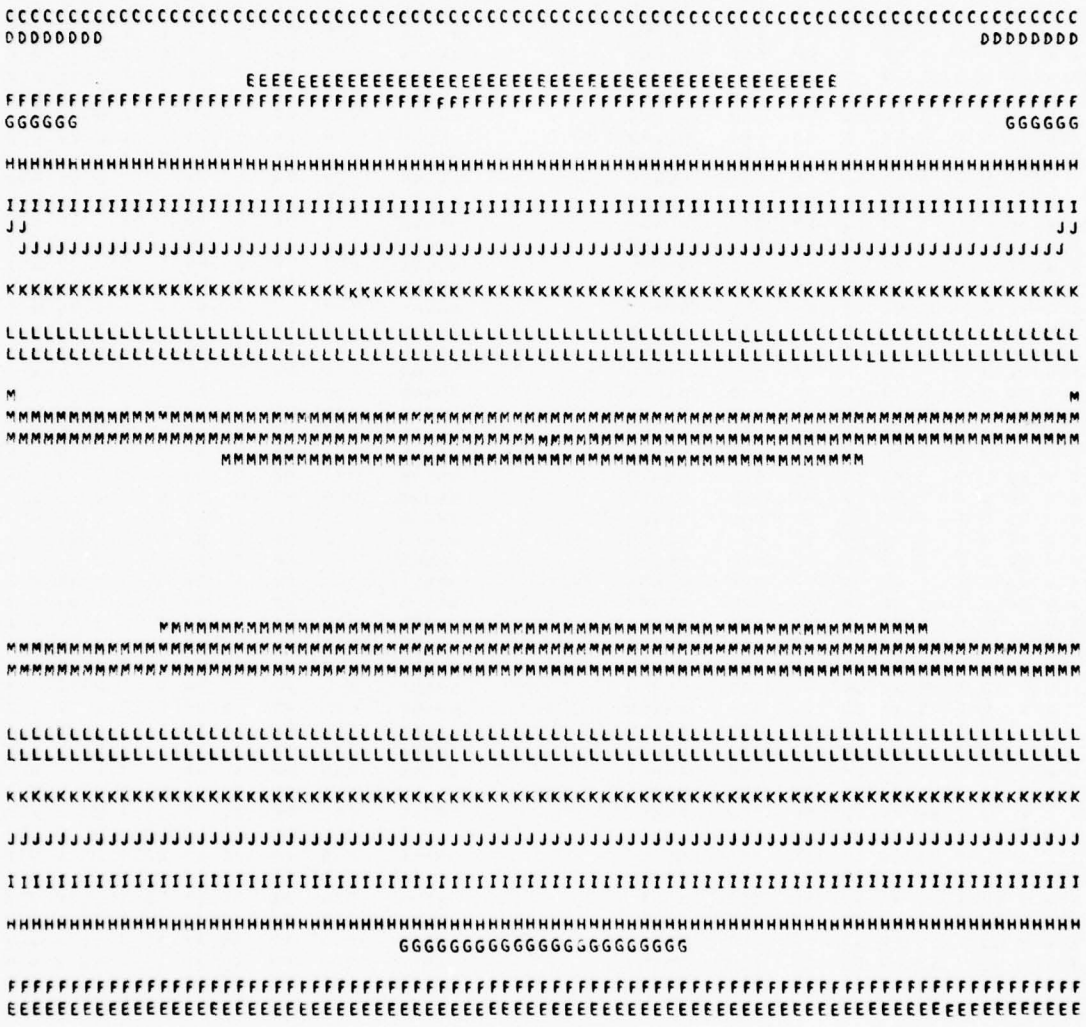

Figure 19. Z configuration, θ_1 = 10°, RBT = 0, ΔL = -1.333 cm, $\Delta\theta_2$ = -0.04233 rad. The curvature along the x-coordinate has been reduced to approximately zero.

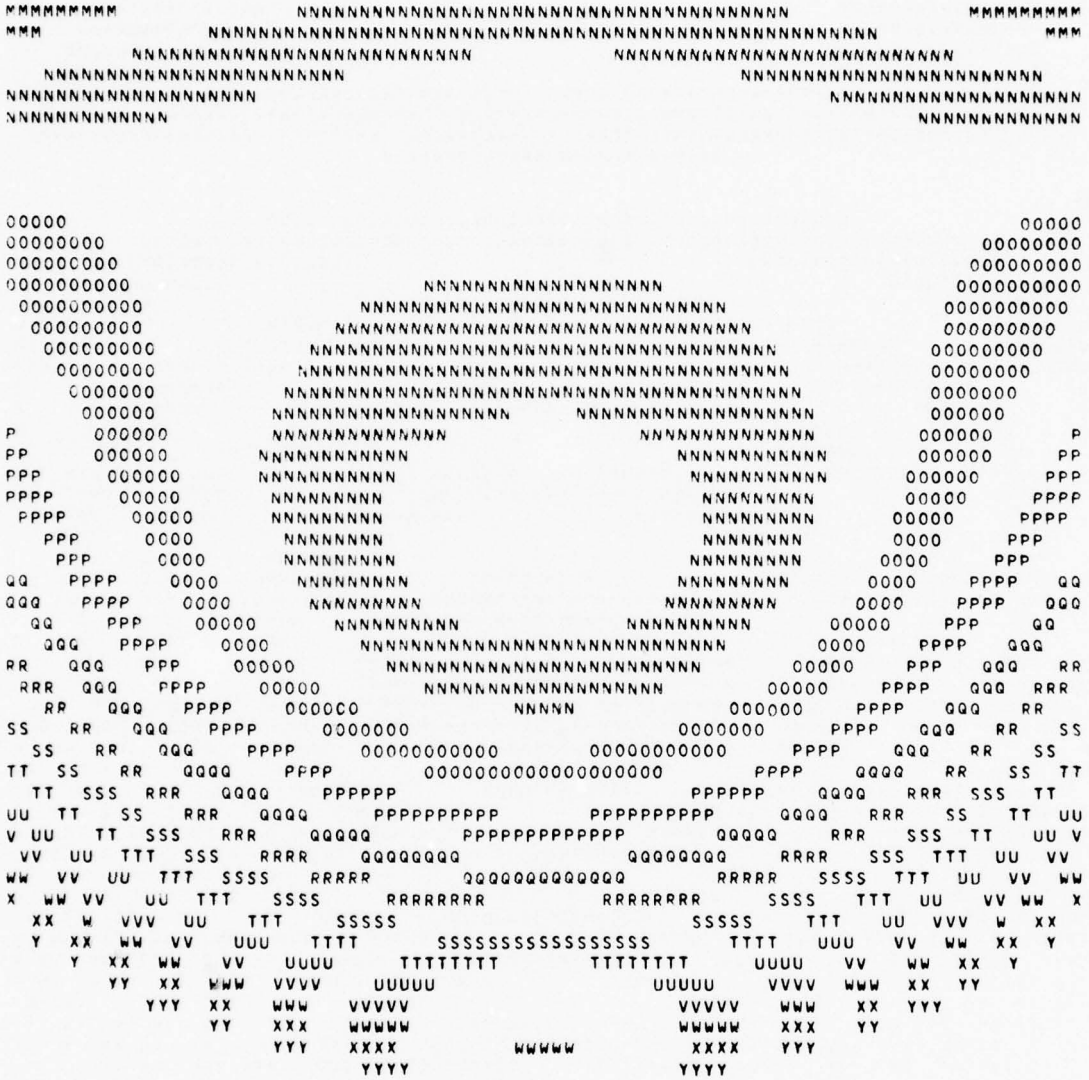

Figure 20. Z configuration, θ_1 = 45°, RBT = 0 (-0.379), ΔL = 1.0 cm, $\Delta\theta_2$ = 0.

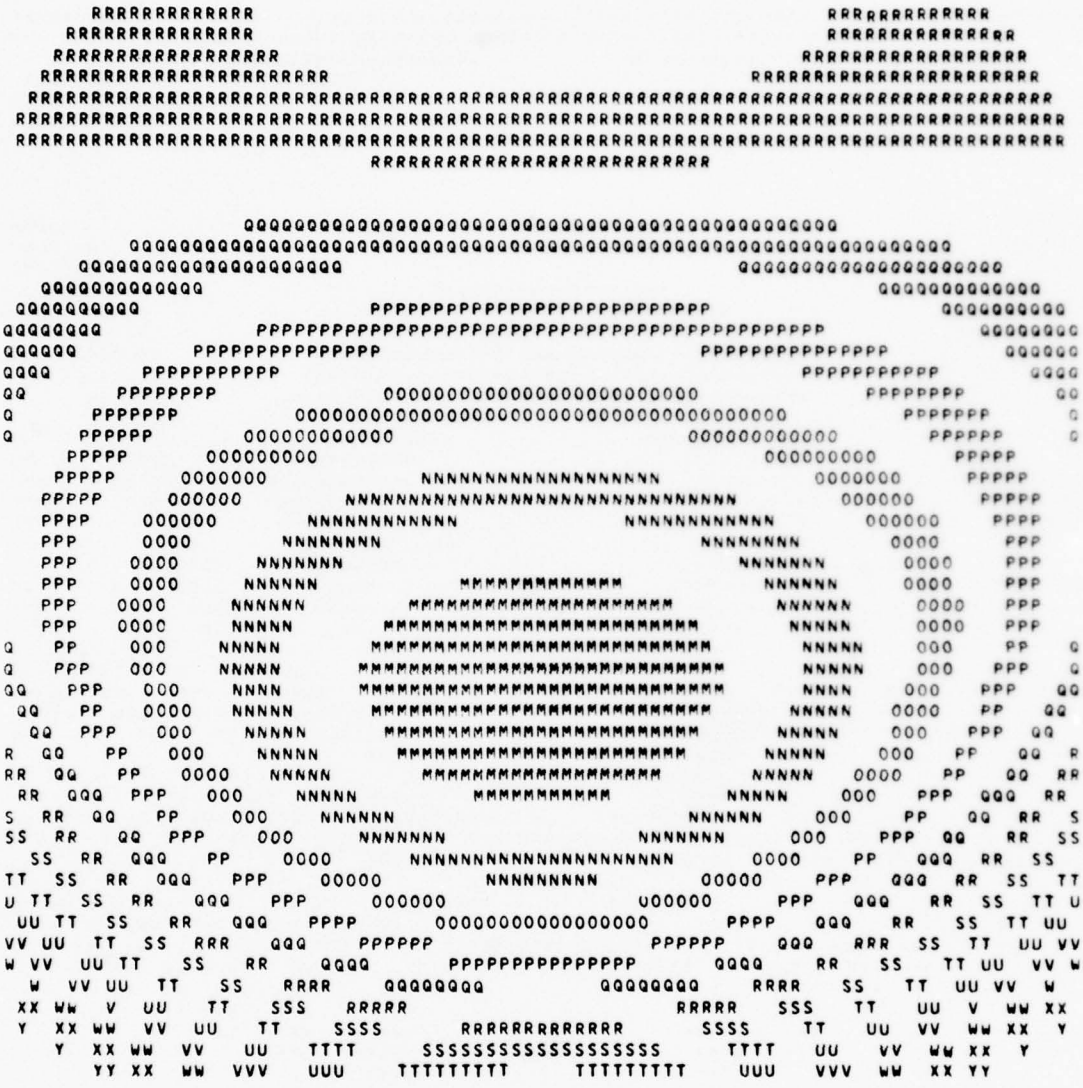

Figure 21. Z configuration, θ_1 = 45°, RBT = -0.379 (-0.379), ΔL = 1.0 cm, $\Delta\theta_2$ = 0.

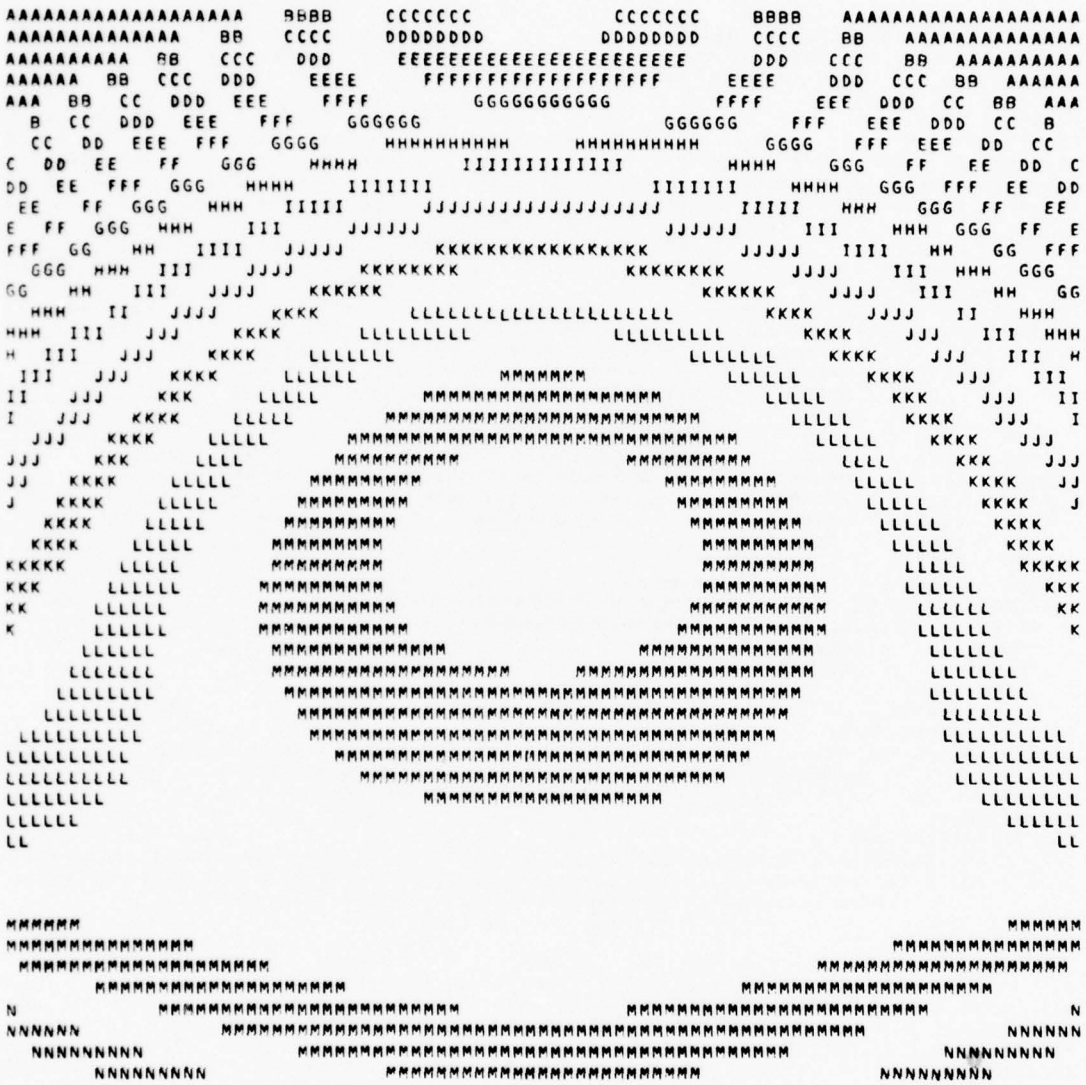

Figure 22. Z configuration, θ_1 = 45°, RBT = 0 (-0.361), L = -1.0 cm, θ_2 = 0.

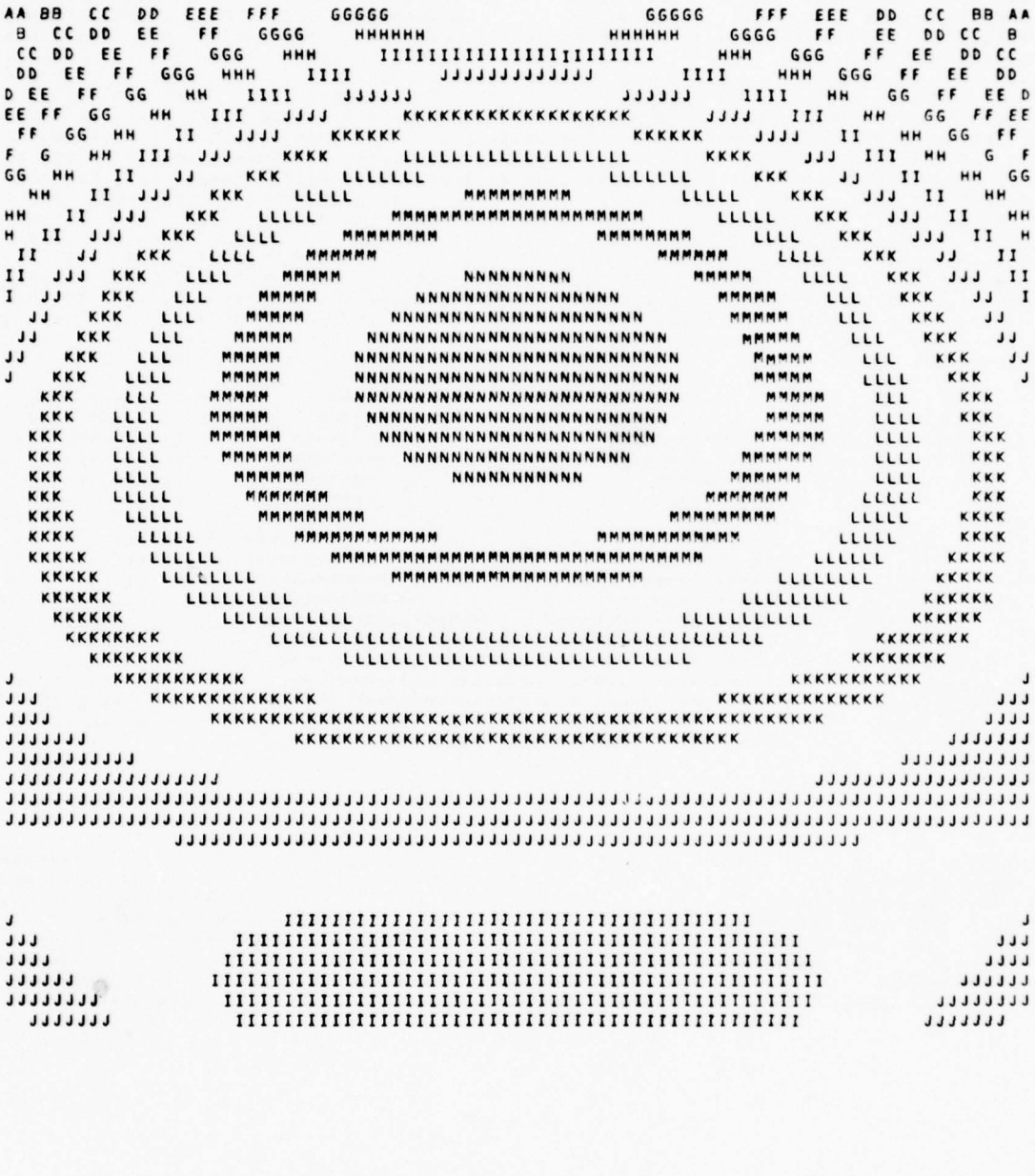

Figure 23. Z configuration, θ_1 = 45°, RBT = -0.361 (-0.361), ΔL = -1.0 cm, $\Delta\theta_2$ = 0.

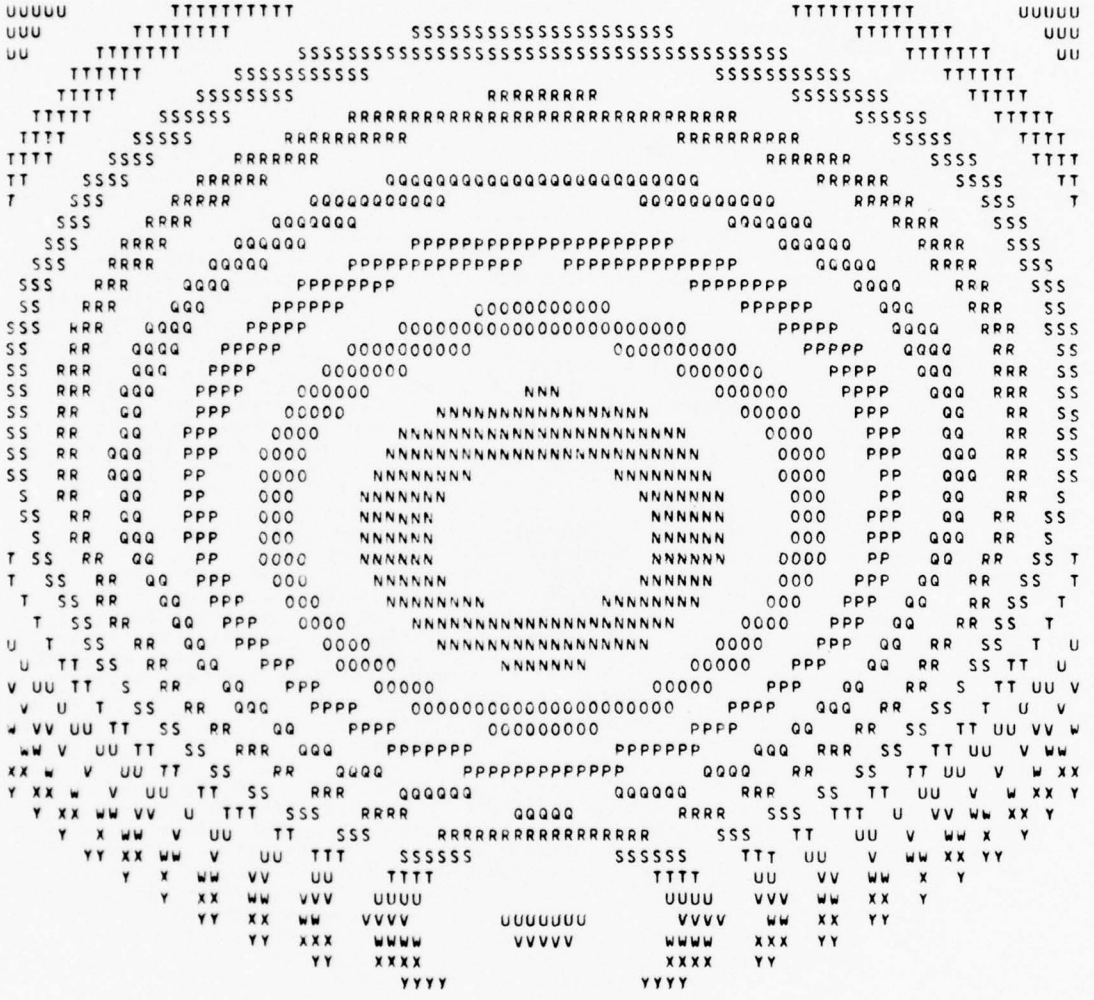

Figure 24. Z configuration, θ_1 = 45°, RBT = 0 (-0.389), ΔL = 2.0 cm, $\Delta\theta_2$ = 0.

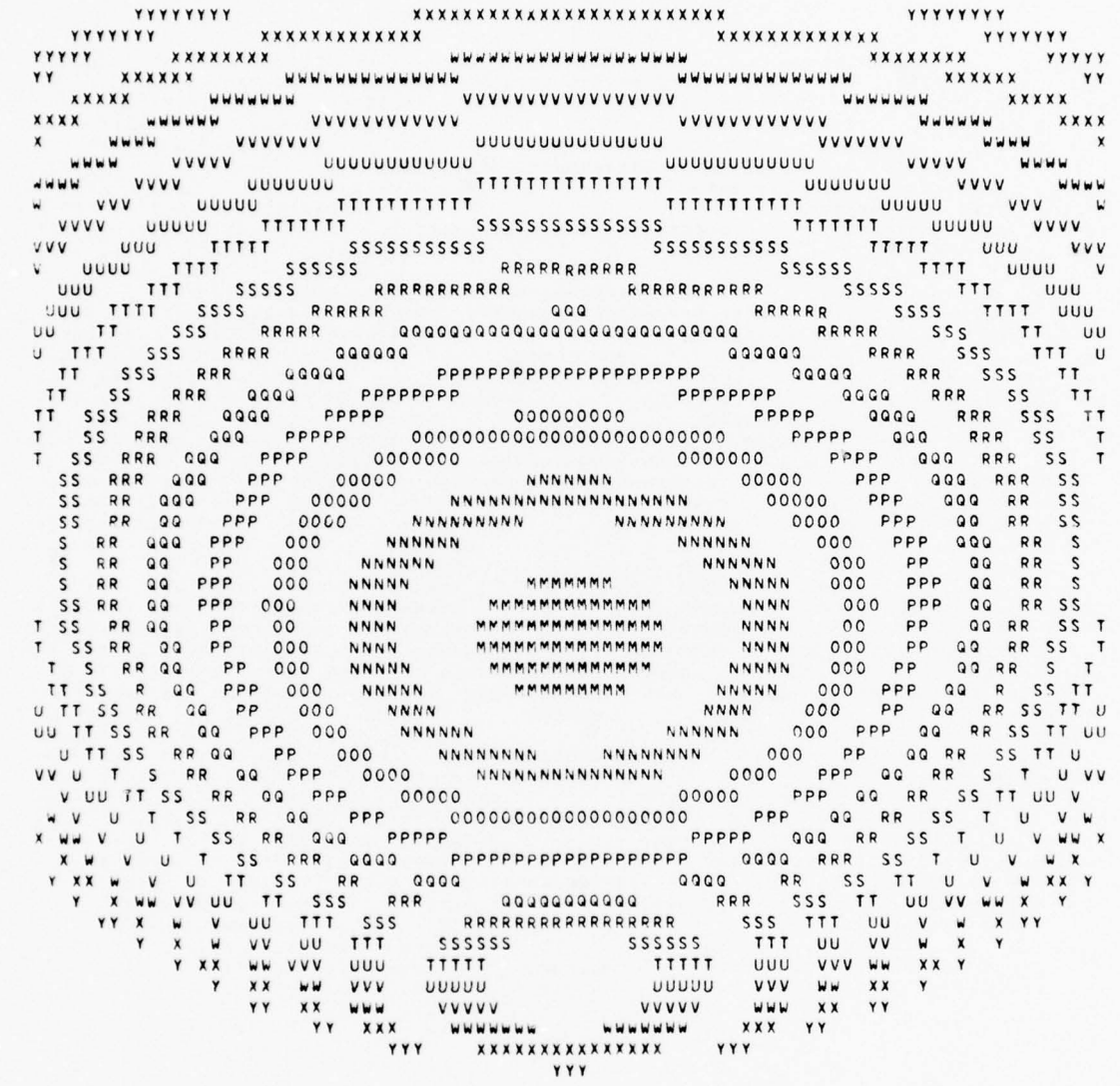

Figure 25. Z configuration, θ_1 = 45°, RBT = -0.389 (-0.389), ΔL = 2.0 cm, $\Delta\theta_2$ = 0.

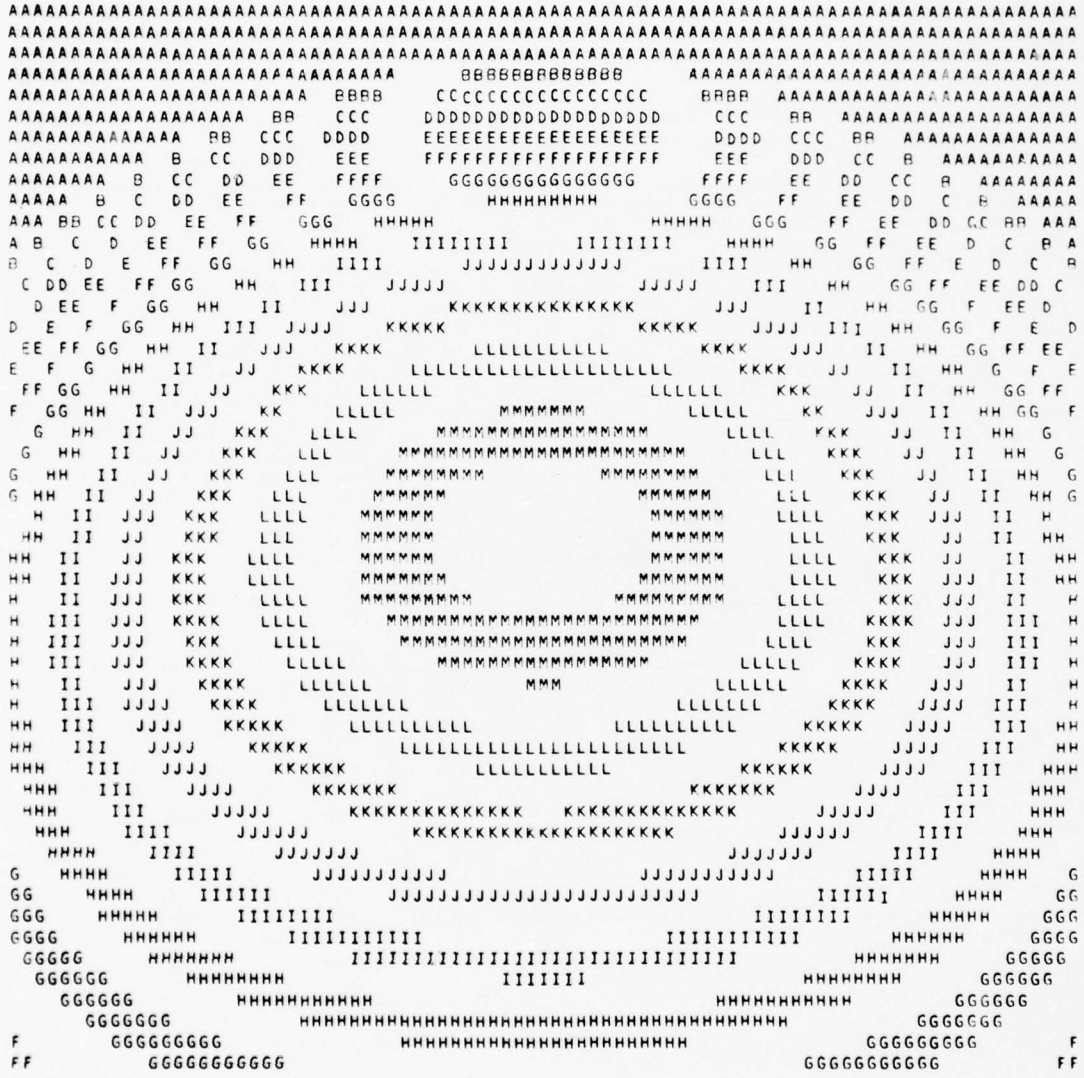

Figure 26. Z configuration, θ_1 = 45°, RBT = -0 (-0.351)
ΔL = -2.0 cm, $\Delta\theta_2$ = 0.

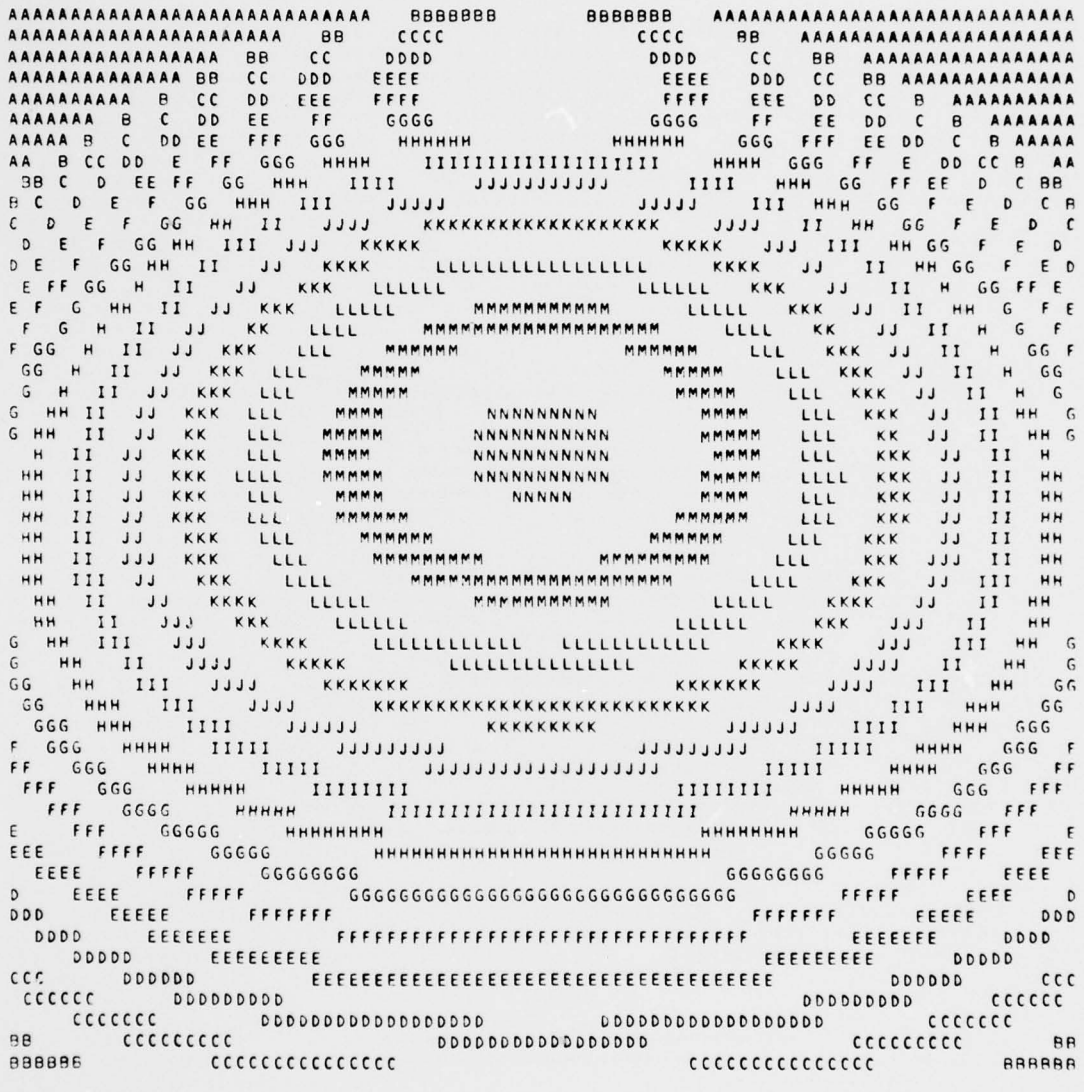

Figure 27. Z configuration, θ_1 = 45°, RBT = -0.351 (-0.351), ΔL = -2.0 cm, $\Delta\theta_2$ = 0.

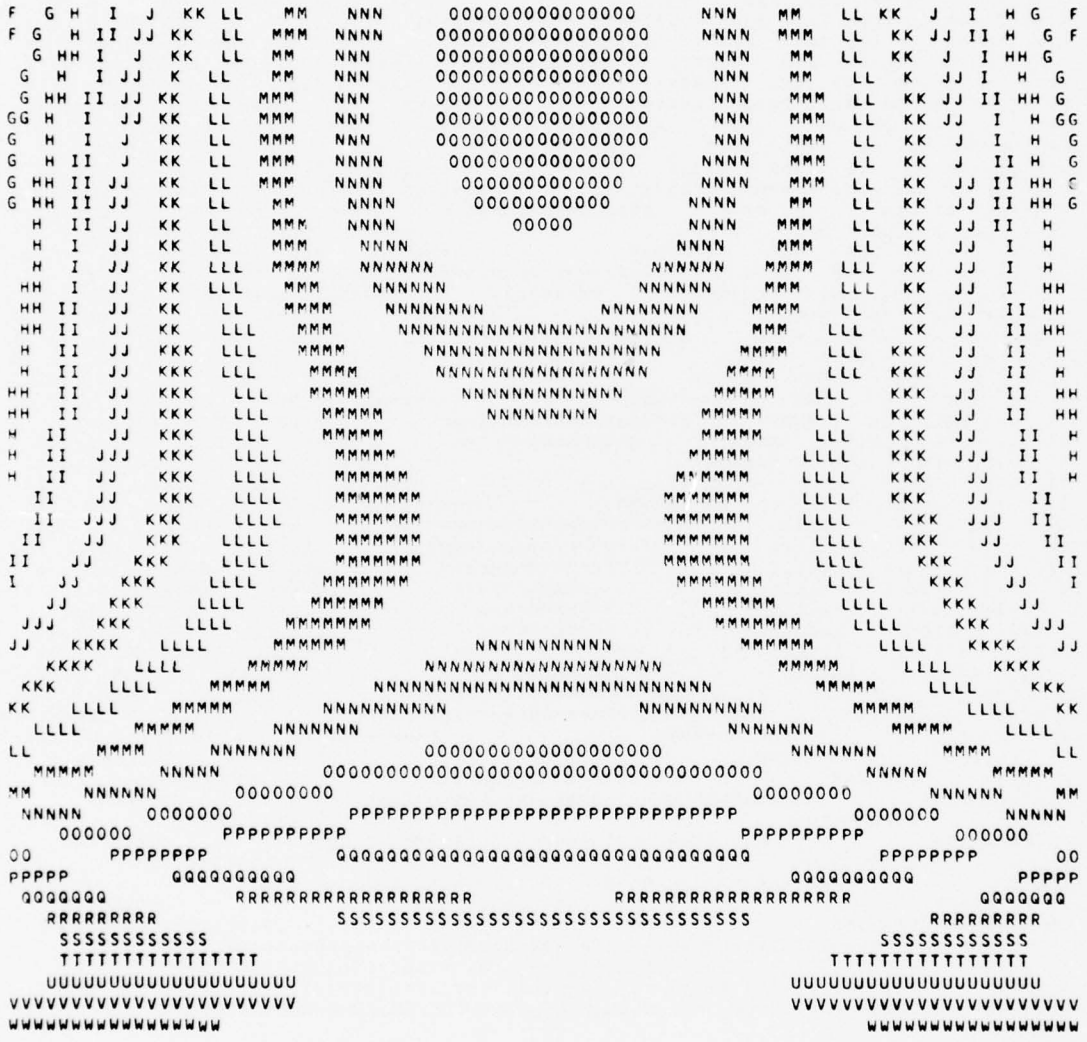

Figure 28. Z configuration, θ_1 = 45°, RBT = 0 (-0.392), ΔL = 0, $\Delta\theta_2$ = 0.007 rad.

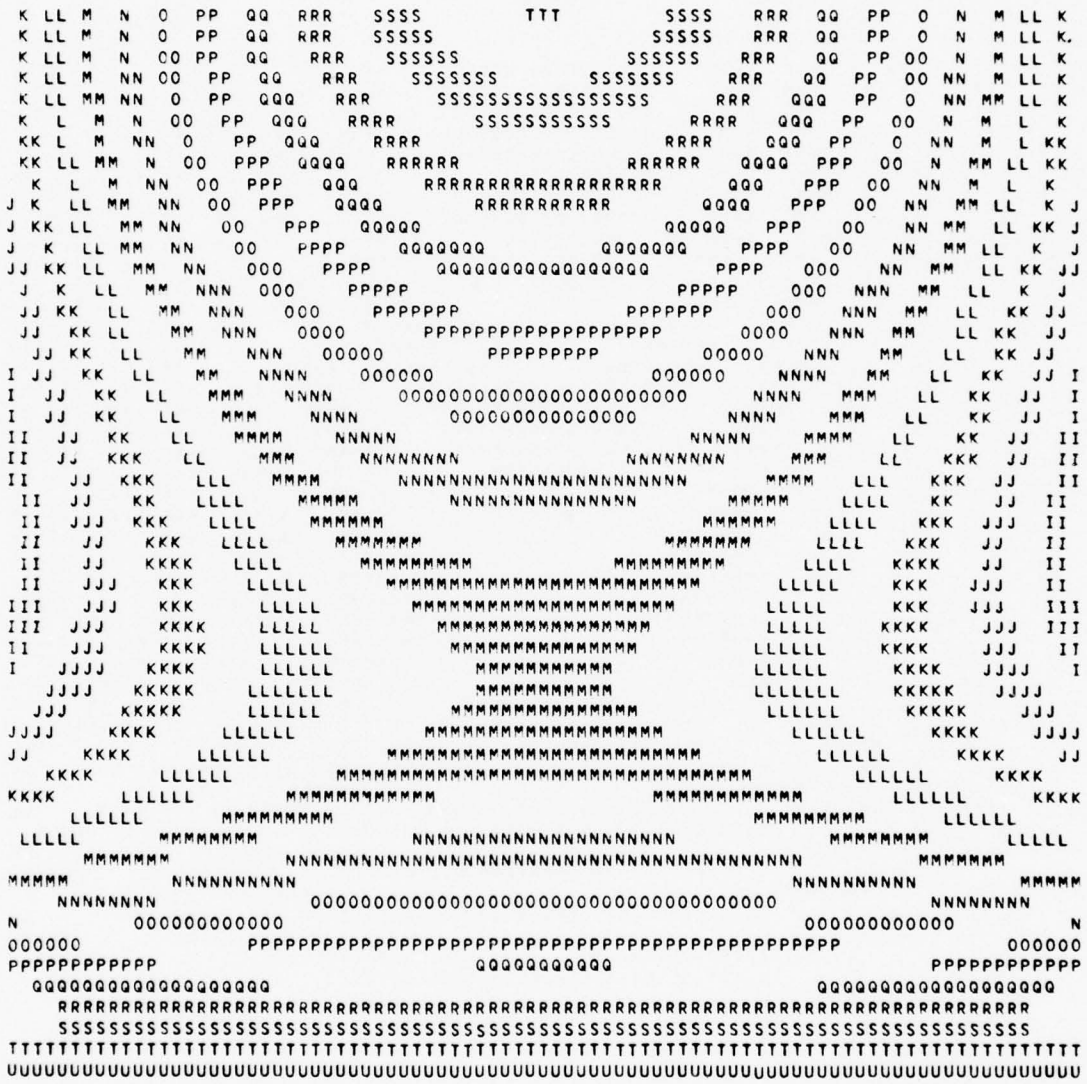

Figure 29. Z configuration, θ_1 = 45°, RBT = -0.392 (-0.392), ΔL = 0, $\Delta\theta_2$ = 0.007 rad.

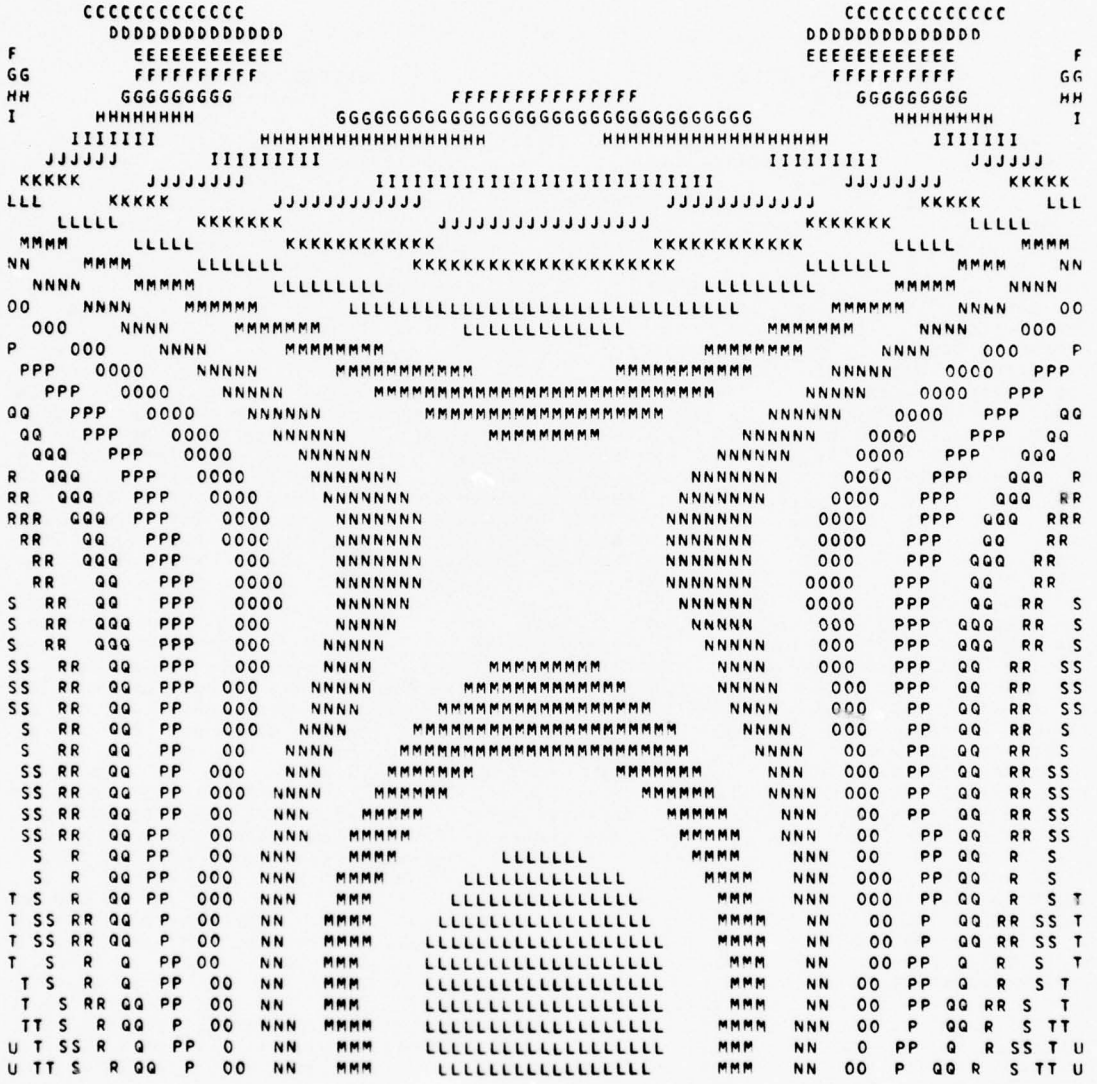

Figure 30. Z configuration, θ_1 = 45°, RBT = 0 (-0.348), ΔL = 0, $\Delta\theta_2$ = -0.007 rad.

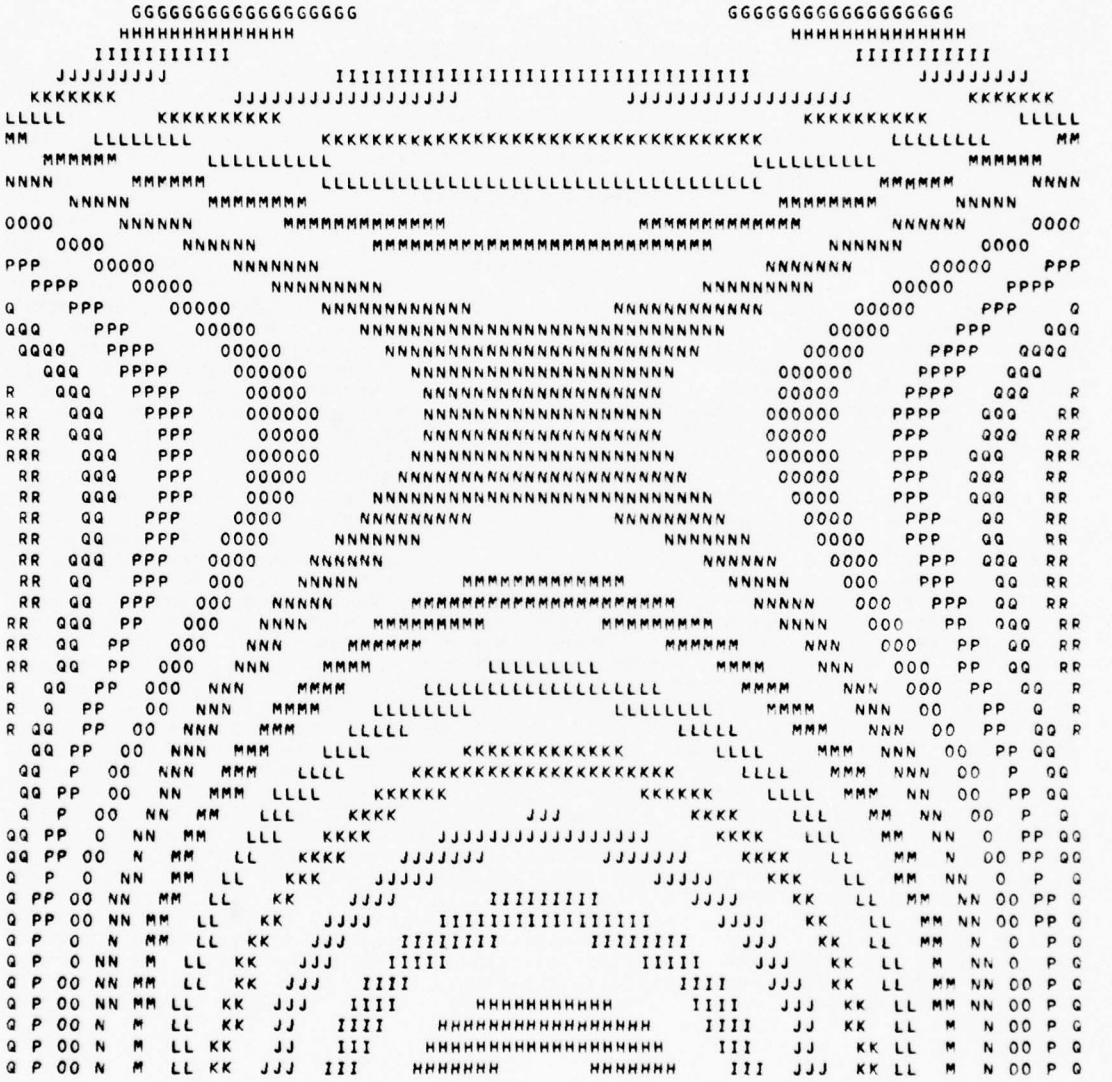

Figure 31. Z configuration, θ_1 = 45°, RBT = -0.348 (-0.348), ΔL = 0, $\Delta\theta_2$ = -0.007 rad.

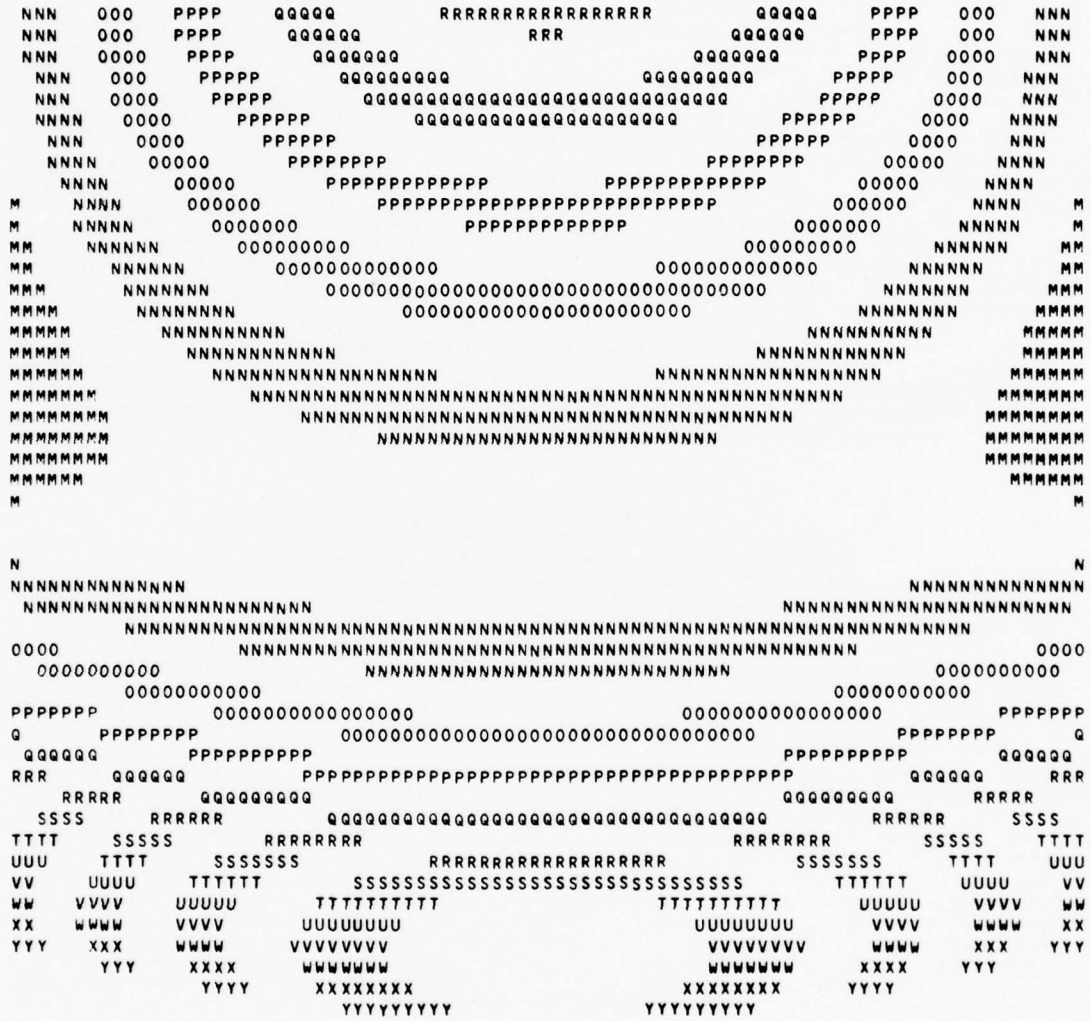

Figure 32. Z configuration θ_1 = 45°, RBT = 0 (-0.393), ΔL = 1.0 cm, $\Delta\theta_2$ = 0.00428 rad. The curvature along the x-coordinate has been reduced to approximately zero.

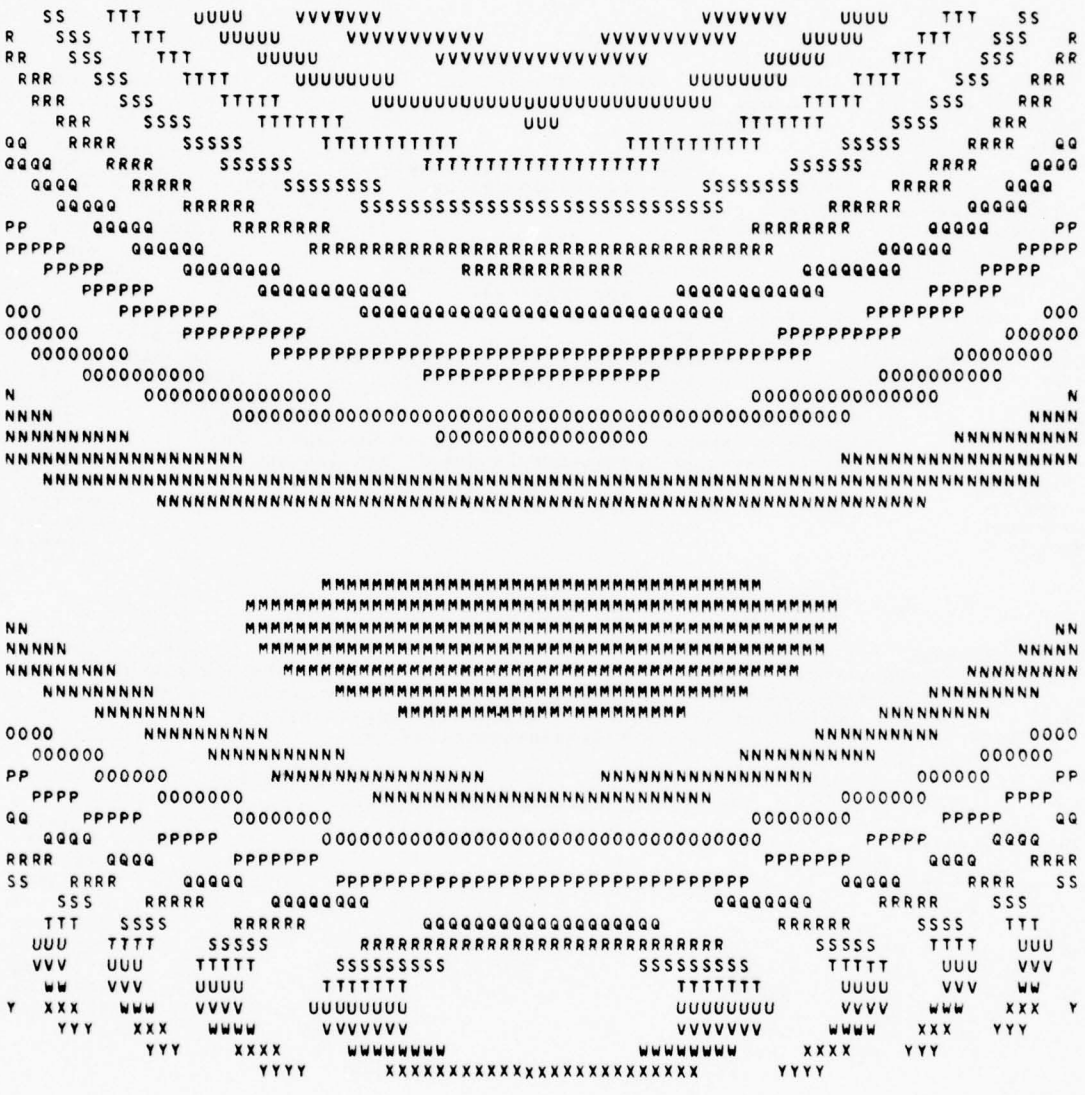

Figure 33. Z configuration, θ_1 = 45°, RBT = -0.393 (-0.393), ΔL = 1.0 cm, $\Delta\theta_2$ = 0.00428 rad. The curvature along the x-coordinate has been reduced to approximately zero.

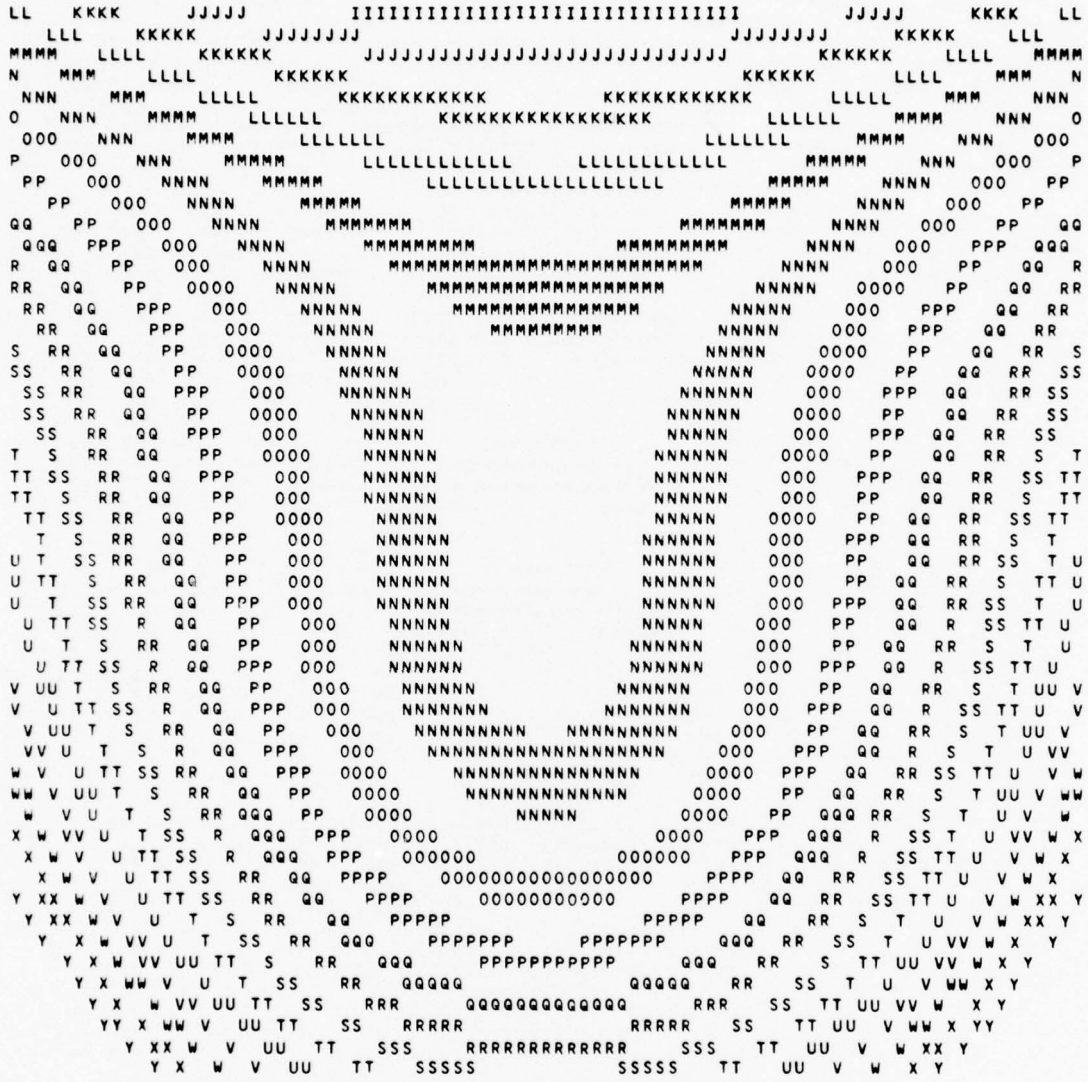

Figure 34. Z configuration, θ_1 = 45°, RBT = 0 (-0.361), ΔL = 1.0 cm, $\Delta\theta_2$ = -0.00580 rad. The curvature along the y-coordinate has been reduced to approximately zero.

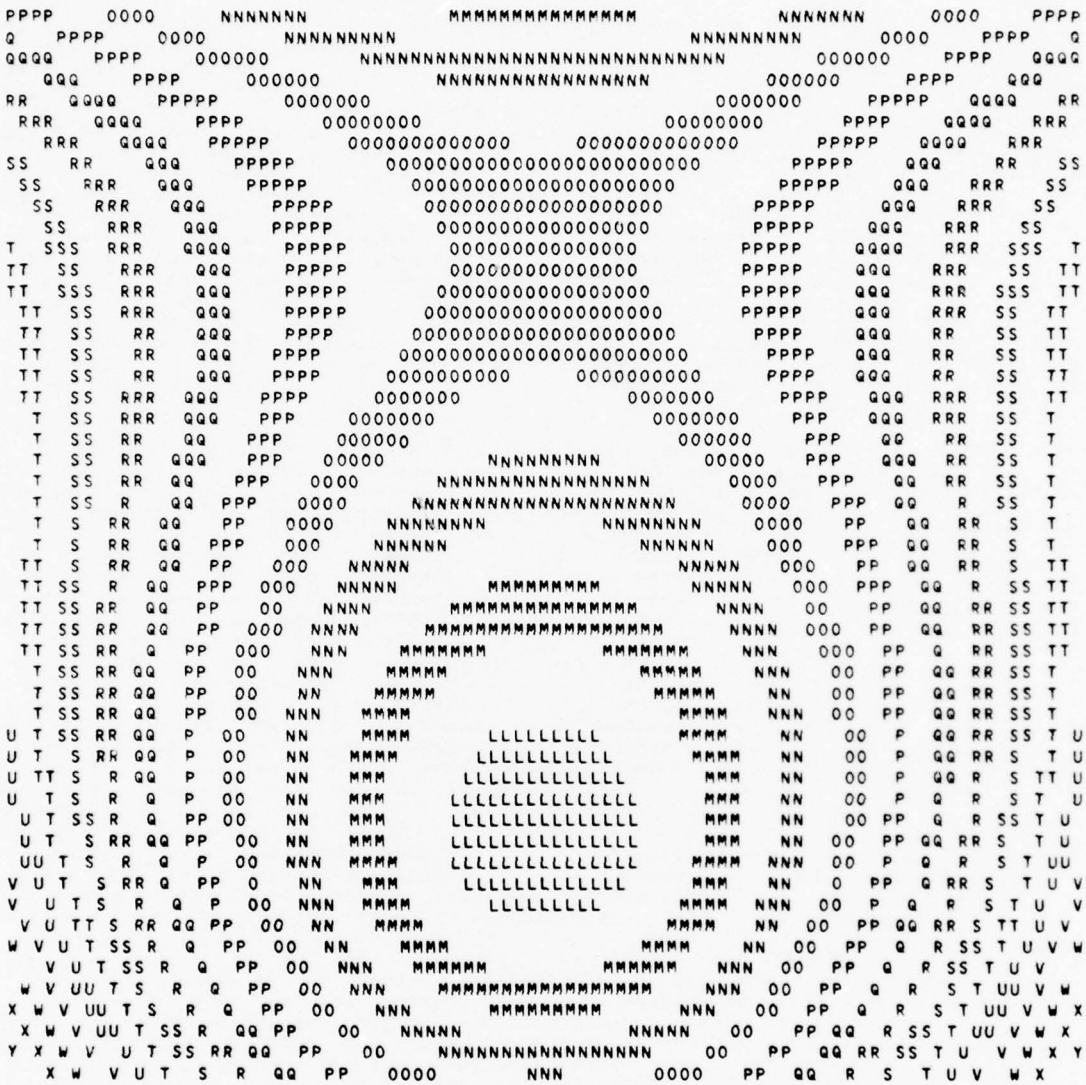

Figure 35. Z configuration, θ_1 = 45°, RBT = -0.361 (-0.361), ΔL = 1.0 cm, $\Delta\theta_2$ = -0.00580 rad. The curvature along the y-coordinate has been reduced to approximately zero.

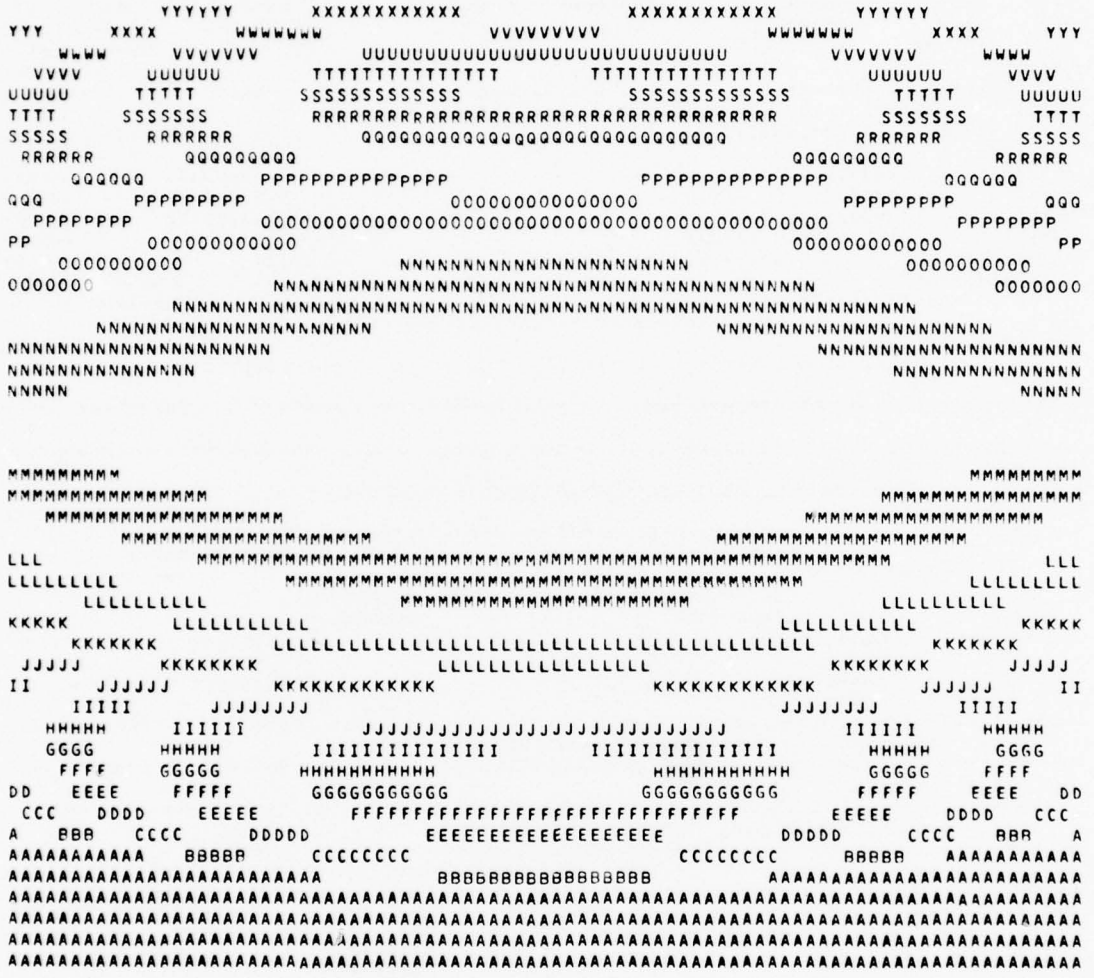

Figure 36. U configuration, $\theta_1 = 45°$, RBT = 0 (1.102), $\Delta L = \Delta\theta_2 = 0$.

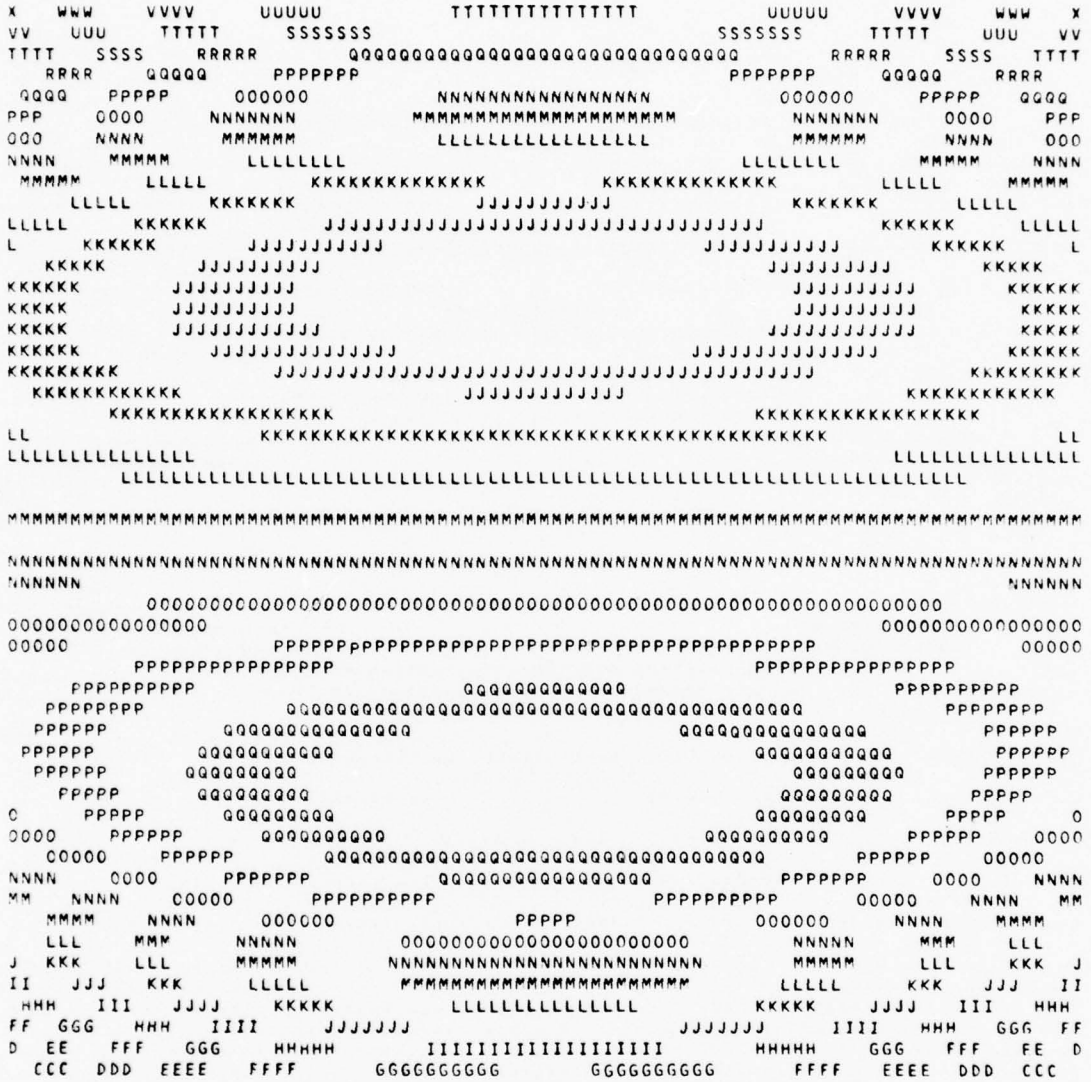

Figure 37. U configuration, θ_1 = 45°, RBT = 1.102 (1.10), $\Delta L = \Delta\theta_2 = 0$.

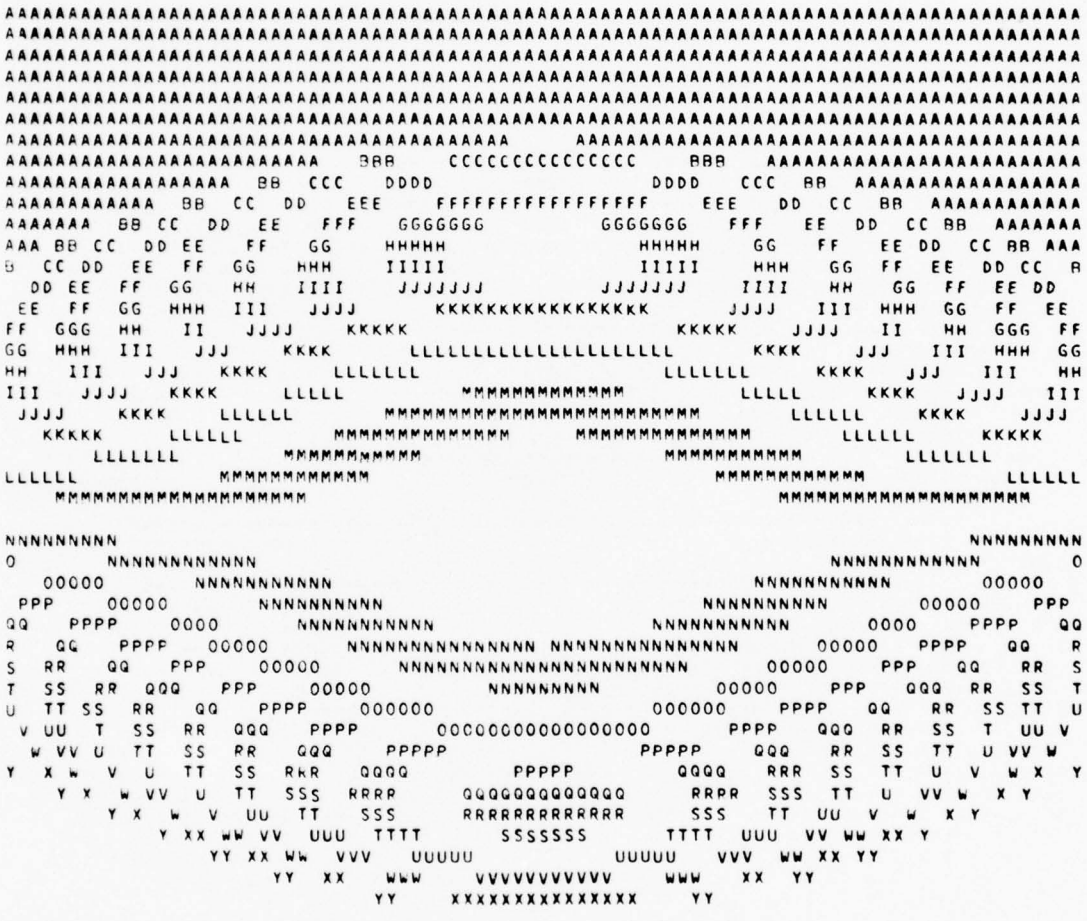

Figure 38. Z configuration, θ_1 = 70°, RBT = 0 (-1.997).

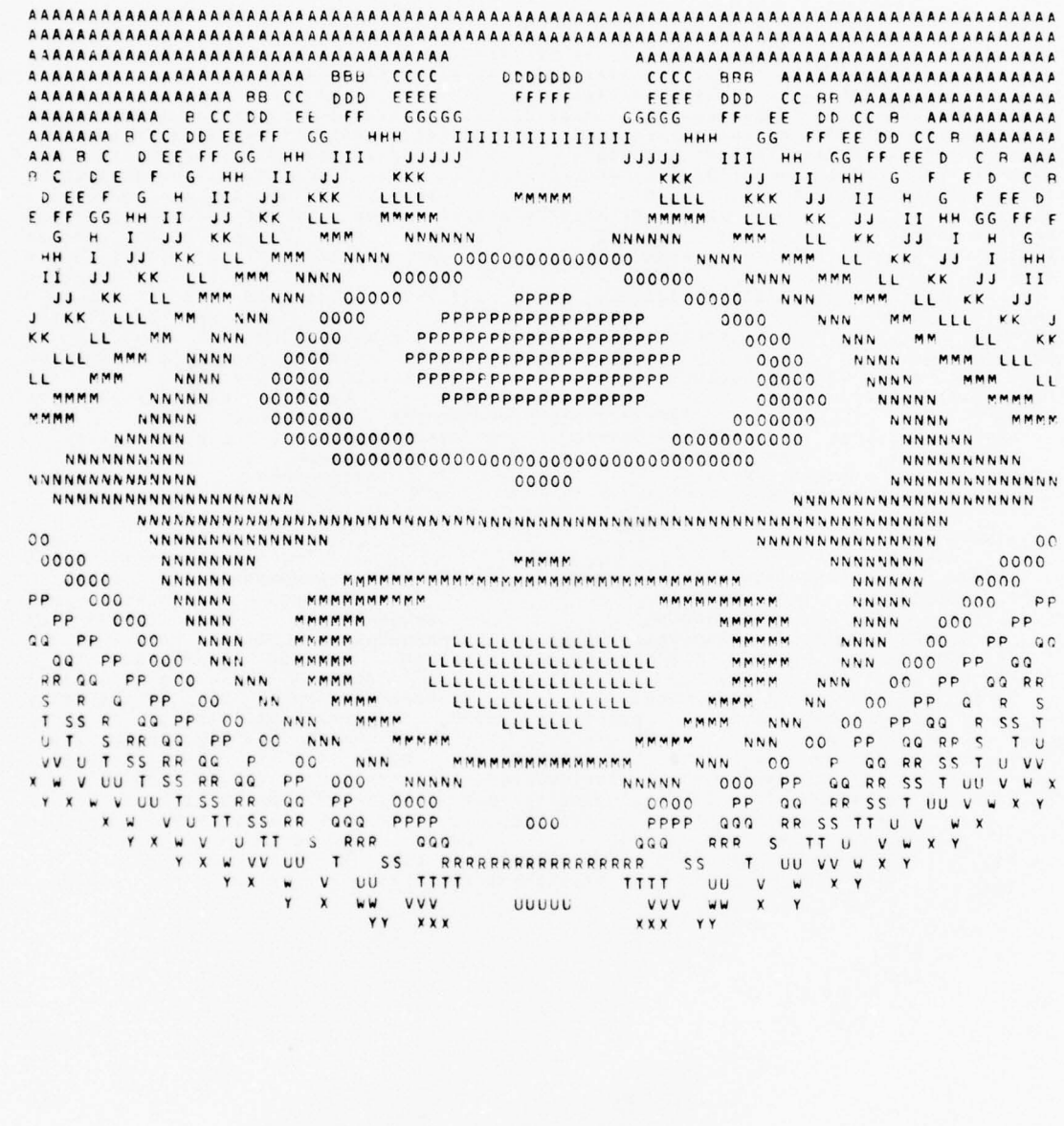

Figure 39. Z configuration, θ_1 = 70°, RBT = -0.799 (-1.997).

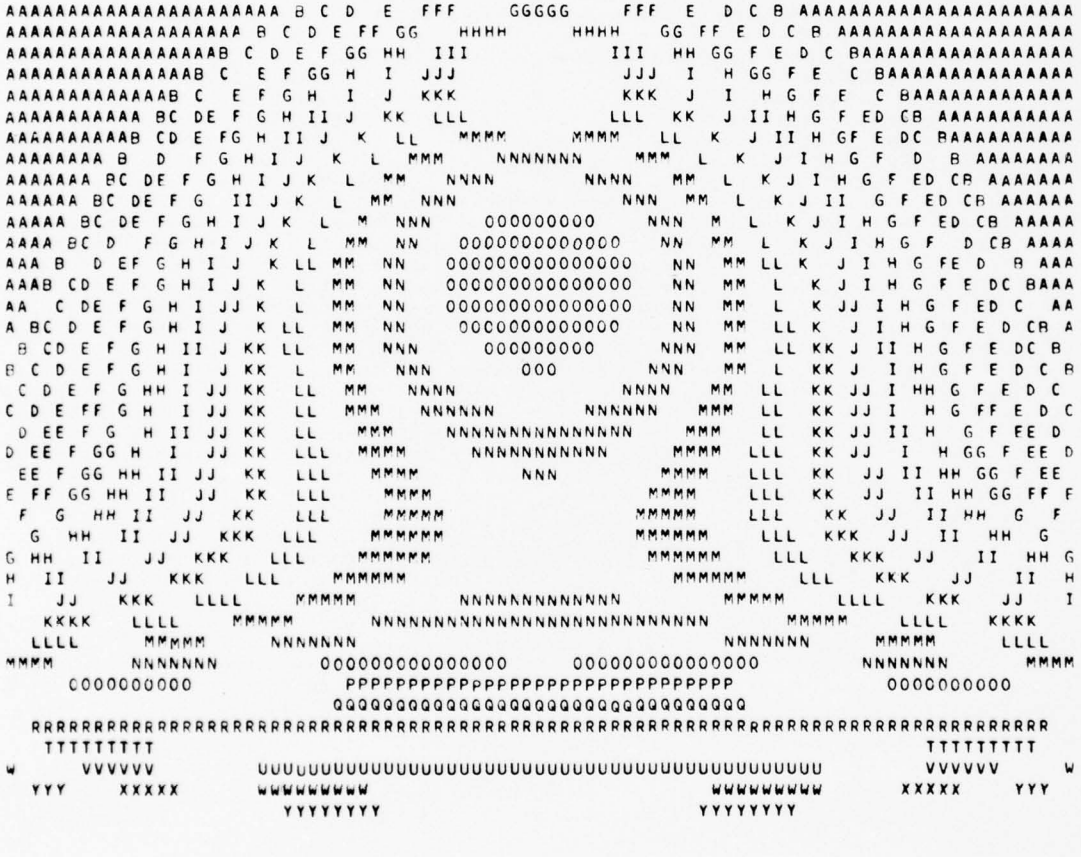

Figure 40. Z configuration, θ_1 = 70°, RBT = 0 (-2.166), $\Delta\theta$ = +0.007.

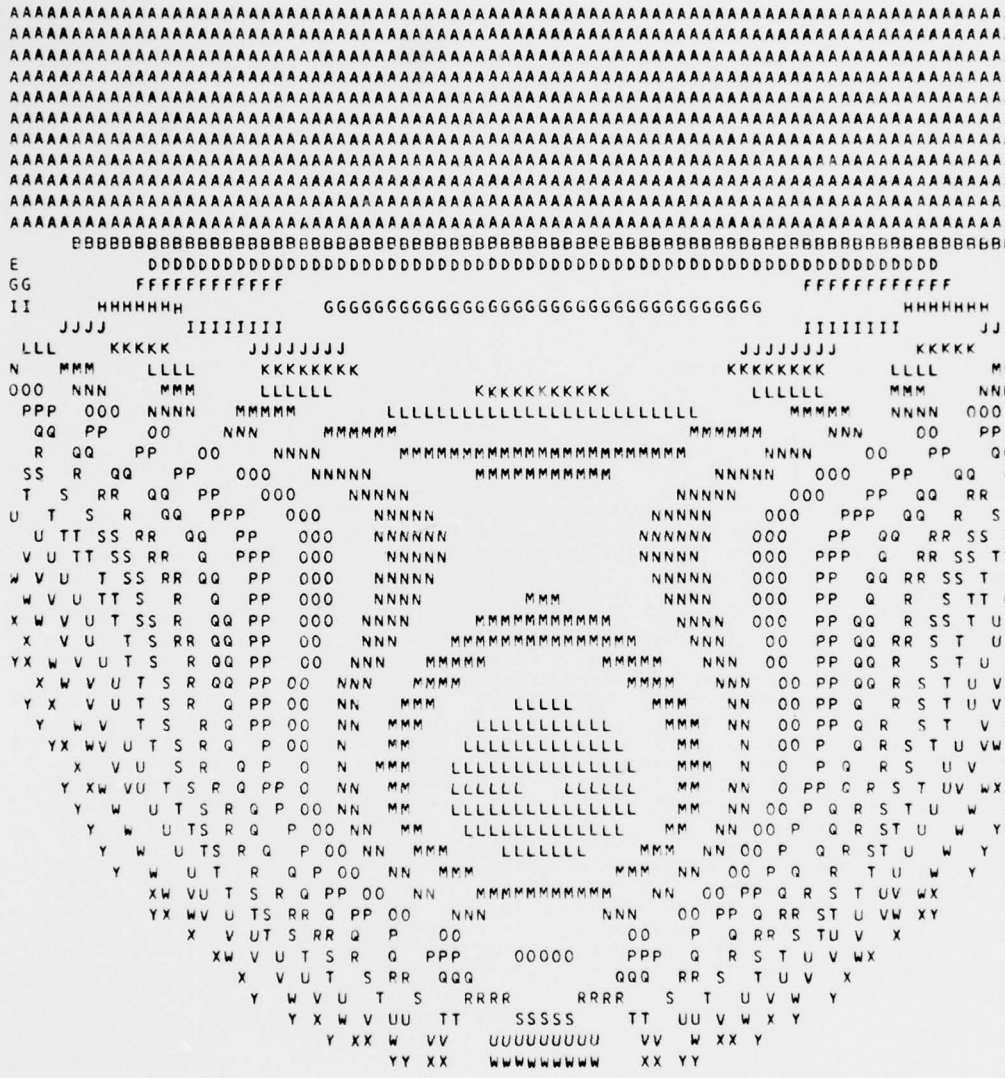

Figure 41. Z configuration, θ_1 = 70°, RBT = 0 (-1.837), $\Delta\theta$ = -0.007.

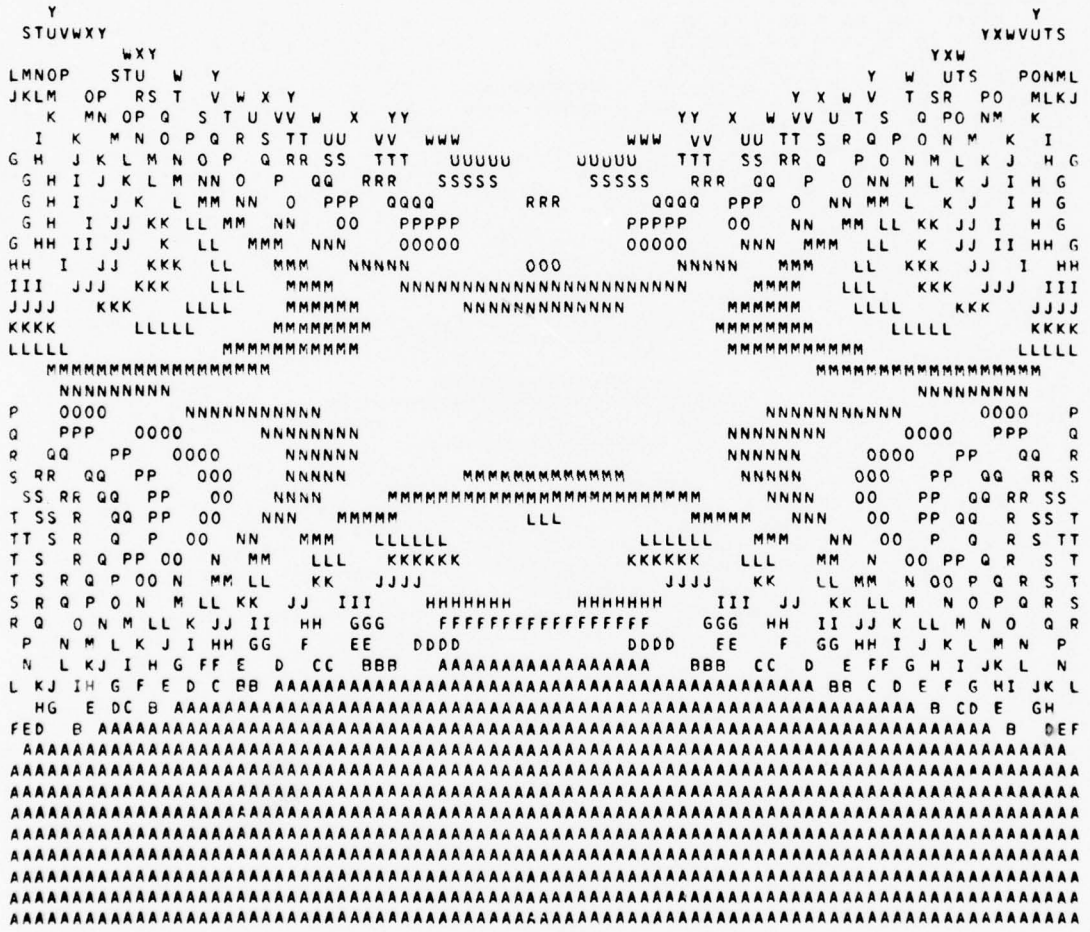

Figure 42. U configuration, $\theta_1 = 70°$, RBT = 0 (3.698), $\Delta L = \Delta\theta_2 = 0$.

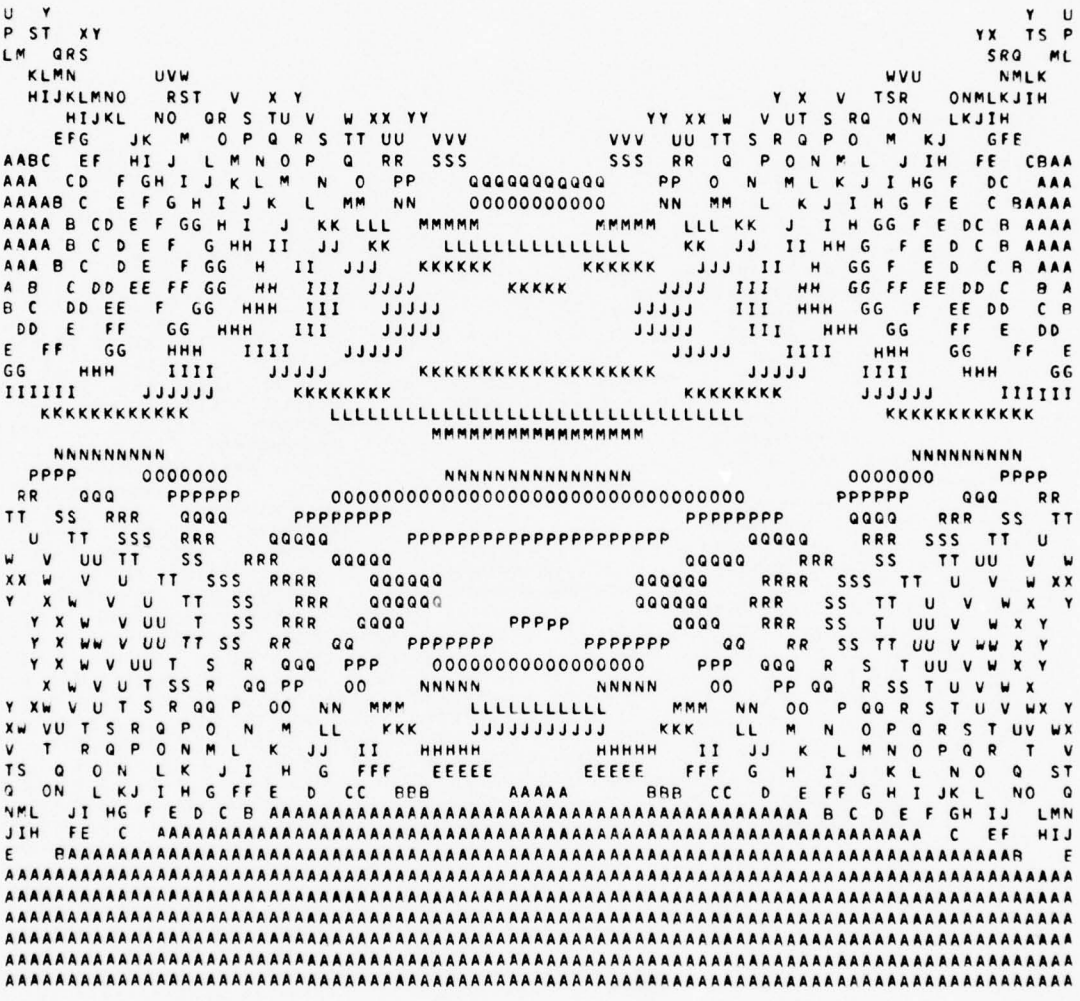

Figure 43. U configuration, θ_1 = 70°, RBT = 1.48 (3.698), $\Delta L = \Delta\theta_2 = 0$.

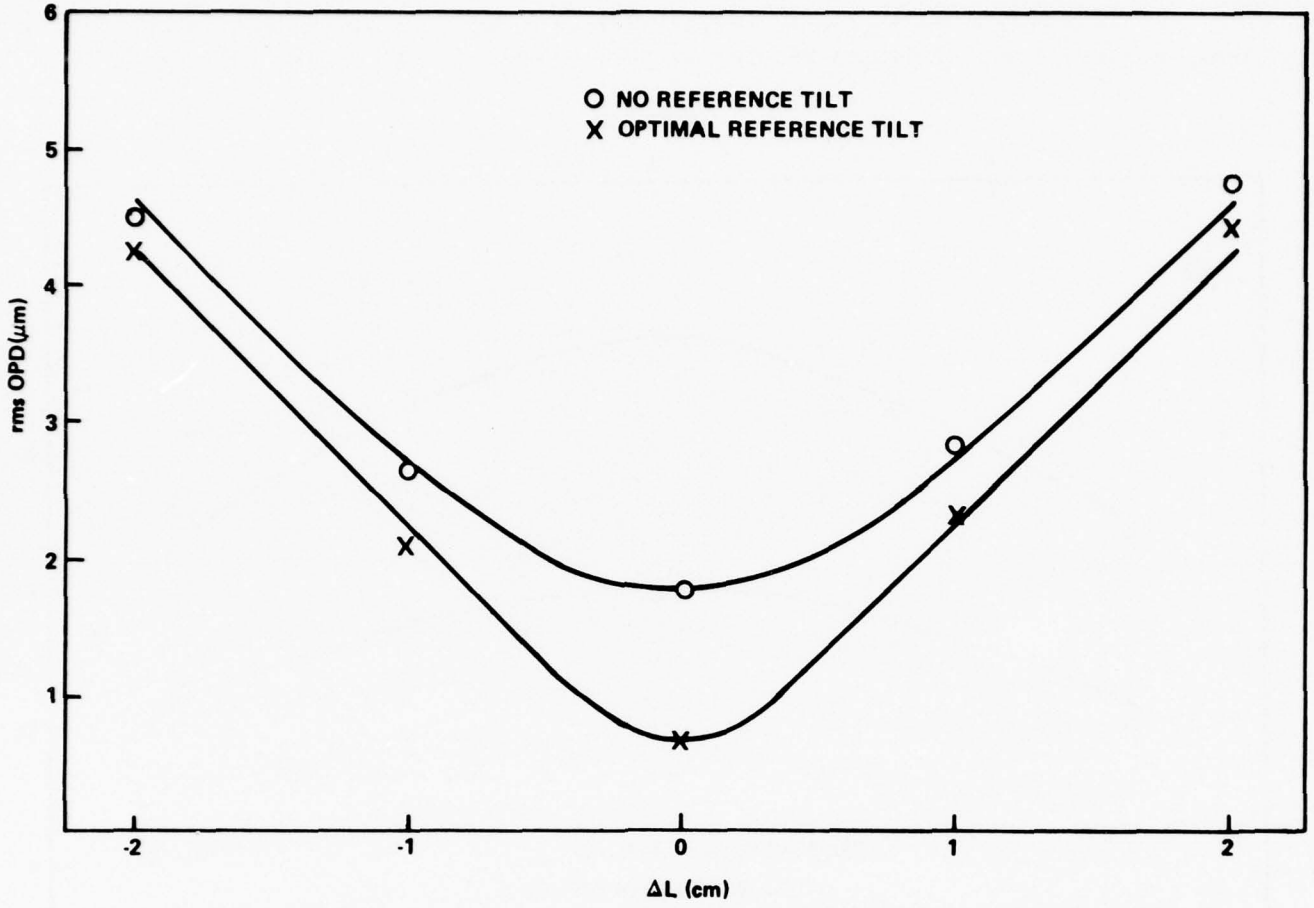

Figure 44. Predicted values (smooth curves) and calculated values of the root-mean-square OPD in microns as a function of ΔL, for Z configuration, $\theta_1 = 45°$, $\Delta\theta_2 = 0$.

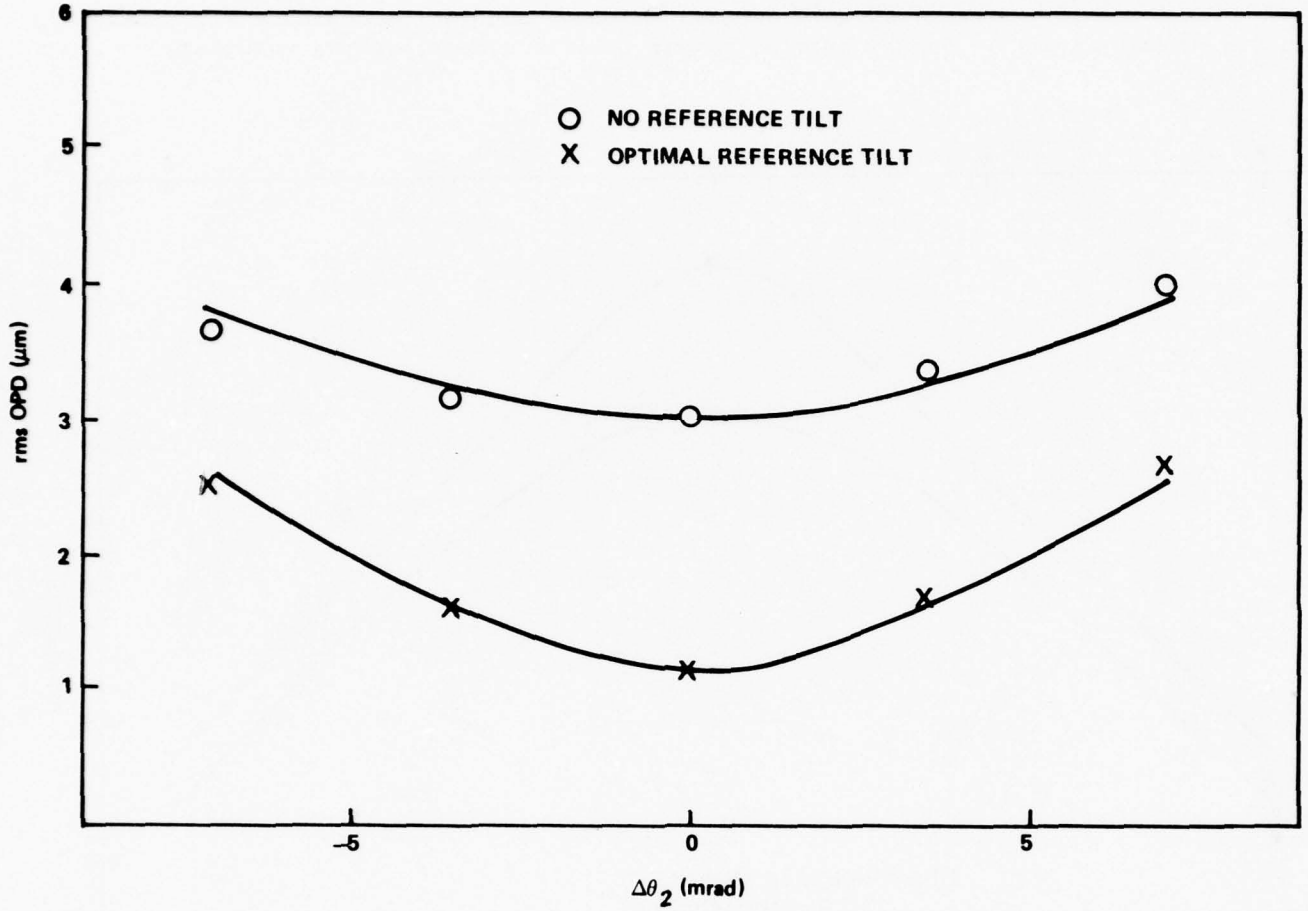

Figure 45. Predicted values (smooth curves) and calculated values of the root-mean-square OPD in microns as a function of $\Delta\theta_2$, for Z configuration, $\theta_1 = 55°$, $\Delta L = 0$.

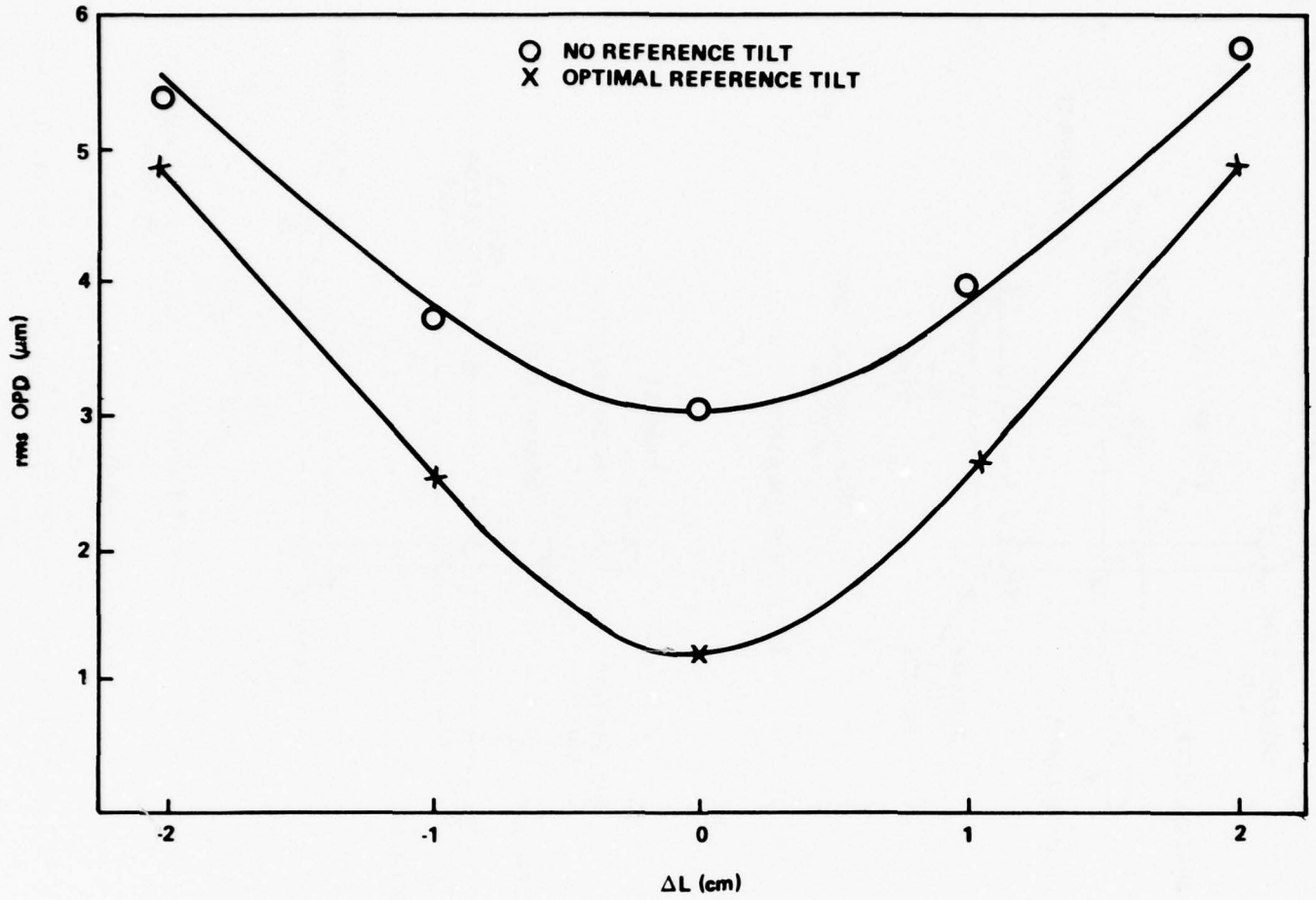

Figure 46. Predicted values (smooth curves) and calculated values of the root-mean-square OPD in microns as a function of ΔL, for Z configuration, $\theta_1 = 55°$, $\Delta\theta_2 = 0$.

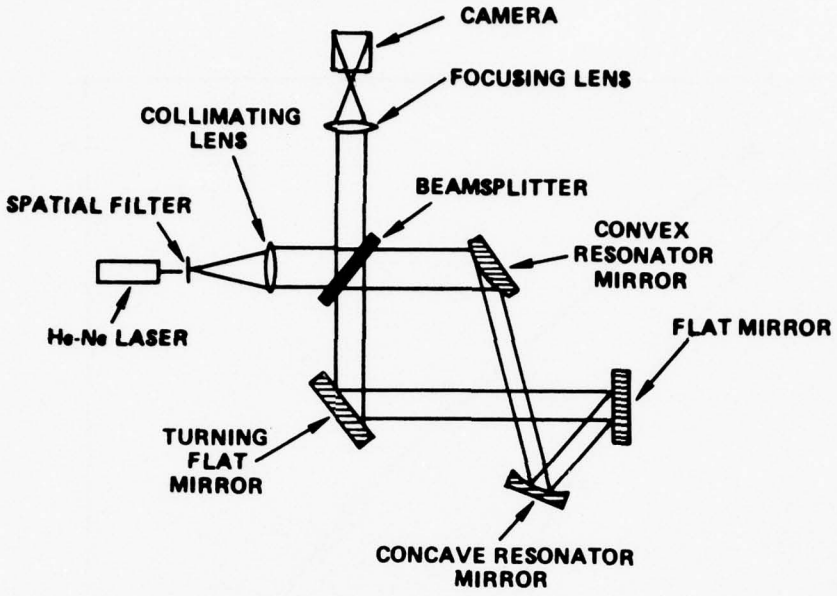

(a) Z CONFIGURATION

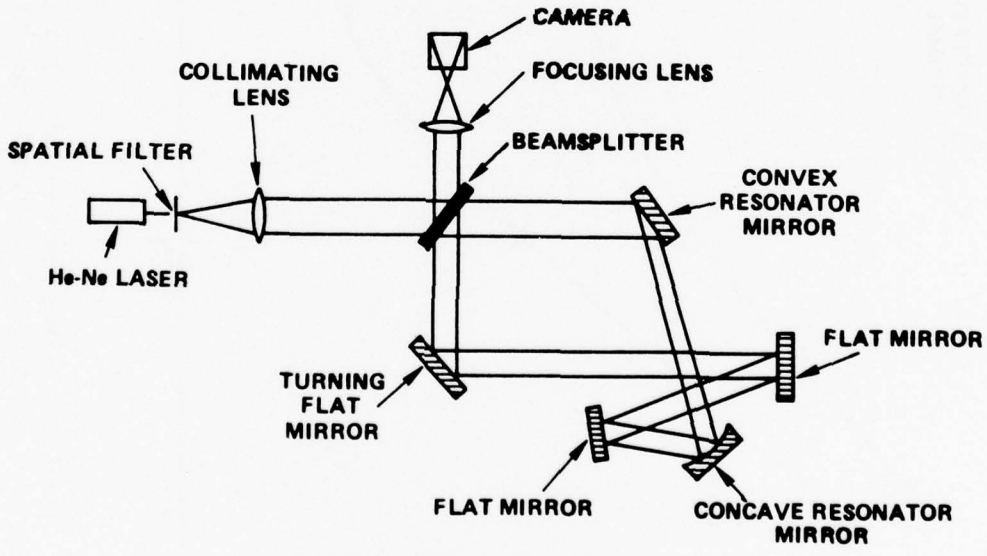

(b) U CONFIGURATION

Figure 47. Experimental arrangement for obtaining interferograms.

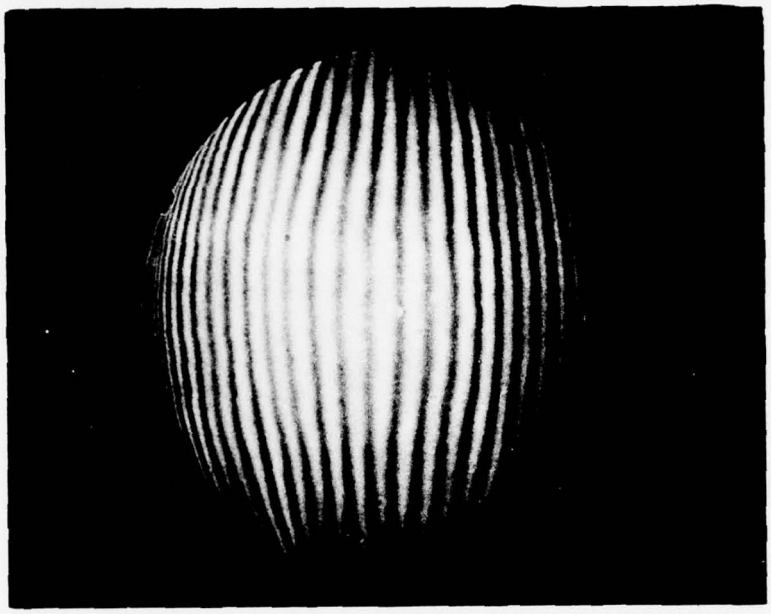

Figure 48. Variation of RBT, θ_1 = 45°, Z configuration.

NO THEORETICAL OPD AVAILABLE

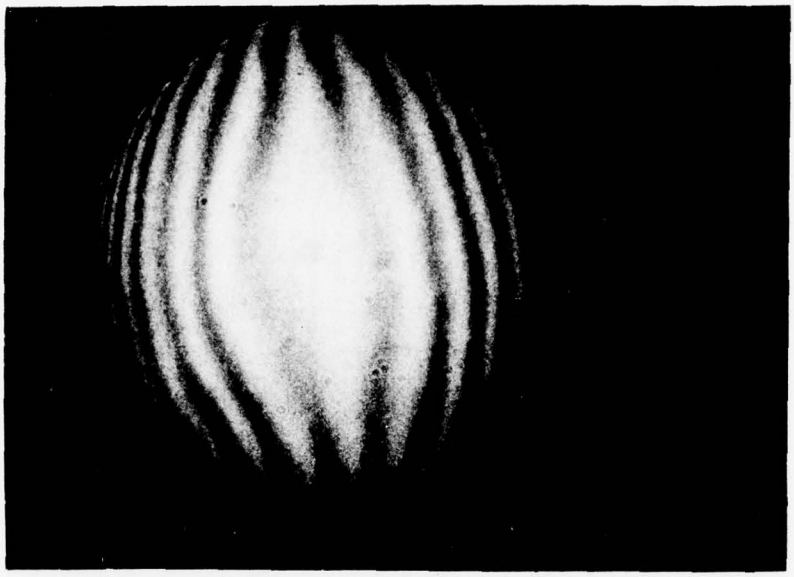

Figure 49(a). Variation of RBT, θ_1 = 45°, Z configuration.

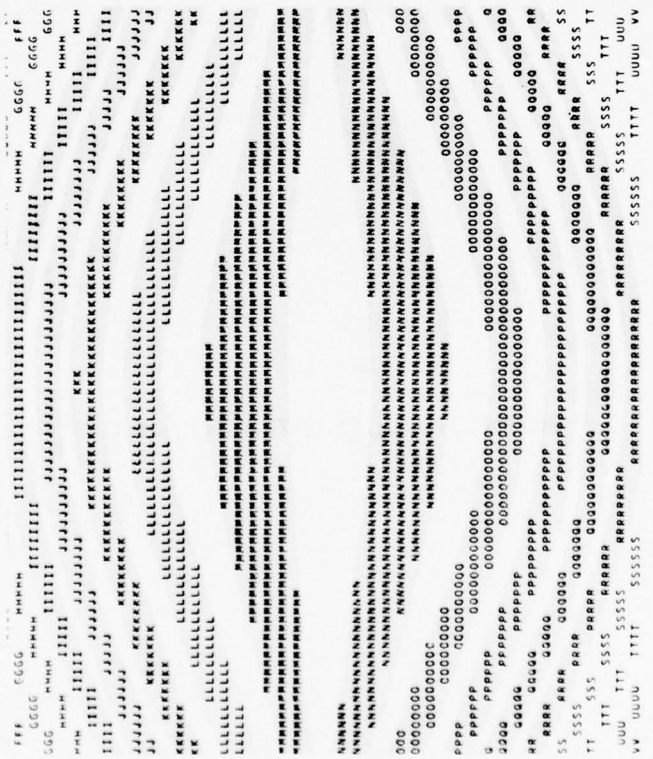

Figure 49(b). Theoretical OPD calculation, Z configuration, θ_1 = 45°, RBT = 0.148 (-0.370).

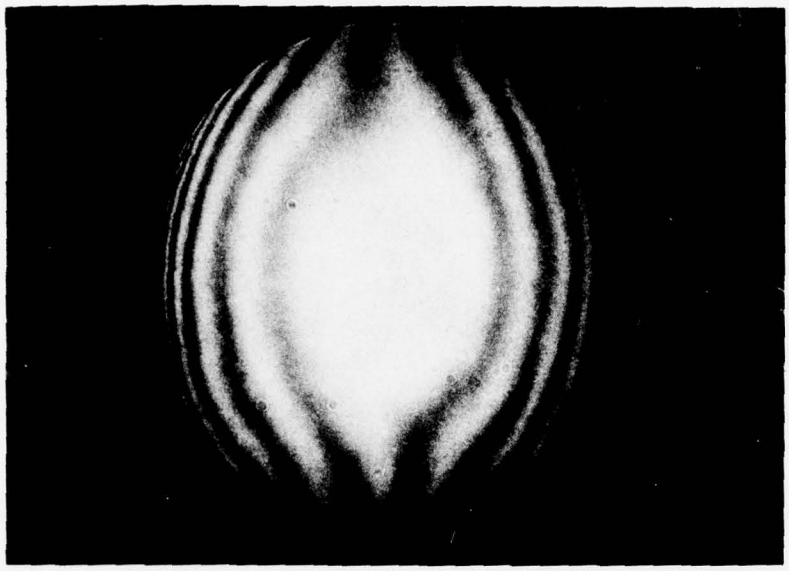

Figure 50(a). Variation of RBT, θ_1 = 45°, Z configuration.

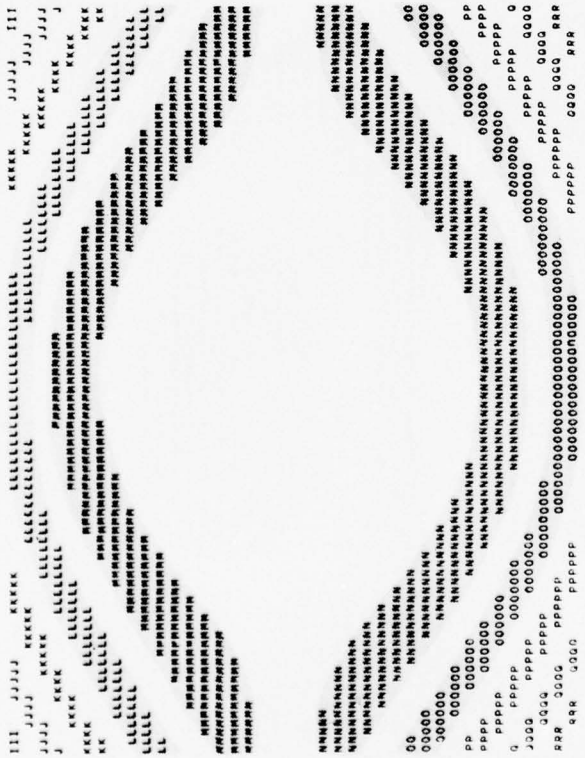

Figure 50(b). Z configuration, θ_1 = 45°, RBT = -0.074 (-0.370).

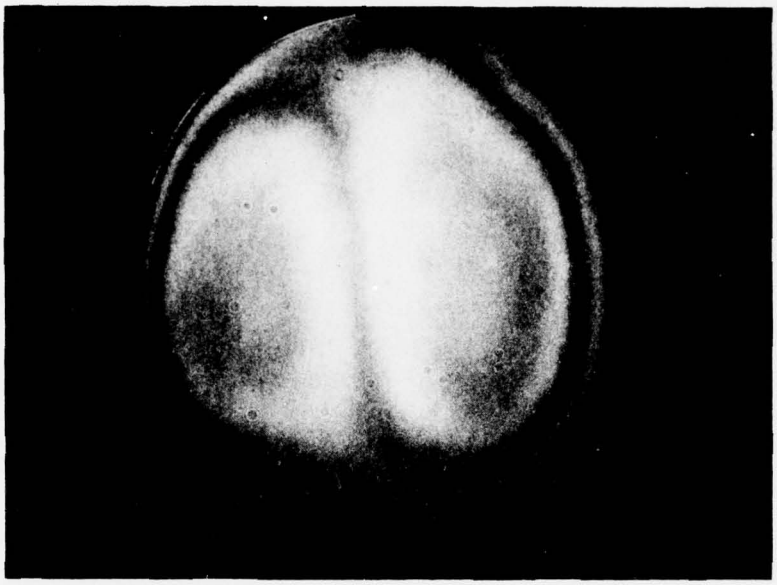

Figure 51(a). Variation of RBT, θ_1 = 45°, Z configuration.

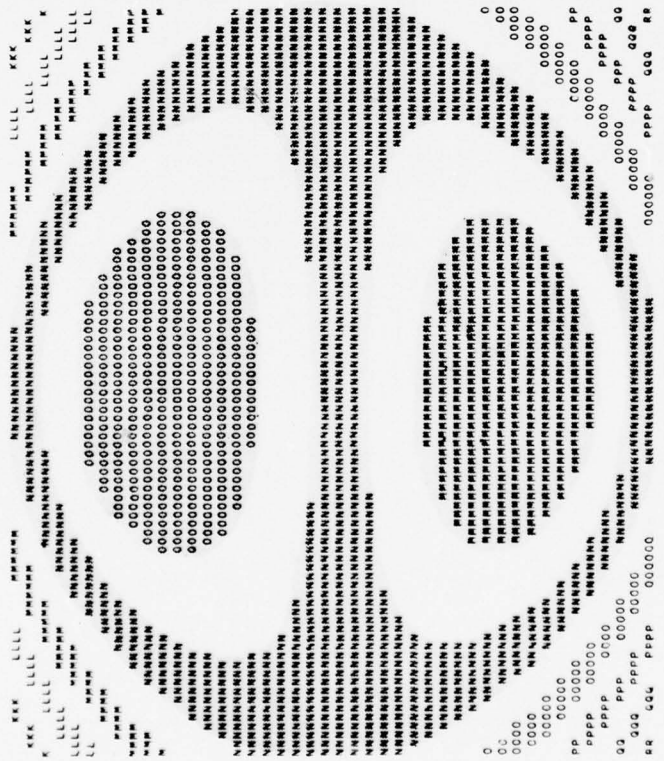

Figure 51(b). Z configuration, θ_1 = 45°, RBT = -0.296 (-0.370).

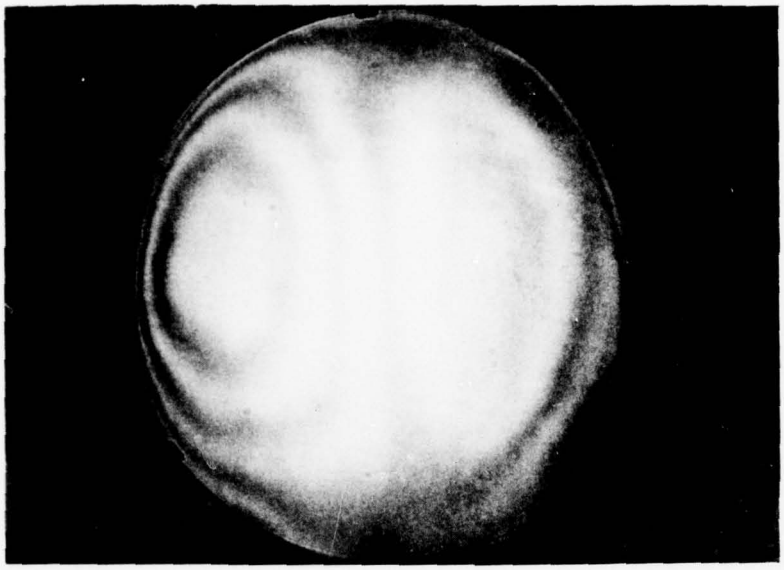

Figure 52(a). Variation of RBT. θ_1 = 45°, Z configuration.

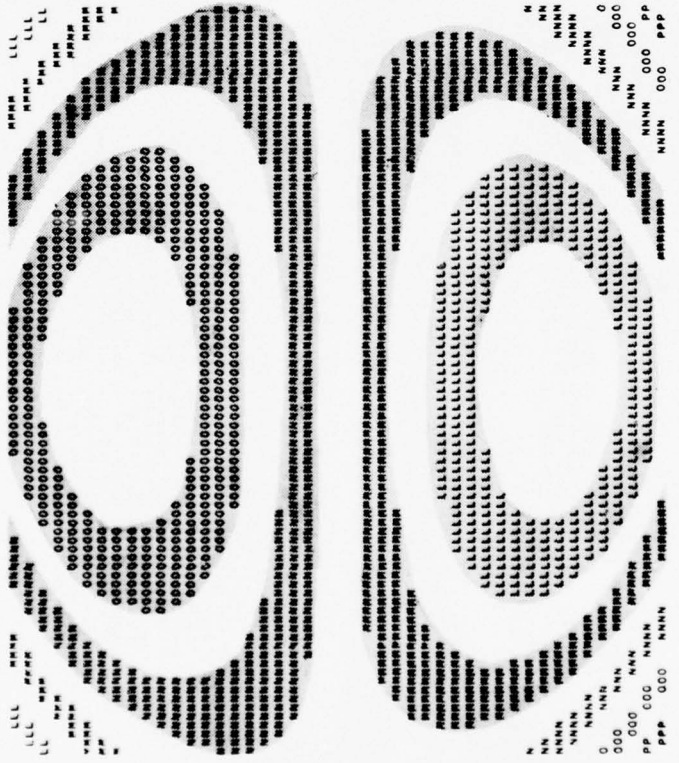

Figure 52(b). Z configuration, θ_1 = 45°, RBT = -0.444 (-0.370).

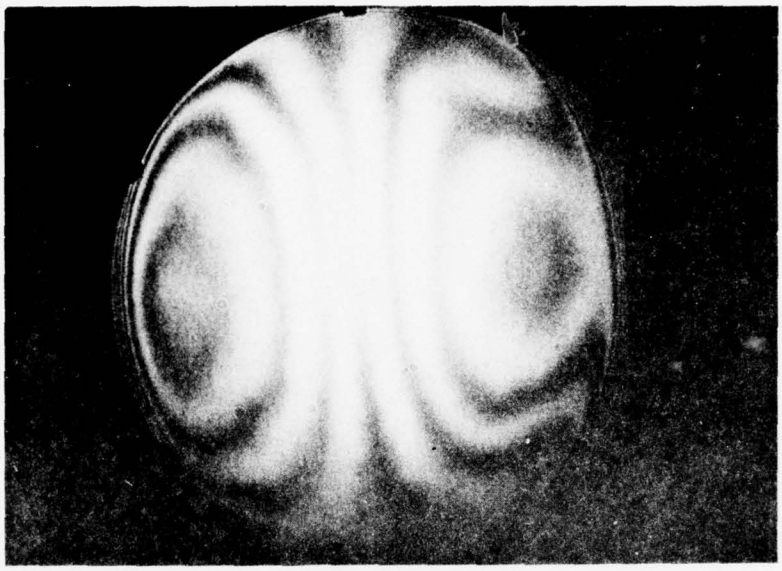

Figure 53(a). Variation of RBT, θ_1 = 45°, Z configuration.

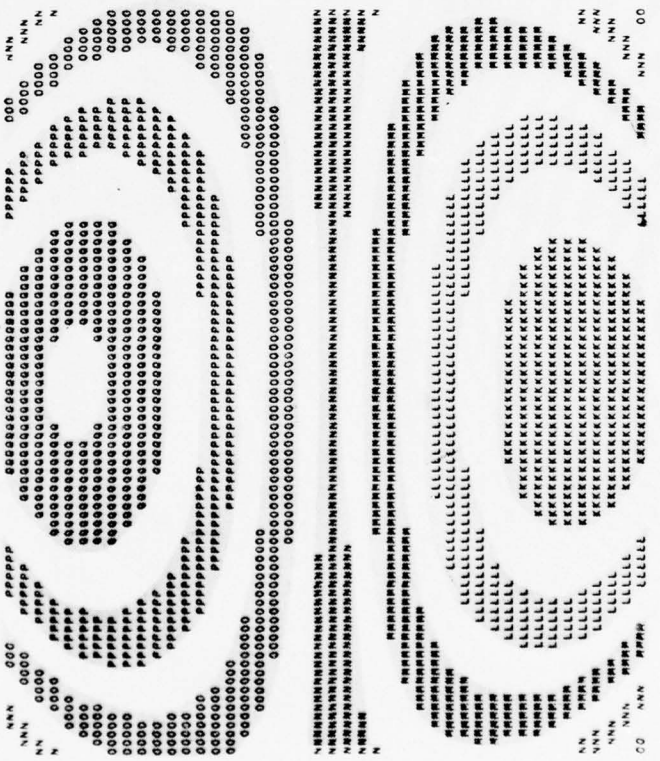

Figure 53(b). Z configuration, θ_1 = 45°, RBT = -0.592 (0.370).

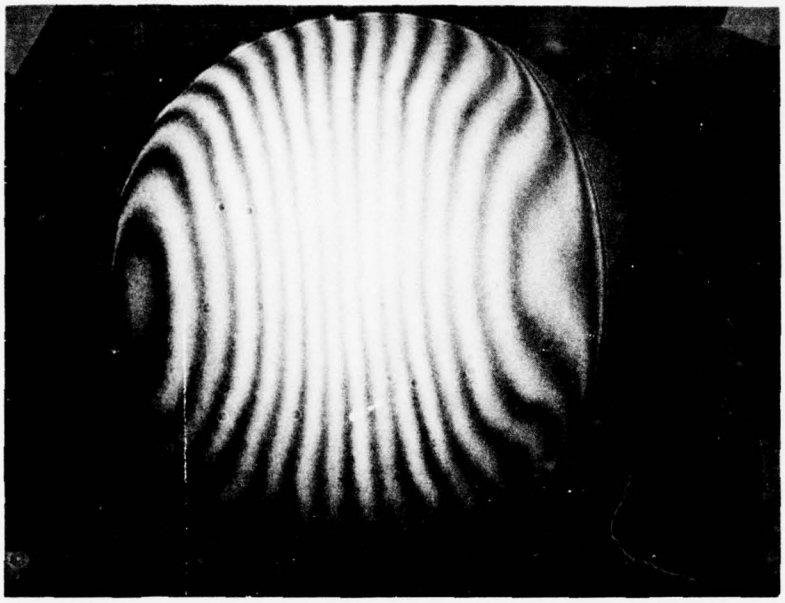

Figure 54(a). Variation in RBT, $\theta_1 = 45°$, Z configuration.

NO THEORETICAL OPD AVAILABLE

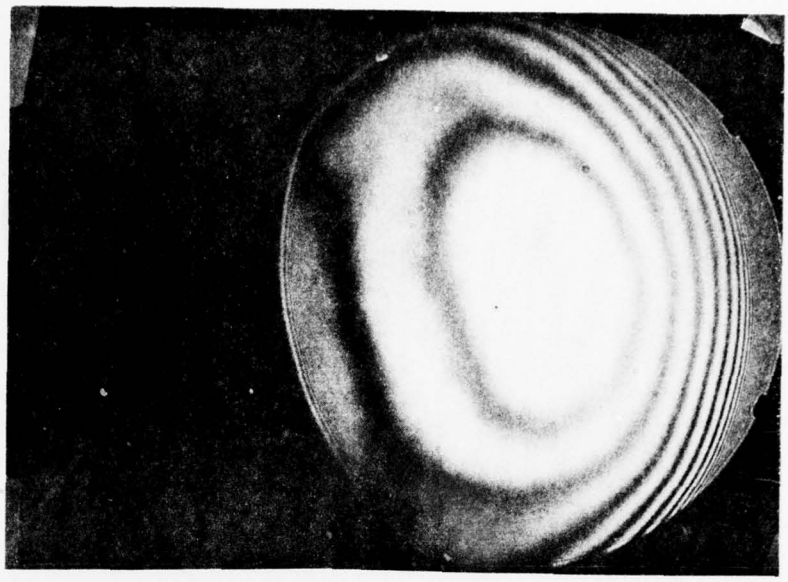

Figure 55(a). Misalignment in L, ΔL = 1 cm, $\theta_1 = 45°$, Z configuration.

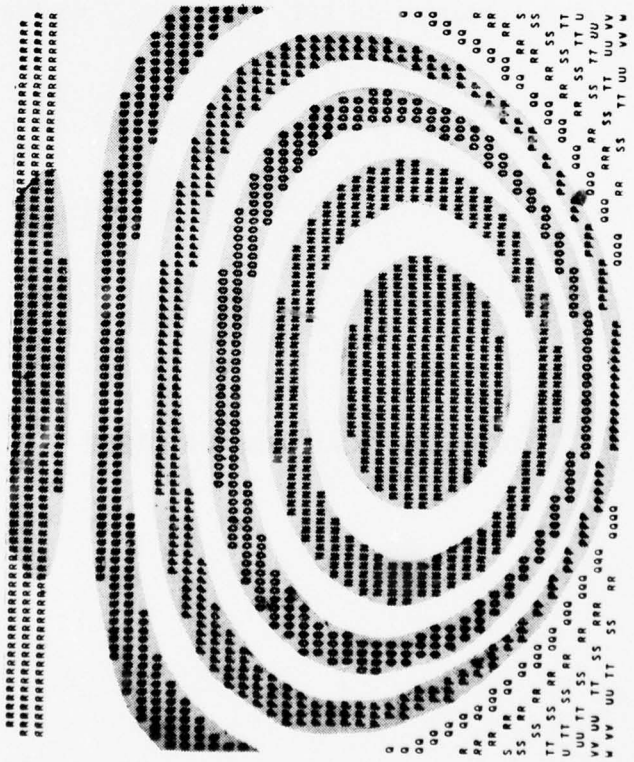

Figure 55(b). Z configuration, $\theta_1 = 45°$, RBT = 0 (-0.361), L = 1.0 cm.

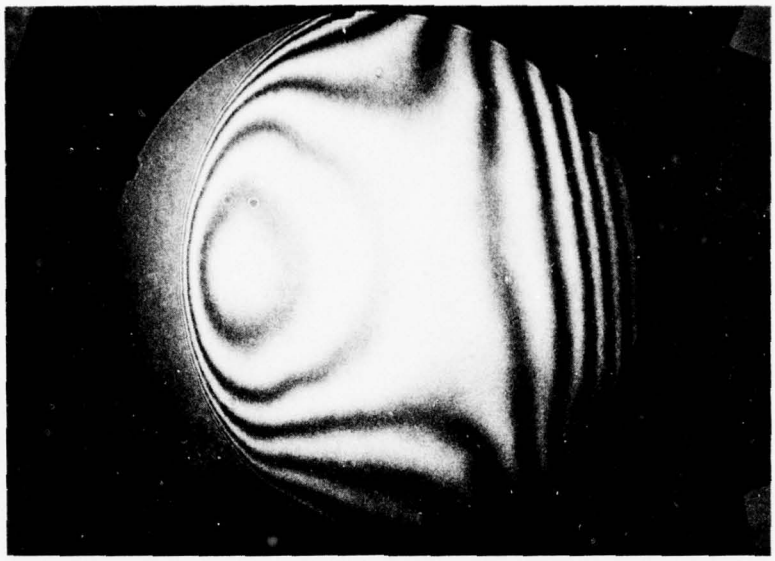

Figure 56(a). Misalignment in θ_2, $\Delta\theta_2$ = 7 mrad, θ_1 = 45°, Z configuration.

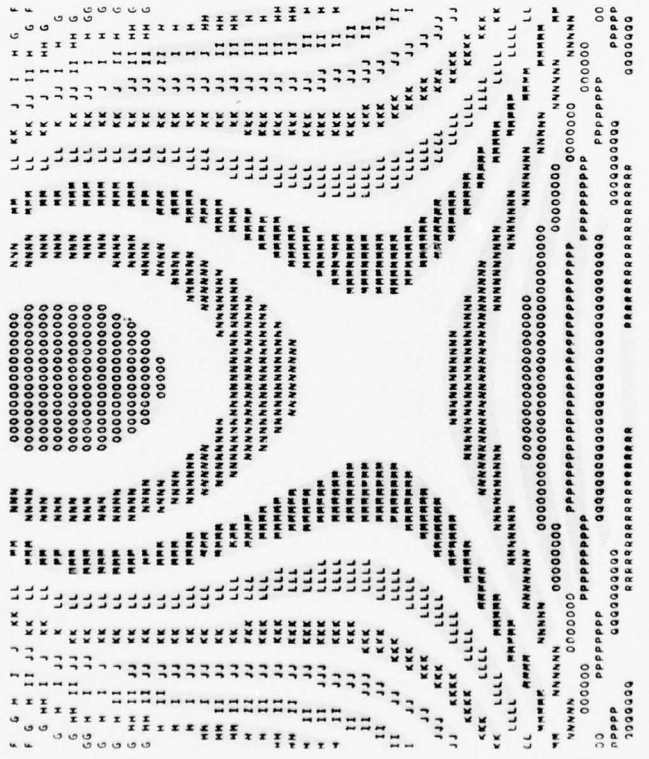

Figure 56(b). θ_1 = 45°, RBT = 0 (-0.392), $\Delta\theta_2$ = 0.007 rad, Z configuration.

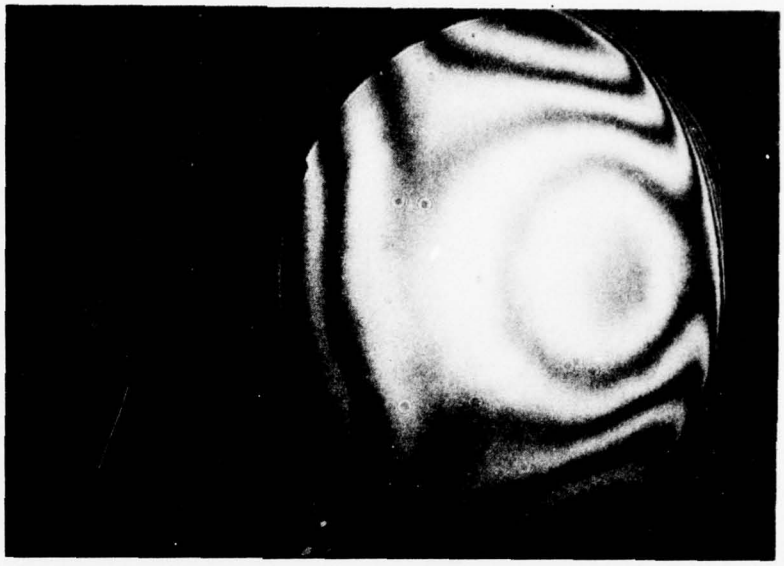

Figure 57(a). Misalignment in $\theta_2 + \Delta\theta_2 = -7$ mrad, $\theta_1 = 45°$, Z configuration.

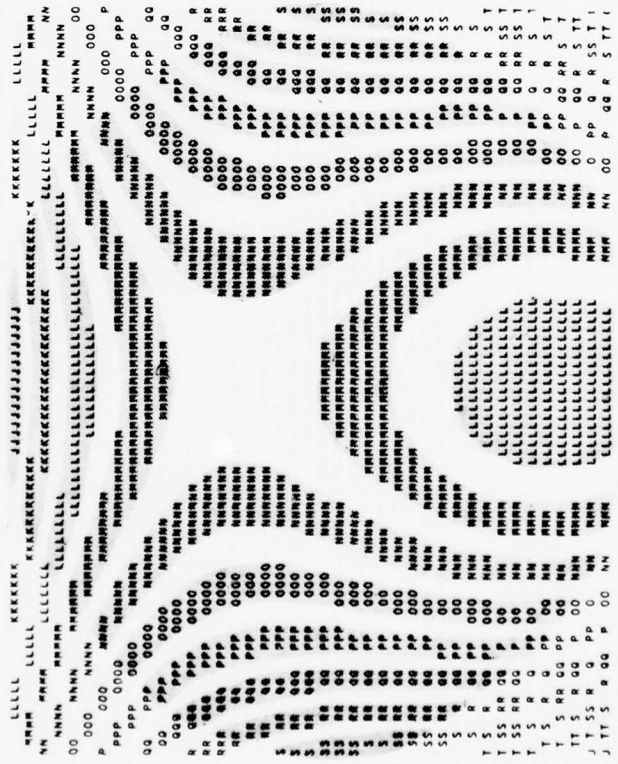

Figure 57(b). Z configuration, $\theta_1 = 45°$, RBT = 0 (-0.348), $\Delta\theta_2 = -0.007$ rad.

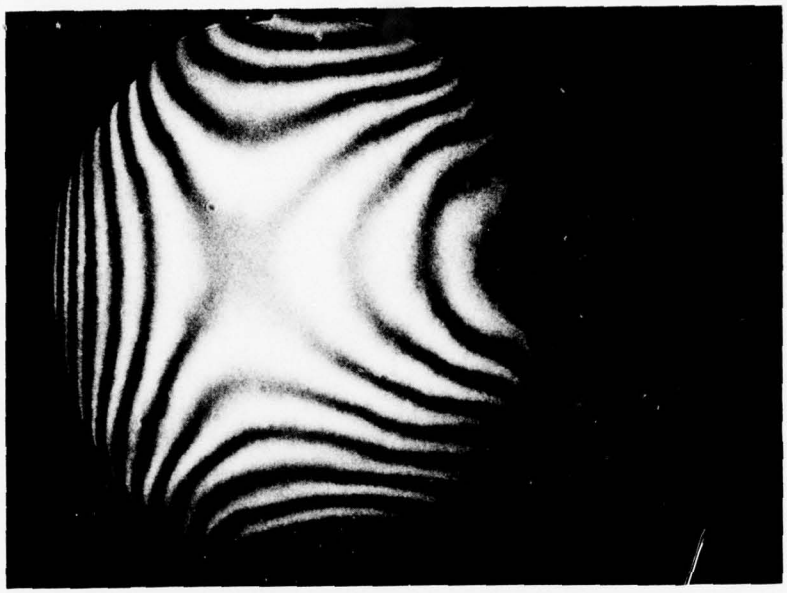

Figure 58. Misalignment in θ_2, $\Delta\theta_2$ = 14 mrad, θ_1 = 45°, Z configuration.

NO THEORETICAL OPD AVAILABLE

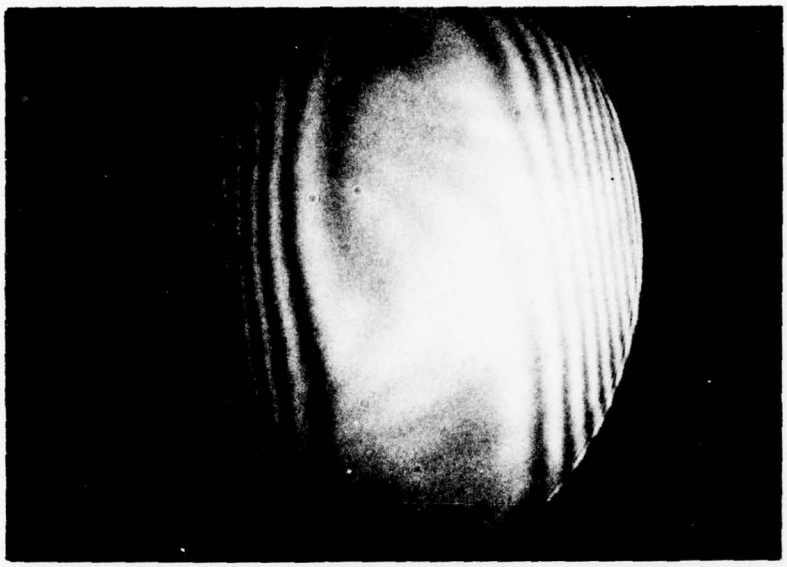

Figure 59(a). Variation of RBT, θ_1 = 45°, U configuration.

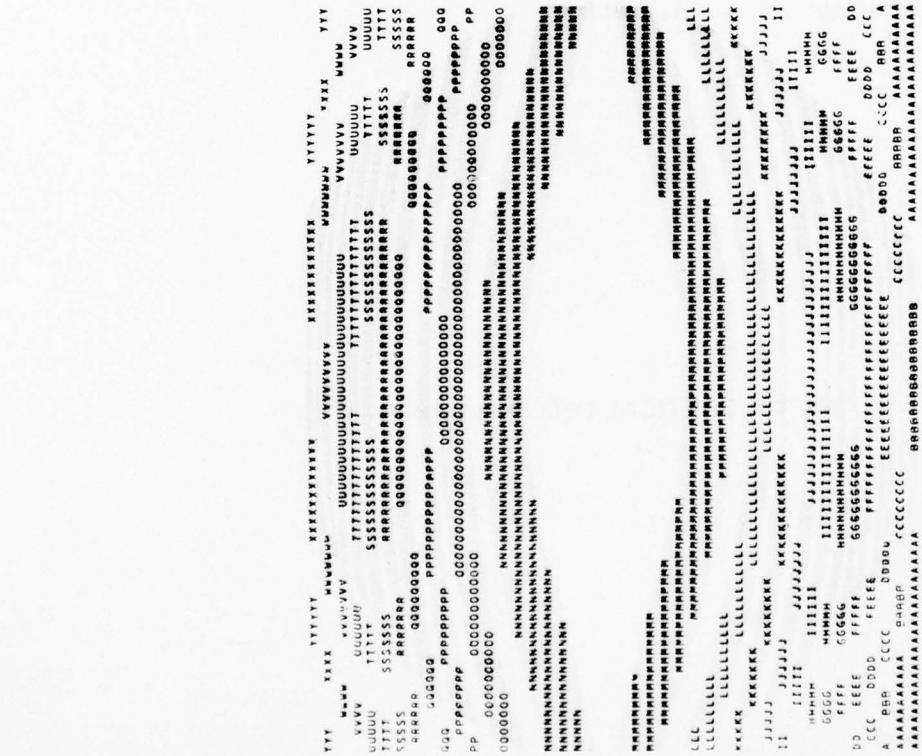

Figure 59(b). RBT = 0 (+1.102), θ_1 = 45°, U configuration.

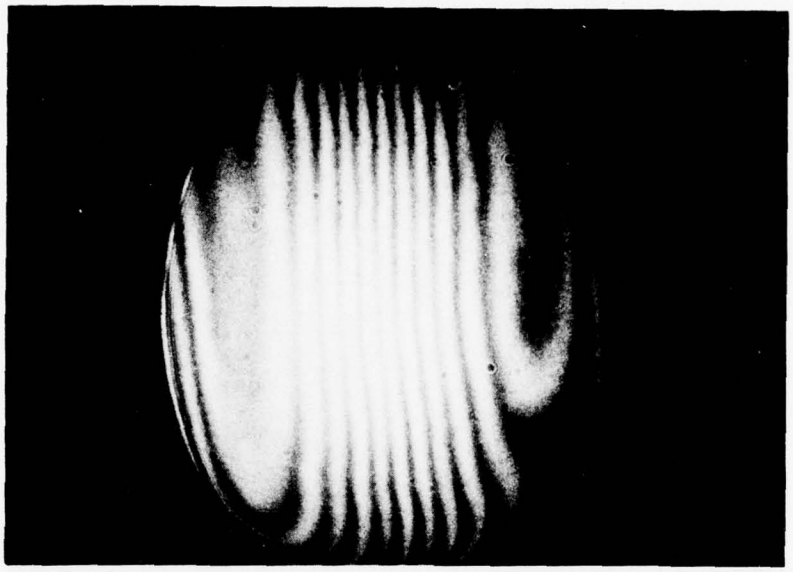

Figure 60(a). Variation of RBT, θ_1 = 45°, U configuration.

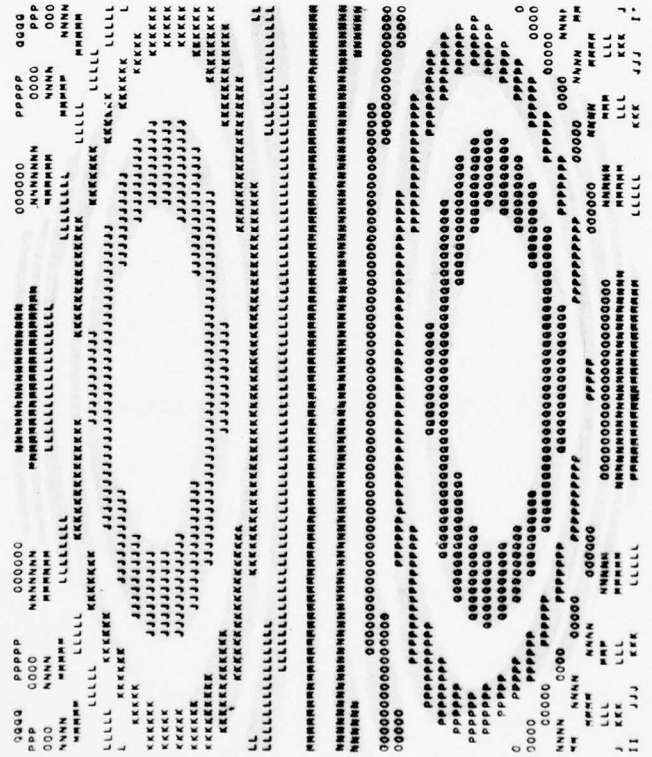

Figure 60(b). RBT = 1.102 (1.102), θ_1 = 45°, U configuration.

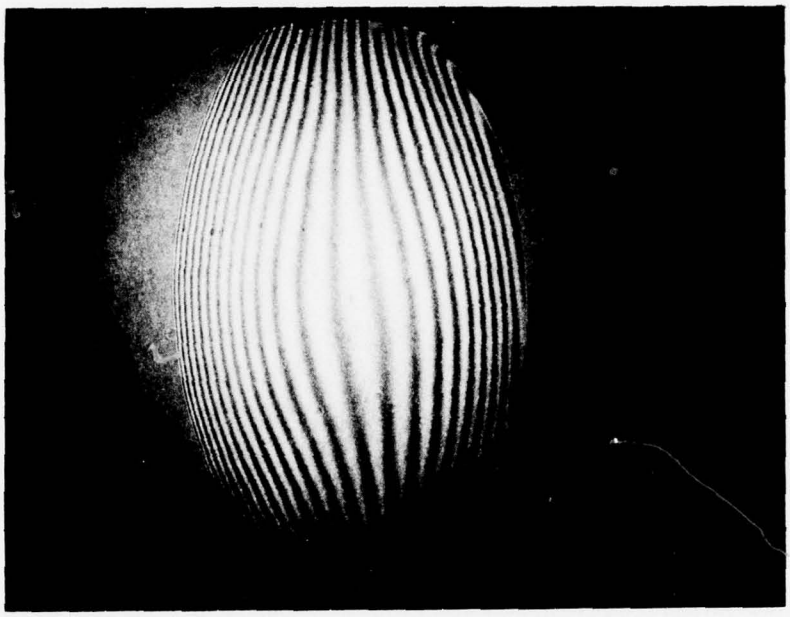

Figure 61. Variation of RBT, θ_1 = 70°, Z configuration.

NO THEORETICAL OPD AVAILABLE

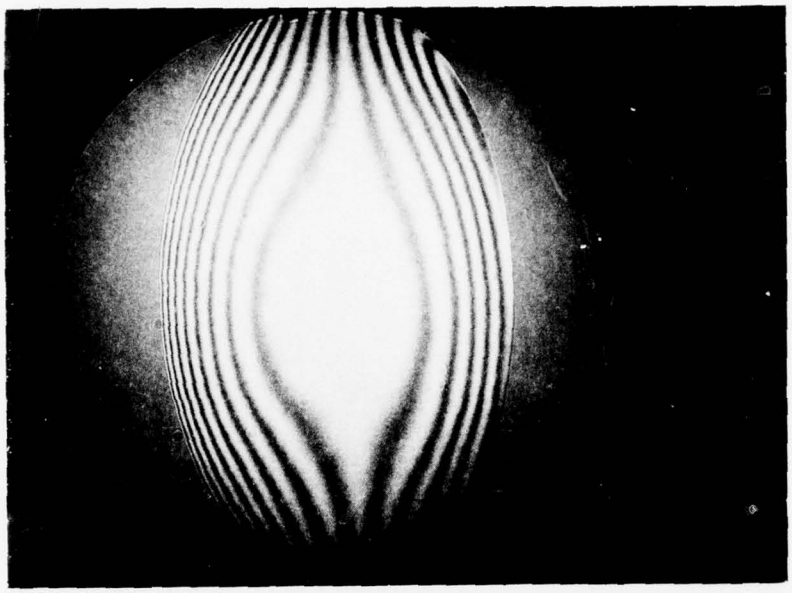

Figure 62(a). Variation of RBT, $\theta_1 \approx 70°$, Z configuration.

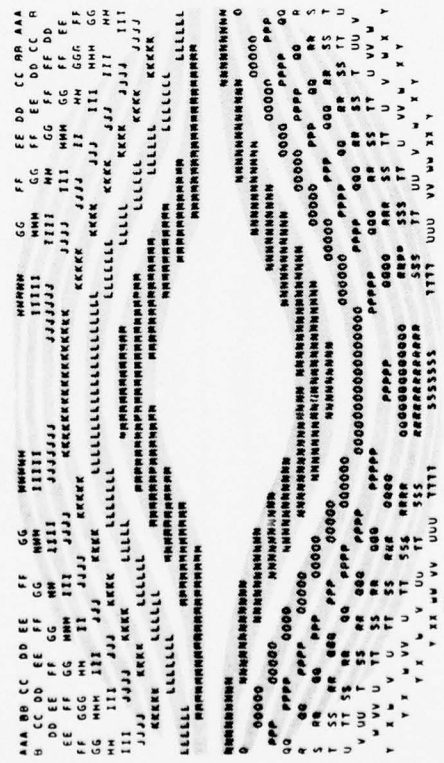

Figure 62(b). RBT = 0 (-1.997), $\theta_1 \approx 70°$, Z configuration.

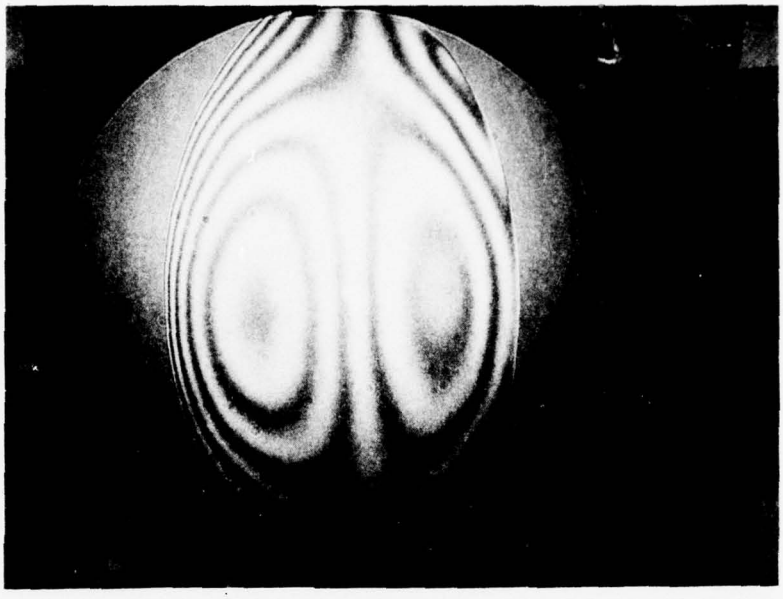

Figure 63(a). Variation of RBT, θ_1 = 70°, Z configuration.

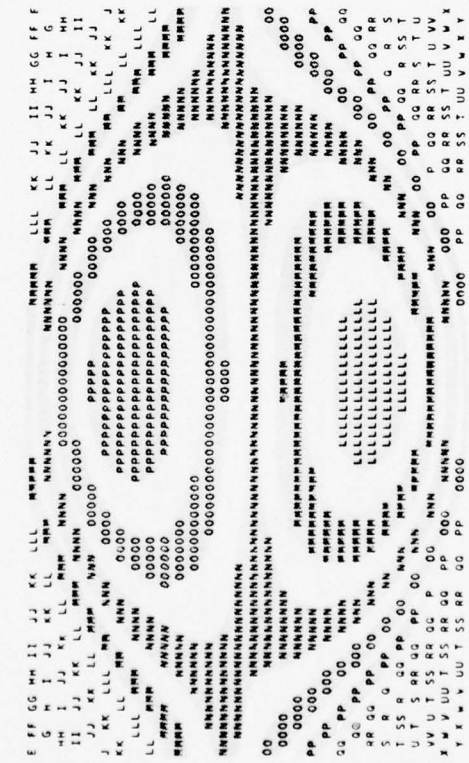

Figure 63(b). RBT = -0.799 (-1.997), θ_1 = 70°, Z configuration.

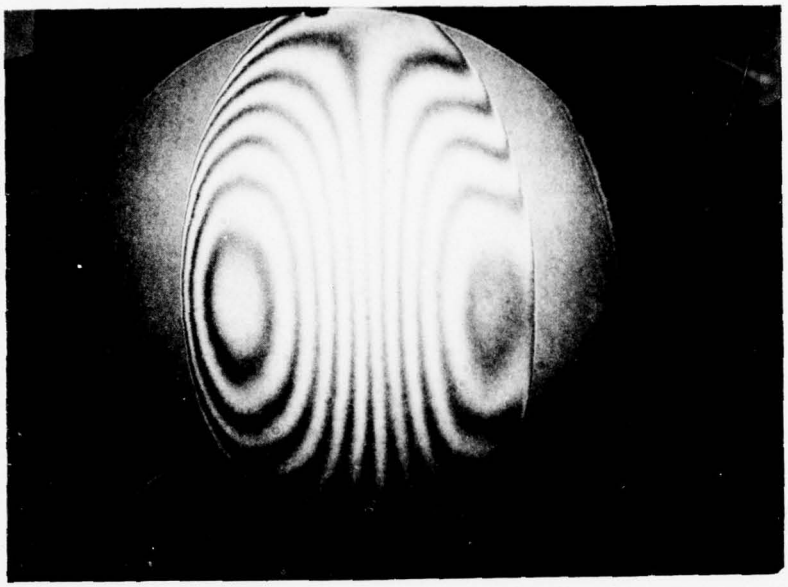

Figure 64. Variation of RBT, θ_1 = 70°, Z configuration.

NO THEORETICAL OPD AVAILABLE

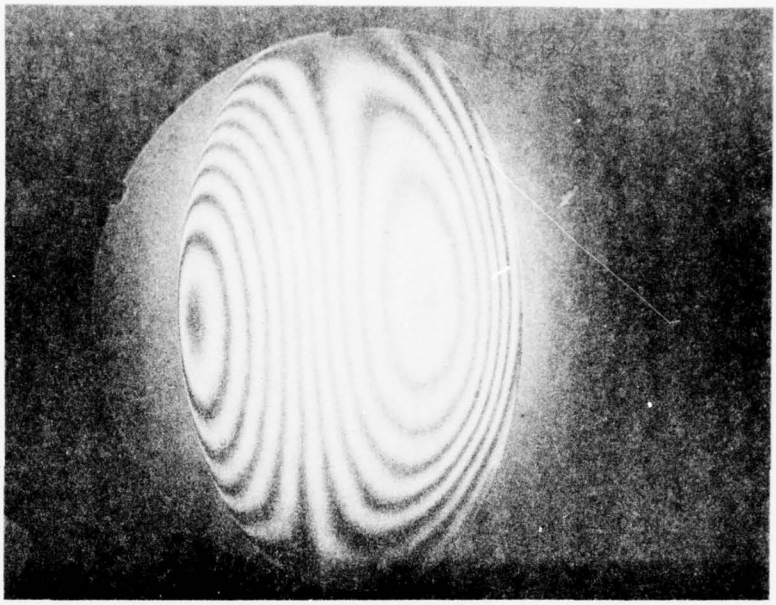

Figure 65. Misalignment in L, ΔL = 2 cm, θ_1 = 70°, Z configuration.

NO THEORETICAL OPD AVAILABLE

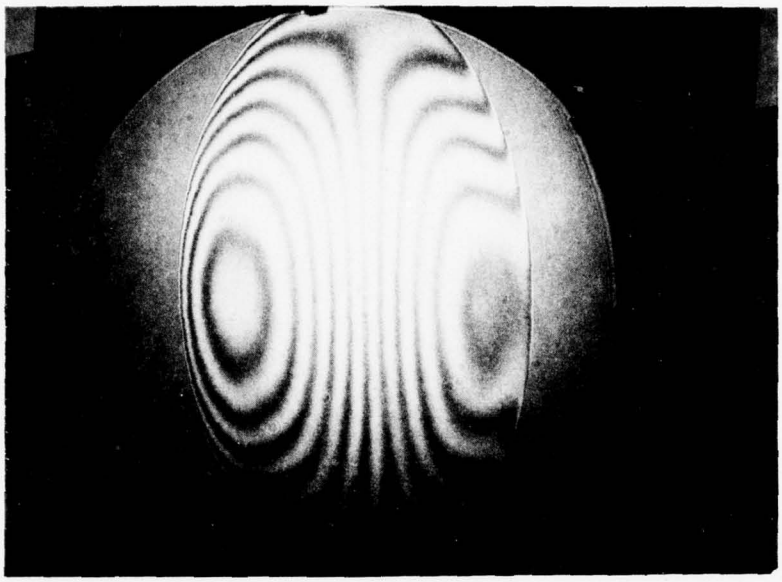

Figure 64. Variation of RBT, θ_1 = 70°, Z configuration.

NO THEORETICAL OPD AVAILABLE

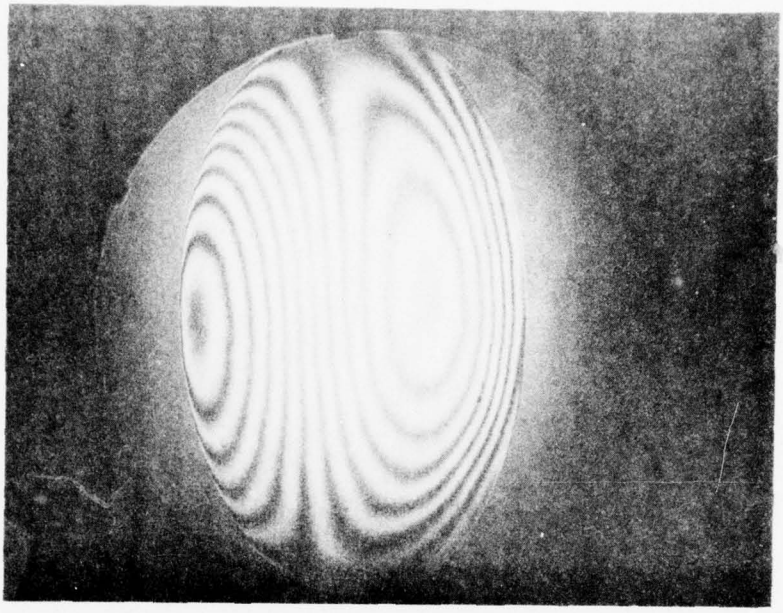

Figure 65. Misalignment in L, ΔL = 2 cm, θ_1 = 70°, Z configuration.

NO THEORETICAL OPD AVAILABLE

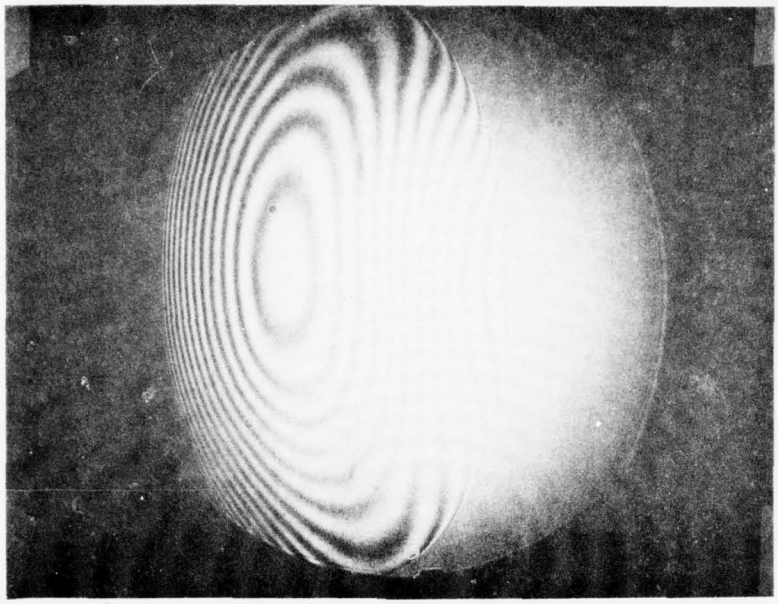

Figure 66. Misalignment in L, $\Delta L = -2$ cm, $\theta_1 = 70°$, Z configuration.

NO THEORETICAL OPD AVAILABLE

AD-A068 015 OFFICE OF THE PROJECT MANAGER HIGH ENERGY LASER REDS--ETC F/G 20/6
OPTICAL QUALITY OF TILTED SPHERICAL MIRROR UNSTABLE RESONATORS.(U)
JAN 79 R W JONES, J C NIXON, C CASON

UNCLASSIFIED DRCPM-HEL-79-2 NL

2 OF 2
AD
A068015

END
DATE
FILMED
6-79
DDC

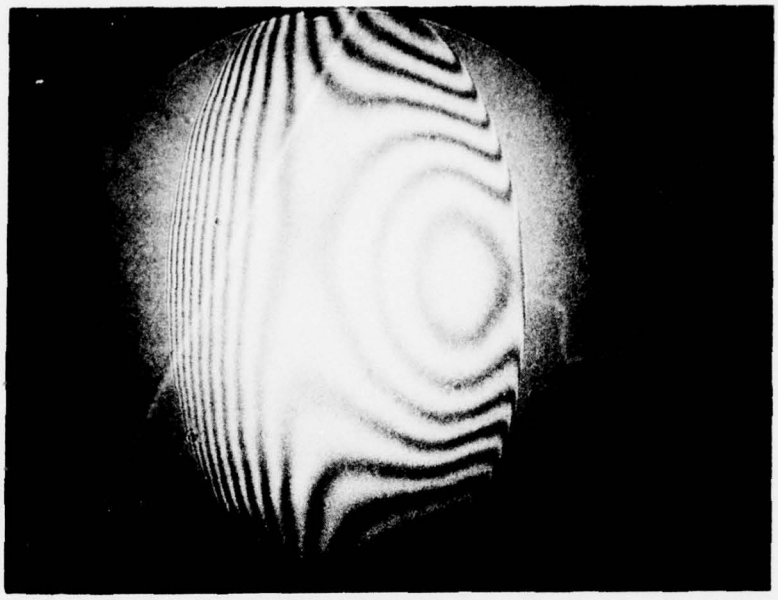

Figure 67(a). Misalignment of θ_2, $\Delta\theta_2$ = -7 mrad, θ_1 = 70°, Z configuration.

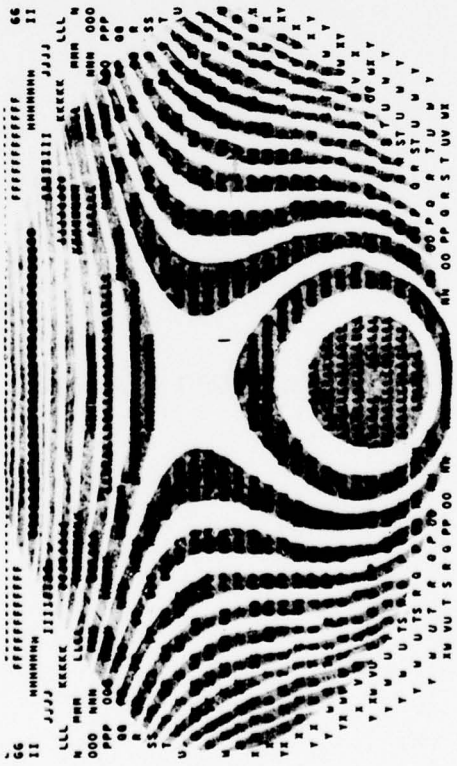

Figure 67(b). RBT = 0 (-1.837), θ_1 = 70°, $\Delta\theta_2$ = -7 mrad.

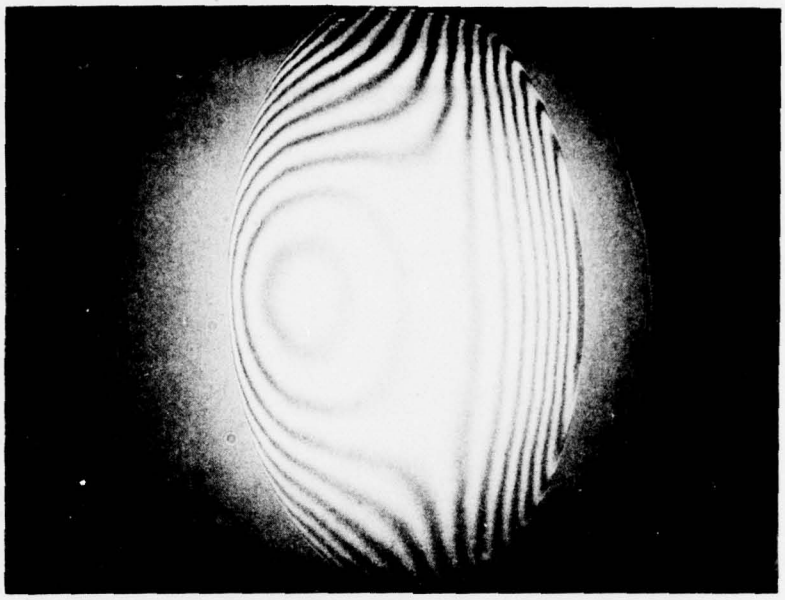

Figure 68(a). Misalignment of θ_2, $\Delta\theta_2$ = 7 mrad, θ_1 = 70°, Z configuration.

Figure 68(b). RBT = 0 (-2.166), θ_1 = 70°, Z configuration, $\Delta\theta_2$ = 7 mrad.

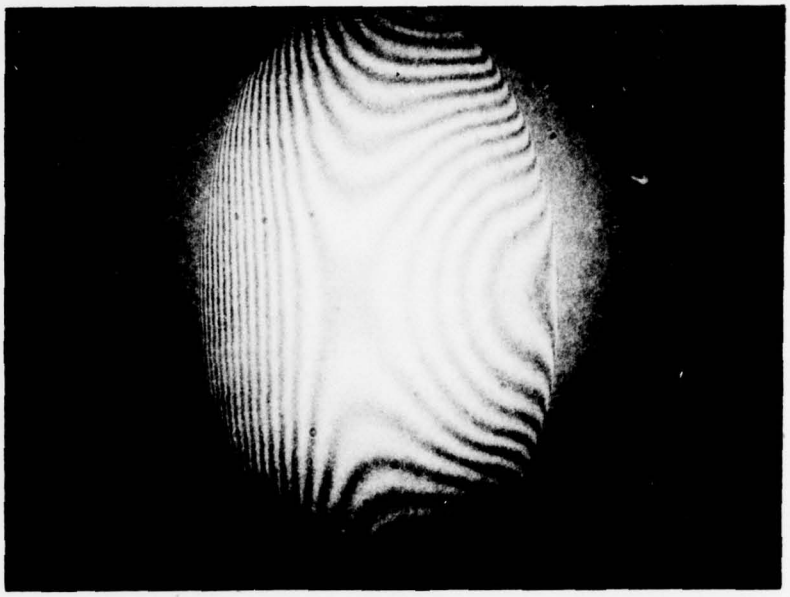

Figure 69. Misalignment in θ_2, $\Delta\theta_2$ = -14 mrad, θ_1 = 70°, Z configuration.

NO THEORETICAL OPD AVAILABLE

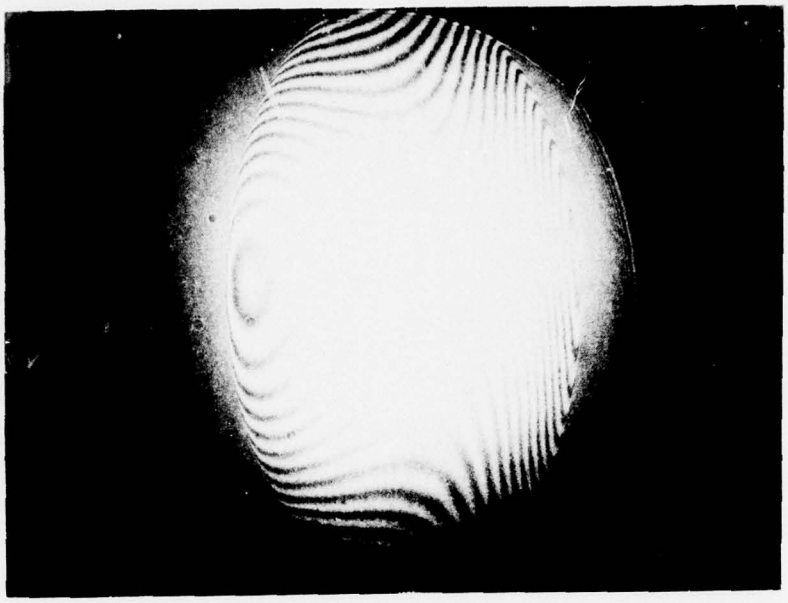

Figure 70. Misalignment in θ_2, $\Delta\theta_2$ = 14 mrad, θ_1 = 70°, Z configuration.

NO THEORETICAL OPD AVAILABLE

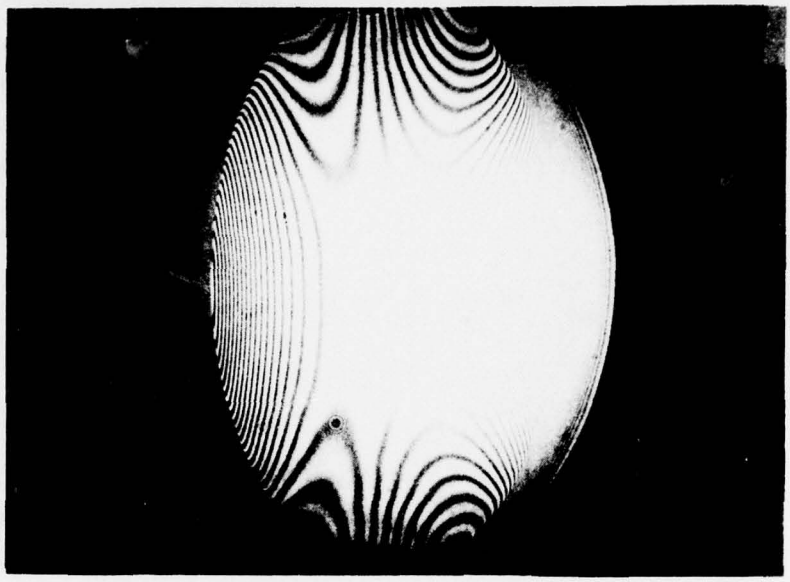

Figure 71(a). Variation of RBT, θ_1 = 70°, U configuration.

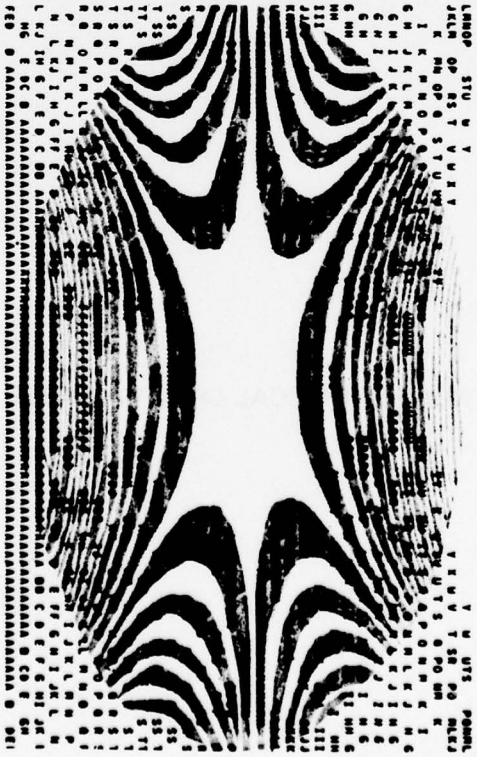

Figure 71(b). U configuration, θ_1 = 70°, RBT = 0 (3.698).

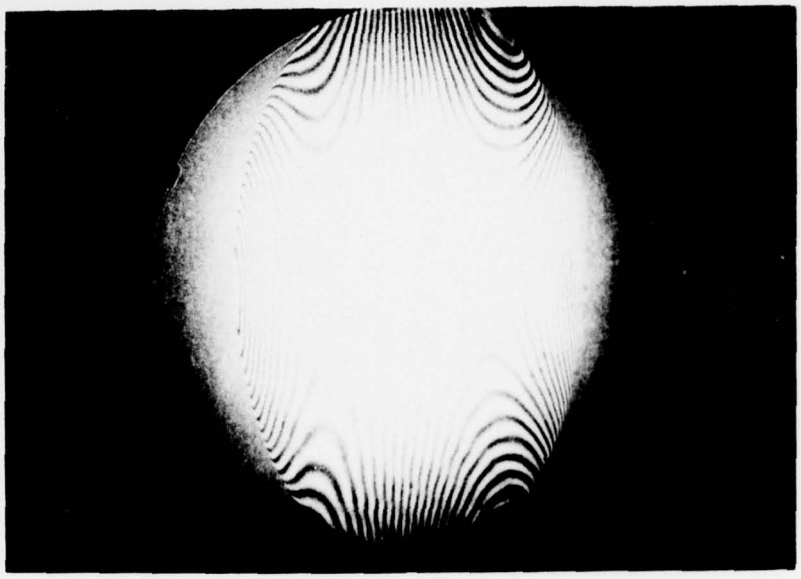

Figure 72(a). Variation of RBT, θ_1 = 70°, U configuration.

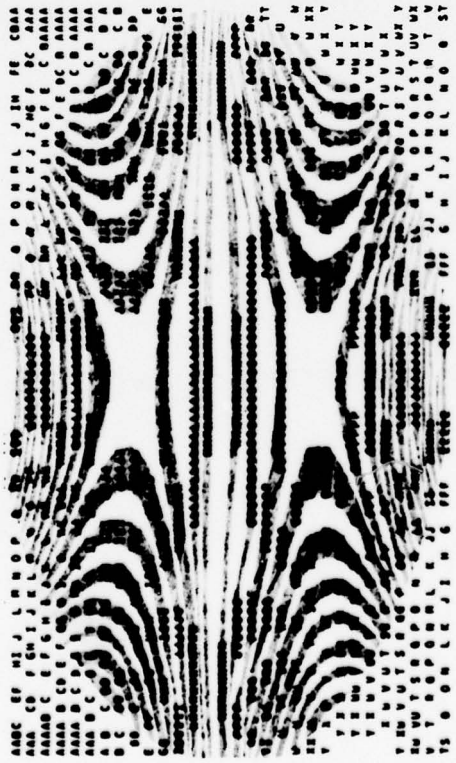

Figure 72(b). U configuration, θ_1 = 70°, RBT = 1.48 (3.698).

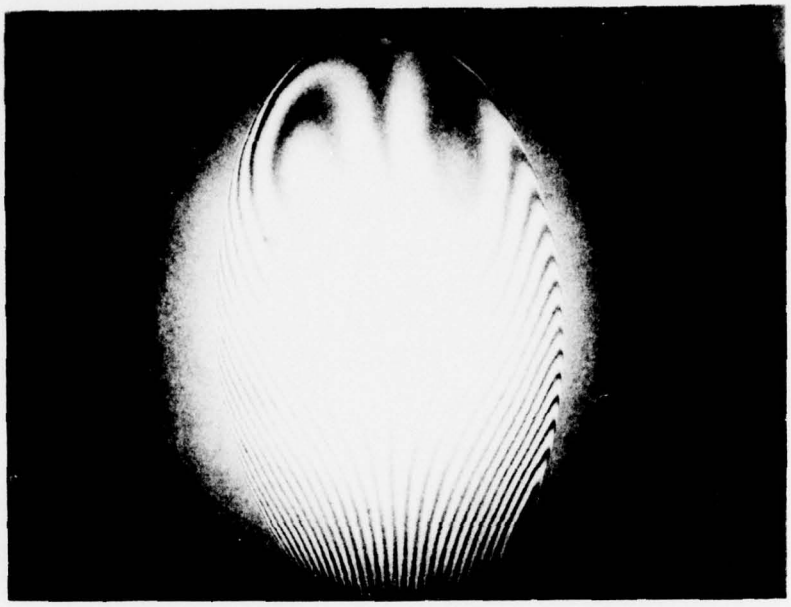

Figure 73. Tilt in θ_2 in a plane orthogonal to the plane of rotation of θ_1 and θ_2, $\Delta\theta_2'$ = 7 mrad, θ_1 = 70°, Z configuration.

NO THEORETICAL OPD AVAILABLE

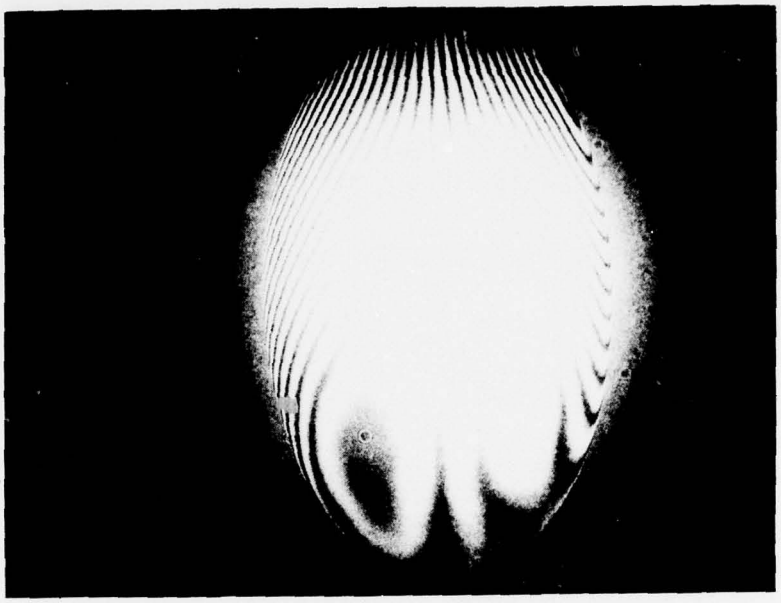

Figure 74. Tilt in θ_2 in a plane orthogonal to the plane of rotation of θ_1 and θ_2, $\Delta\theta_2' = -7$ mrad, $\theta_1 = 70°$, Z configuration.

NO THEORETICAL OPD AVAILABLE

Appendix A. EQUATIONS FOR THREE-DIMENSIONAL RAY TRACING

The coordinate system used at a particular stage of ray-tracing calculations will ordinarily be chosen such that the central ray is along the positive z axis. Usually the origin of coordinates is at the intersection of the central ray with the spherical-mirror surface. The equations can be related to Figure A-1, which depicts the case of a convex mirror. Provision is made for the mirror to be tilted about the x-axis, i.e., in the y-z plane, by an angle T. The coordinate system is left-handed.

The basic ray-optics equation for reflection is simply

$$\bar{e}_r = \bar{e}_i - 2\,\bar{n}\cos\theta, \tag{A-1}$$

where $\bar{e}_i$ and $\bar{e}_r$ are unit vectors along the incident and reflected rays, respectively, $\bar{n}$ is a unit normal vector (pointed from the intersection point toward the mirror center), and θ is the angle between the incident (or reflected) ray and the mirror normal $\bar{n}$.

The mirror tilt angle T is taken as positive for counterclockwise rotation, i.e., from the positive z direction toward the positive y direction. The convention is adopted that the mirror curvature R is negative for convex mirrors. The coordinates of the mirror center are then 0, -R sin T, -R cos T; this is valid for either sign of R. The equation of the mirror surface is

$$\phi\ (x,y,z) = \text{const} = R^2 = x^2 + (y + R\sin T)^2 + (z + R\cos T)^2\ . \tag{A-2}$$

The unit normal vector can be determined by taking the gradient of this function, i.e.,

$$\bar{n} = \frac{1}{2R}\,\Delta\phi = \frac{x}{R}\ ,\ \frac{y}{R} + \sin T,\ \frac{z}{R} + \cos T \tag{A-3}$$

Now z can be eliminated:

$$\bar{n} = \left(\frac{x}{R}\ ,\left(\frac{y}{R} + \sin T\right)\ ,\ \sqrt{1 - \left(\frac{x}{R}\right)^2 - \left(\frac{y}{R} + \sin T\right)^2}\right) \tag{A-4}$$

The direction cosines of the incident ray are denoted by a, b, and c, i.e., giving vector equation:

$$\bar{e}_i = (a,b,c) \tag{A-5}$$

and similarly, (using primes to denote the reflected ray),

$$\bar{e}_r = (a', b', c') \quad . \tag{A-6}$$

The cosine of the angle θ between the incident ray and the surface normal is given by the dot product of the corresponding unit vectors, that is:

$$\cos\theta = \bar{e}_i \cdot \bar{n} \quad . \tag{A-7}$$

This gives the explicit result:

$$\cos = \theta\ a\left(\frac{x}{R}\right) + b\left(\frac{y}{R}\right) + c\sqrt{1 - \left(\frac{x}{R}\right)^2 - \left(\frac{y}{R} + \sin T\right)^2} \quad . \tag{A-8}$$

This equation can conveniently be used to determine the numerical value of θ. The direction cosines of the reflected ray can then be determined from the following equations:

$$a' = a - 2\cos\theta \cdot \frac{x}{R} \quad , \tag{A-9}$$

$$b' = b - 2\cos\theta \cdot \left(\frac{y}{R} + \sin T\right) \quad , \tag{A-10}$$

$$c' = c - 2\cos\theta \cdot \sqrt{1 - \left(\frac{x}{R}\right)^2 - \left(\frac{y}{R} + \sin T\right)^2} \quad . \tag{A-11}$$

For the special case of an incident ray parallel to the z-axis, i.e., for $a = b = 0$, the following is noted:

$$c' = c - 2\cos^2\theta \quad . \tag{A-12}$$

The necessary relationship between the direction cosines

$$(a')^2 + (b')^2 + (c')^2 = 1 \tag{A-13}$$

is reserved here for a possible test, but is not used to determine the value of c', because an Equation (11-A) which determines the sign as well as the magnitude of c' is needed.

Equations (9-A) through (11-A) for direction cosines of reflected ray require knowledge not only of direction cosines of incident ray but also of the coordinates of the point of intersection of the incident ray with the mirror. In general, these must be determined from a separate calculation. For the special case of the incident ray parallel to the

z-axis, encountered in starting some ray-tracing problems, x and y will be given, and z can be determined from the equation obtained by solving Equation (A-2) for z:

$$z = -R \cos T - \sqrt{R^2 - x^2 - (y + R \sin T)^2} \quad . \tag{A-14}$$

At various stages in the calculations, it will be desirable to make rotational coordinate transformation. In particular, such a rotation of coordinates will be made after each reflection from a spherical mirror. As indicated in Figure A-2, the direction of the central ray is changed such that the associated angle in the z-y plane is increased by $\pi + 2\,T$, where T is the mirror tilt angle, taken as positive for counterclockwise rotations. This is denoted by Θ, i.e.:

$$\Theta = \pi + 2\,T \quad . \tag{A-15}$$

With reference to Figure A-3, a rotational transformation from an unprimed to a primed coordinate system as shown has the transformation equations:

$$z' = z \cos \Theta + y \sin \Theta \quad , \tag{A-16}$$

$$y' = -z \sin \Theta + y \cos \Theta \quad . \tag{A-17}$$

The effect of the coordinate rotation on direction cosines can be derived by reference to Figure A-4. The polar and azimuthal angles V and W define the direction of the ray vector $\bar{e}$, which is alternatively defined by the direction cosines a, b, and c. Thus the following can be written:

$$a = \cos V \quad , \tag{A-18}$$

$$b = \sin V \sin W \quad , \tag{A-19}$$

$$c = \sin V \cos W \quad . \tag{A-20}$$

These equations can be readily solved for V and W:

$$V = \cos^{-1}(a) \quad , \tag{A-21}$$

$$W = \sin^{-1}\left(\frac{b}{\sin V}\right) = \cos^{-1}\left(\frac{c}{\sin V}\right) \quad . \tag{A-22}$$

The effect of a rotation about the x-axis, measured as positive in the sense discussed previously is to reduce W algebraically by the magnitude of the rotation angle, while the polar angle V is unaffected. Thus, the following can be written:

$$V' = V \quad , \tag{A-23}$$

$$W' = W - \Theta \quad . \tag{A-24}$$

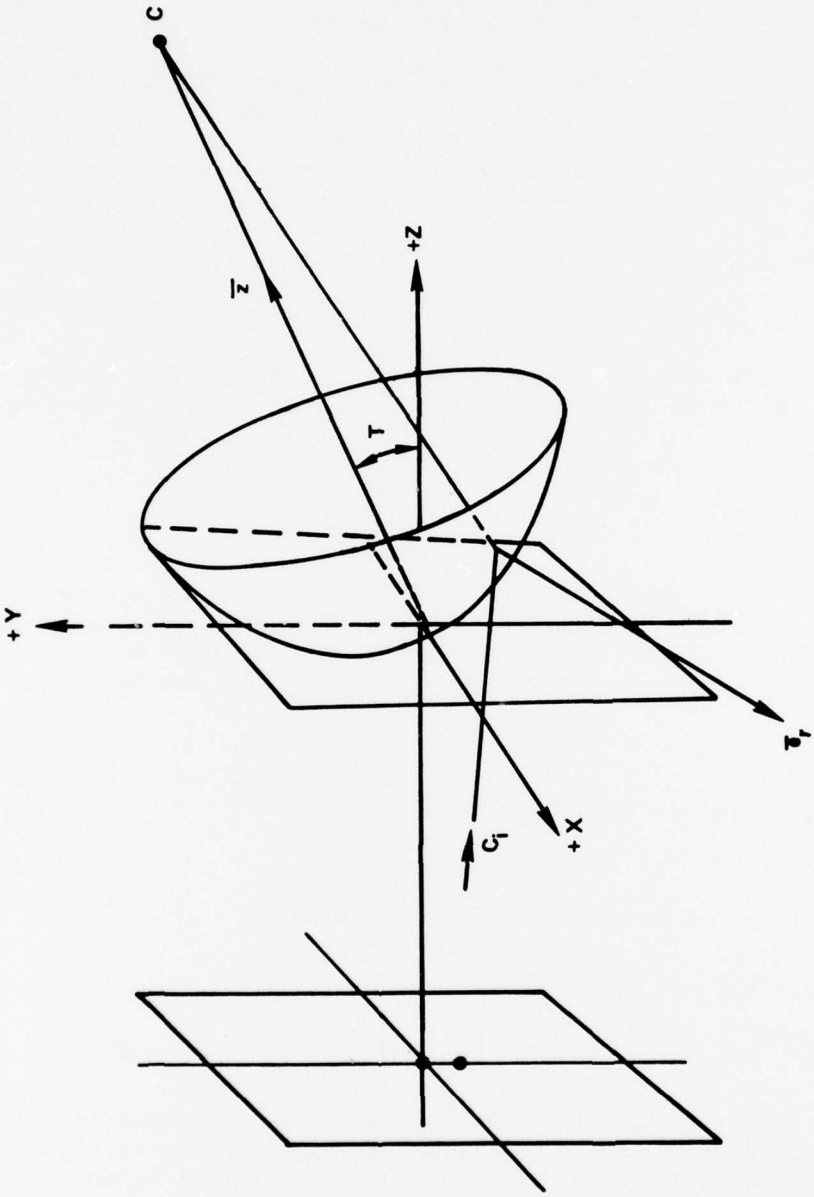

Figure A-1. Convex mirror.

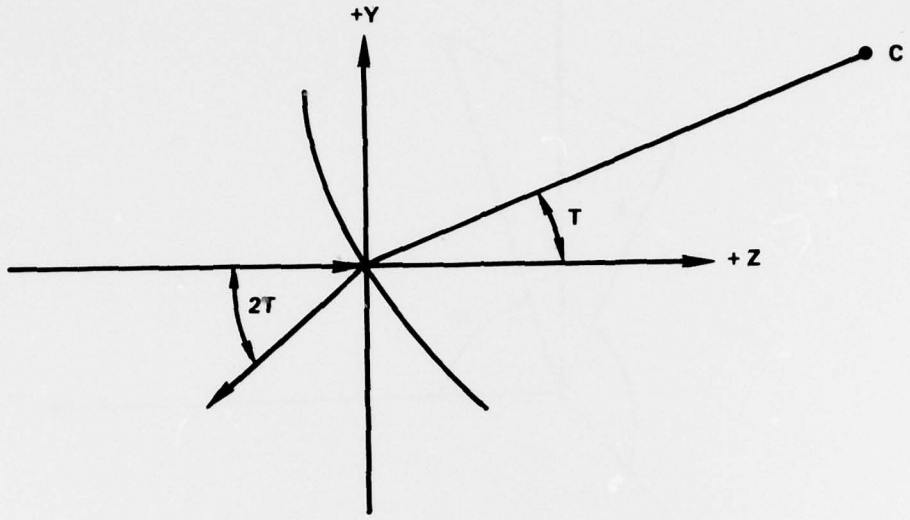

Figure A-2. Direction of the central ray.

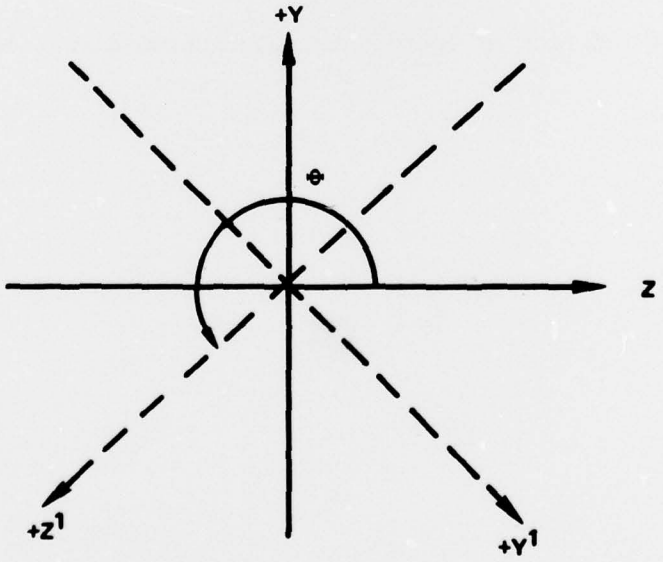

Figure A-3. Rotational transformation.

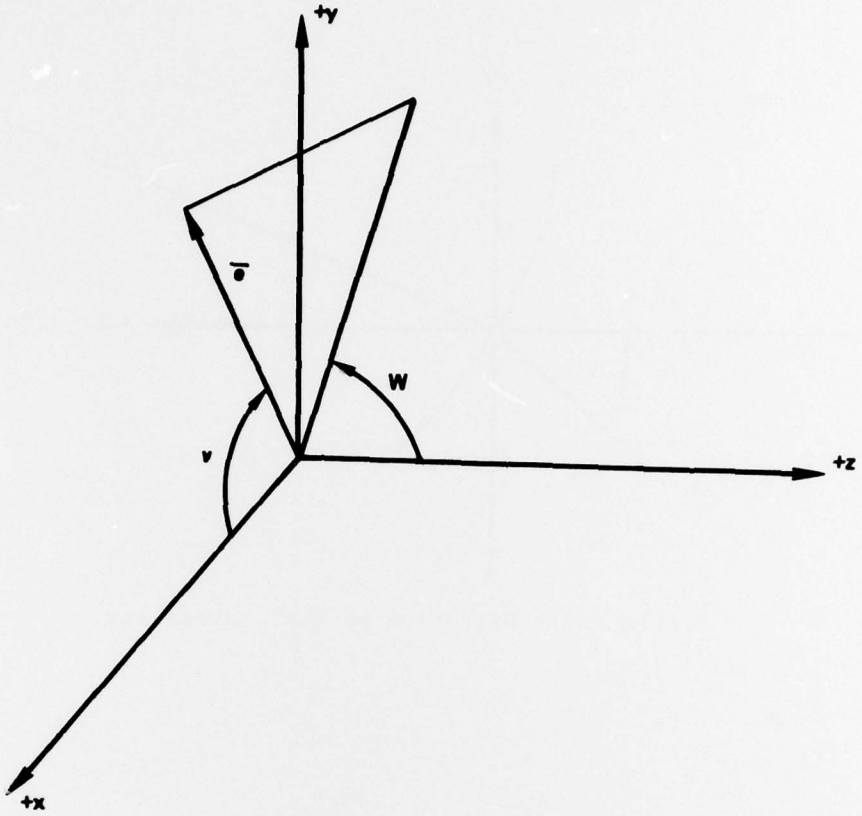

Figure A-4. Effect of coordinate rotation on direction cosines.

The direction cosines can then be written in the rotated frame in terms of the new angles:

$$a'' = \sin(V) = a \quad , \tag{A-25}$$

$$b'' = \sin(V) \sin(W') \quad , \tag{A-26}$$

$$c'' = \sin(V) \cos(W') \quad . \tag{A-27}$$

Here double primes are used on the a, b, and c simply to distinguish from the equations relating to the change in direction cosines as a result of reflection from a spherical mirror.

For computer evaluation of W, the proper quadrant must be chosen. A suitable method is evaluating the magnitude of W from the second part of Equation (A-22) involving the $\cos^{-1}$ function, but with the sign of W chosen to conform to the first part of Equation (A-22), involving the $\sin^{-1}$ function.

After finding the direction cosines and coordinates at the mirror-intersection point, referred to a coordinate system with positive z-axis along central ray, the case that the next mirror is also a spherical mirror is considered. First the point of intersection of the ray with this mirror is found. For this purpose, the parametric equations with t are written for the ray as:

$$x' = x + a\,t \quad , \tag{A-28}$$

$$y' = y + b\,t \quad , \tag{A-29}$$

$$z' = z + c\,t \quad . \tag{A-30}$$

Equation (A-2) can be rewritten defining the mirror surface:

$$(x')^2 + (y' + R \sin T)^2 + (z' + R \cos T)^2 = R^2 \quad . \tag{A-31}$$

Substituting Equations (A-28) through (A-30) gives:

$$(x + at)^2 + (y + R \sin T + bt)^2 + (z + R \cos T + ct)^2 = R^2 . \tag{A-32}$$

This can be expressed as:

$$t^2 + 2\,B\,t + C = 0 \quad , \tag{A-33}$$

where

$$B = ax + b(y + R \sin T) + c(z + R \cos T) \quad , \tag{A-34}$$

$$C = x^2 + (y + R \sin T)^2 + (z + R \cos T)^2 - R^2 \quad . \tag{A-35}$$

The solution to Equation (A-33) is simply:

$$t = -B \pm \sqrt{B^2} = C \quad . \tag{A-37}$$

The choice of sign in front of the square root should be such as to obtain a positive solution. It should be the smaller in magnitude of the two in the event that there are two positive roots.

Appendix B. EFFECTS OF INCREMENTS TO MIRROR SPACING L AND TO CONCAVE-MIRROR TILT ANGLE θ_2

By the nature of the concept, there will be no net focusing or defocusing, i.e., no second-power term in x or y in the equation for a constant-phase surface, in the output when both L and θ_2 are set precisely at their nominal values. This fact is of considerable practical importance. But because there may be small departures of ΔL and $\Delta\theta_2$ from their nominal values, it is appropriate to investigate the predicted effects (i.e., predicted in a fairly simple closed-form analysis as given in this appendix) of such departures and to compare these predictions to results of detailed calculations.

First, increments ΔL are considered. The effective focal lengths of the mirrors in the x-z plane are denoted by F_{1x} and F_{2x}. Similar notation will be employed for the y-z plane; differences in the two cases arise only from the presence of $\cos\theta_2$ or $\sec\theta_2$. F_{Tx} denotes the effective focal length in the x-z plane of the output beam. The following lens-type equation can then be written:

$$\frac{1}{F_{Tx}} = \frac{1}{F_{1x} - L - \Delta L} + \frac{1}{F_{2x}}$$

$$= \frac{F_{2x} + (F_{1x} - L - \Delta L)}{(F_{1x} - L - \Delta L)F_{2x}} \quad .$$

But L has a value such that the output is collimated, i.e.,

$$F_{2x} + F_{1x} - L = 0.$$

It is here understood that F_{1x} is negative. Then, to a good approximation, the following can be written:

$$\frac{1}{F_{Tx}} = \frac{\Delta L}{(F_{2x})^2}$$

Now the incremental optical path length for the case of a wave focusing with focal length F_{Tx} is simply

$$z = C_{20}\, x^2 \quad .$$

Similarly, for focusing in the y-z plane, the following is obtained:

$$z = C_{02}\, y^2 \quad .$$

The corresponding value of C_{20} is given by

$$C_{20} = -\frac{1}{2F_{Tx}} \quad .$$

The specific expression for F_{2x} is

$$F_{2x} = \frac{R_2}{2} \sec \theta_2 \quad ;$$

hence,

$$C_{20} = -\frac{2\Delta L}{R_2^2} \cos^2 \theta_2 \quad .$$

Similarly, the following is obtained:

$$C_{02} = -\frac{2\Delta L}{R_2^2} \sec^2 \theta_2 \quad .$$

A numerical example with $R_2 = 675$ cm, $\theta_1 = 55°$, $\theta_2 = 38.76°$ has been considered. The predictions of the preceding equations for this example are

$$C_{20} = -0.267 \times 10^{-5}\, \Delta L \quad ,$$

$$C_{02} = -0.722 \times 10^{-5}\, \Delta L \quad .$$

The values of C_{20} and C_{02} have also been determined by simple function-fitting to results of numerical OPD calculations. A comparison of these latter calculated results with the predicted results derived is given in Table B-1. The agreement is satisfactory.

It should be noted that the signs of C_{20} and C_{02} are the same for increments in mirror-spacing L. That is to say, the net focusing or defocusing (converging or diverging) effect is qualitatively the same (though quantitatively different) in the two transverse planes.

Next, the effect of an incremental tilt angle $\Delta\theta_2$ is considered. The equation for focal length of output in x-z plane is now

$$\frac{1}{F_{Tx}} = \frac{1}{F_{1x} - L} + \frac{1}{F_{2x} + \Delta F_{2x}} \quad ,$$

which reduces to a high degree of approximation to

$$\frac{1}{F_{Tx}} = - \frac{\Delta F_{2x}}{(F_{2x})^2} \quad .$$

but,

$$F_{2x} = \frac{R_2}{2} \sec \theta_2 \quad ,$$

and hence

$$\Delta F_{2x} = \frac{R_2}{2} \sec \theta_2 \tan \theta_2 \, \Delta\theta_2 \quad .$$

This leads to

$$\frac{1}{F_{Tx}} = - \frac{2}{R_2} \sin \theta_2 \, \Delta\theta_2$$

but again,

$$C_{20} = - \frac{1}{2F_{Tx}} \quad .$$

This finally gives

$$C_{20} = \frac{1}{R_2} \sin \theta_2 \, \Delta\theta_2 \quad .$$

For the yz plane, the following is obtained:

$$F_{2y} = -\frac{R_2}{2} \cos \theta_2 \quad .$$

The following is readily obtained:

$$F_{2y} = \frac{R_2}{2} (-\sin \theta_2) \, \Delta\theta_2 \quad .$$

This finally gives

$$C_{02} = -\frac{1}{R_2} \sin \theta_2 \sec^2 (\theta_2) \, \Delta\theta_2 \quad .$$

In the preceding equations $\Delta\theta_2$ is assumed to be in radians.

A numerical example with $R_1 = -290$ cm, $R_2 = 675$ cm, $\theta_1 = 0.95993$ rad (55°), and $\theta_2 = 0.67647$ rad (38.76°) has been considered. The predicted values of the quadratic parameters C_{20} and C_{02} are

$$C_{20} = 0.927 \times 10^{-3} \, \Delta\theta_2 \quad .$$

$$C_{02} = -1.525 \times 10^{-3} \, \Delta\theta_2 \quad .$$

A comparison of values predicted in this way with values obtained by function-fitting to numerically calculated OPDs is given in Table B-2. The agreement is satisfactory.

C_{20} and C_{02} have opposite signs for the case of increments in tilt angle θ_2. This is readily understood by noting that the effective focal lengths in the two transverse planes are changed in opposite directions by such an incremental tilt angle. This behavior is in contrast to the behavior with regard to increments in mirror spacing.

TABLE B-1. COMPARISON OF PREDICTED AND CALCULATED VALUES OF BEAM CURVATURE PARAMETERS C_{20} AND C_{02} RESULTING FROM INCREMENTS ΔL IN MIRROR SEPARATION. (R_1 = -290 cm, R_2 = 675 cm, θ_1 = 55°, θ_2 = 38.76°, L = 180.01005 cm)*

	C_{20}		C_{20}	
L (cm)	Predicted	Calculated	Predicted	Calculated
+1.0	-0.267E-5	-0.268E-5	-0.722E-5	-0.728E-5
-1.0	+0.267E-5	+0.266E-5	+0.722E-5	+0.716E-5
+2.0	-0.534E-5	-0.536E-5	-1.444E-5	-1.457E-5
-2.0	+0.534E-5	+0.531E-5	+1.444E-5	+1.430E-5

*Predicted values are the same for Z and U configurations; calculated values are for Z configurations.

TABLE B-2. COMPARISON OF PREDICTED AND CALCULATED VALUES OF BEAM CURVATURE PARAMETERS C_{20} AND C_{02} RESULTING FROM INCREMENTS $\Delta\theta_2$ IN CONCAVE-MIRROR TILT ANGLE. (R_1 = -290 cm, R_2 = 675 cm, θ_1 = 0.95993 rad (55°), θ_2 = 0.67647 rad (38.76°), L = 180.01005 cm)*

	C_{20}		C_{02}	
θ_2	Predicted	Calculated	Predicted	Calculated
+0.0035	+0.324E-5	+0.325E-5	-0.534E-5	-0.540E-5
-0.0035	-0.324E-5	-0.324E-5	+0.534E-5	+0.528E-5
+0.0070	+0.648E-5	+0.652E-5	-1.068E-5	-0.082E-5
-0.0070	-0.648E-5	-0.646E-5	+1.068E-5	+1.054E-5

*Predicted values are the same for Z and U configurations; calculated values are for Z configurations. Note that 0.0035 rad 0.2°.

DISTRIBUTION

No. of Copies		No. of Copies
12	Defense Documentation Center Attn: DDC-TCA Cameron Station Alexandria, VA 22314	
1	McDonnell Douglas Research Laboratory Attn: Dr. Thomas J. Menne Post Office Box 516 St. Louis, MO 63166	
1	General Electric Attn: Mr. Bill East 3198 Chestnut Street Philadelphia, PA 19101	
1	Aerospace Corporation Attn: W. Warren Post Office Box 95085 El Segundo, CA 90045	
1	Air Force Weapons Laboratory Attn: AFWL-ALC, Dr. B. Hogge Kirtland AFB, NM 87117	
1	Commander Wright-Patterson Air Force Base Attn: ARL/LP, Dr. J. Drewry Wright-Patterson AFB, OH 45433	
1	Commander US Army Research Office - Durham Box CM, Duke Station Durham, NC 27706	
2	Science Applications, Inc. Attn: Steade Howie 2028 Powers Ferry Road Suite 260 Atlanta, GA 30339	
1 1	Navy High Energy Laser Project Office (PM 22/PMS 405) National Center #3 Attn: Dr. Finkleman Dr. Stregack Crystal City, VA 20010	
1	Director of Defense Research & Engineering Attn: Asst. Dir., Space & Advanced Sys. The Pentagon Washington, DC 20301	
1	Director US Army Ballistic Research Laboratory Attn: DRDAR-BLD, Mr. H. Breaux Aberdeen Proving Ground, MD 21005	
1	Director US Army Advanced BMD Technology Center Attn: ATC-T, J. Hagefstration P. O. Box 1500 Huntsville, AL 35807	
1	AVCO Everett Research Laboratory Attn: Dr. G. Sutton 2385 Revere Beach Parkway Everett, MA 02149	
1	General Electric Company Valley Forge Space Center Attn: Mr. W. J. East P. O. Box 8555 Philadelphia, PA 19101	
1	General Research Corporation Attn: Dr. G. K. Warmbrod 307 Wynn Drive Huntsville, AL 35807	
1	Rocketdyne Attn: Mr. Spencer Clapp Canoga Park, CA 91304	
1	W. J. Schafer Associates, Inc. Attn: Dr. G. Zeiders 14 Lakeside Office Park Wakefield, MA 01880	1
1	W. J. Schafer Associates, Inc. Attn: Dr. W. H. Evers 1901 North Fort Myer Drive Arlington, VA 22209	1
1	Bell Aerospace Textron Attn: Dr. Wayne Solomon P. O. Box 1 Buffalo, NY 14240	1
1	Hughes Aircraft Company Attn: Dr. F. Mastrup Centinela & Teale Streets Building 6, Mail Station E 125 Culver City, CA 90230	1
2 1	Lockheed Missile and Space Company Huntsville Research and Engineering Center Attn: R. Mikatorian P. O. Box 1103 Huntsville, AL 35807	1
1	North American Rockwell Corporation Attn: Dr. J. Flanagan Mr. R. M. McHale 6633 Canoga Avenue Canoga Park, CA 91304	1 1
2	United Aircraft Research Lab Attn: Dr. D. Smith 400 Main Street East Hartford, CN 06108	1
1 1	TRW Systems, Bldg. 01 Attn: Dr. S. Forbes Mr. D. Culler Mr. Dwight Moberg One Space Park Redondo Beach, CA 90278	1 1 1
1	United Technologies Research Center Attn: Dr. Casper Ultee Silver Lane East Hartford, CT 06108	1
1	United Technologies Corporation Pratt & Whitney Aircraft Group, GPD Attn: Mr. George McLafferty P. O. Box 2691 West Palm Beach, FL 33402	1
1	Air Force Weapons Laboratory/ALC Attn: CPT John Opray Kirtland AFB, NM 87117	1
1	Space and Missile System Organization/YAD Attn: LTC John Doughtey P. O. Box 92960 Worldway Postal Center Los Angeles, CA 90009	1
1	Defense Advanced Research Projects Agency Director Laser Div Attn: STO, Dr. R. Sepucha 1400 Wilson Blvd. Arlington, VA 22209	1
1	Charles Stark Draper Laboratories Attn: Dr. C. K. Whitney 555 Technology Square Cambridge, MA 02139	1
1	US Army Materiel Systems Analysis Activity Attn: DRXSY-MP Aberdeen Proving Ground, MD 21005	1

TABLE B-1. COMPARISON OF PREDICTED AND CALCULATED VALUES OF BEAM CURVATURE PARAMETERS C_{20} AND C_{02} RESULTING FROM INCREMENTS ΔL IN MIRROR SEPARATION. (R_1 = -290 cm, R_2 = 675 cm, θ_1 = 55°, θ_2 = 38.76°, L = 180.01005 cm)*

	C_{20}		C_{20}	
L (cm)	Predicted	Calculated	Predicted	Calculated
+1.0	-0.267E-5	-0.268E-5	-0.722E-5	-0.728E-5
-1.0	+0.267E-5	+0.266E-5	+0.722E-5	+0.716E-5
+2.0	-0.534E-5	-0.536E-5	-1.444E-5	-1.457E-5
-2.0	+0.534E-5	+0.531E-5	+1.444E-5	+1.430E-5

*Predicted values are the same for Z and U configurations; calculated values are for Z configurations.

TABLE B-2. COMPARISON OF PREDICTED AND CALCULATED VALUES OF BEAM CURVATURE PARAMETERS C_{20} AND C_{02} RESULTING FROM INCREMENTS $\Delta\theta_2$ IN CONCAVE-MIRROR TILT ANGLE. (R_1 = -290 cm, R_2 = 675 cm, θ_1 = 0.95993 rad (55°), θ_2 = 0.67647 rad (38.76°), L = 180.01005 cm)*

	C_{20}		C_{02}	
θ_2	Predicted	Calculated	Predicted	Calculated
+0.0035	+0.324E-5	+0.325E-5	-0.534E-5	-0.540E-5
-0.0035	-0.324E-5	-0.324E-5	+0.534E-5	+0.528E-5
+0.0070	+0.648E-5	+0.652E-5	-1.068E-5	-0.082E-5
-0.0070	-0.648E-5	-0.646E-5	+1.068E-5	+1.054E-5

*Predicted values are the same for Z and U configurations; calculated values are for Z configurations. Note that 0.0035 rad 0.2°.

DISTRIBUTION

No. of Copies	
12	Defense Documentation Center Attn: DDC-TCA Cameron Station Alexandria, VA 22314
1	McDonnell Douglas Research Laboratory Attn: Dr. Thomas J. Menne Post Office Box 516 St. Louis, MO 63166
1	General Electric Attn: Mr. Bill East 3198 Chestnut Street Philadelphia, PA 19101
1	Aerospace Corporation Attn: W. Warren Post Office Box 95085 El Segundo, CA 90045
2	Air Force Weapons Laboratory Attn: AFWL-ALC, Dr. B. Hogge Kirtland AFB, NM 87117
1	Commander Wright-Patterson Air Force Base Attn: ARL/LP, Dr. J. Drewry Wright-Patterson AFB, OH 45433
1	Commander US Army Research Office - Durham Box CM, Duke Station Durham, NC 27706
2	Science Applications, Inc. Attn: Steade Howie 2028 Powers Ferry Road Suite 260 Atlanta, GA 30339
1 1	Navy High Energy Laser Project Office (PM 22/PMS 405) National Center #3 Attn: Dr. Finkleman Dr. Stregack Crystal City, VA 20010
1	Director of Defense Research & Engineering Attn: Asst. Dir., Space & Advanced Sys. The Pentagon Washington, DC 20301
1	Director US Army Ballistic Research Laboratory Attn: DRDAR-BLD, Mr. H. Breaux Aberdeen Proving Ground, MD 21005
1	Director US Army Advanced BMD Technology Center Attn: ATC-T, J. Hagefstration P. O. Box 1500 Huntsville, AL 35807
1	AVCO Everett Research Laboratory Attn: Dr. G. Sutton 2385 Revere Beach Parkway Everett, MA 02149
1	General Electric Company Valley Forge Space Center Attn: Mr. W. J. East P. O. Box 8555 Philadelphia, PA 19101
1	General Research Corporation Attn: Dr. G. K. Warmbrod 307 Wynn Drive Huntsville, AL 35807
1	Rocketdyne Attn: Mr. Spencer Clapp Canoga Park, CA 91304
1	W. J. Schafer Associates, Inc. Attn: Dr. G. Zeiders 14 Lakeside Office Park Wakefield, MA 01880
1	W. J. Schafer Associates, Inc. Attn: Dr. W. H. Evers 1901 North Fort Myer Drive Arlington, VA 22209
1	Bell Aerospace Textron Attn: Dr. Wayne Solomon P. O. Box 1 Buffalo, NY 14240
1	Hughes Aircraft Company Attn: Dr. F. Mastrup Centinela & Teale Streets Building 6, Mail Station E 125 Culver City, CA 90230
1	Lockheed Missile and Space Company Huntsville Research and Engineering Center Attn: R. Mikatorian P. O. Box 1103 Huntsville, AL 35807
1 1	North American Rockwell Corporation Attn: Dr. J. Flanagan Mr. R. M. McHale 6633 Canoga Avenue Canoga Park, CA 91304
1	United Aircraft Research Lab Attn: Dr. D. Smith 400 Main Street East Hartford, CN 06108
1 1 1 1 1	TRW Systems, Bldg. 01 Attn: Dr. S. Forbes Mr. D. Culler Mr. Dwight Moberg One Space Park Redondo Beach, CA 90278
1	United Technologies Research Center Attn: Dr. Casper Ultee Silver Lane East Hartford, CT 06108
1	United Technologies Corporation Pratt & Whitney Aircraft Group, GPD Attn: Mr. George McLafferty P. O. Box 2691 West Palm Beach, FL 33402
1	Air Force Weapons Laboratory/ALC Attn: CPT John Opray Kirtland AFB, NM 87117
1	Space and Missile System Organization/YAD Attn: LTC John Doughtey P. O. Box 92960 Worldway Postal Center Los Angeles, CA 90009
1	Defense Advanced Research Projects Agency Director Laser Div Attn: STO, Dr. R. Sepucha 1400 Wilson Blvd. Arlington, VA 22209
1	Charles Stark Draper Laboratories Attn: Dr. C. K. Whitney 555 Technology Square Cambridge, MA 02139
1	US Army Materiel Systems Analysis Activity Attn: DRXSY-MP Aberdeen Proving Ground, MD 21005

	No. of Copies
DRCPM-HEL-T, Charles Cason	20
-P	1
-S	1
DRSMI-LP, Mr. Voigt	1
DRDMI-X, Mr. McKinley	1
-T, Dr. Kobler	1
-NS	1
-TBD	3
-TI (Record Copy)	1
(Reference Set)	1